



ARR No. 3I21

*1108.5*  
*148*  
~~\_\_\_\_\_~~

NATIONAL ADVISORY COMMITTEE FOR AERONAUTICS

# WARTIME REPORT

ORIGINALLY ISSUED  
September 1943 as  
Advance Restricted Report 3I21

WIND-TUNNEL INVESTIGATION OF REAR UNDERSLING

FUSELAGE DUCTS

By K. R. Czarnecki and W. J. Nelson

Langley Memorial Aeronautical Laboratory  
Langley Field, Va.

# NACA

WASHINGTON

NACA WARTIME REPORTS are reprints of papers originally issued to provide rapid distribution of advance research results to an authorized group requiring them for the war effort. They were previously held under a security status but are now unclassified. Some of these reports were not technically edited. All have been reproduced without change in order to expedite general distribution.

# NATIONAL ADVISORY COMMITTEE FOR AERONAUTICS

## ADVANCE RESTRICTED REPORT

### WIND-TUNNEL INVESTIGATION OF REAR UNDERSLUNG

#### FUSELAGE DUCTS

By K. R. Ozarnecki and W. J. Nelson

#### SUMMARY

A general investigation of cooling ducts located at various positions on a model of a typical pursuit airplane has been conducted in the NACA full-scale tunnel. Results are given in the present report for a duct located on the bottom of the fuselage with its inlet behind the leading edge of the wing. This installation is designated a rear underslung fuselage duct.

Because of the thick boundary layers that existed at the inlets of rear underslung fuselage ducts, serious losses in total pressure occurred ahead of the heat exchanger. In order to eliminate these losses, tests were made with special vane installations designed to avoid boundary-layer separation and with ducts to bypass the boundary layer away from the main cooling duct.

Good pressure recoveries were obtained in the ducts with the use of either the inlet guide-vane installation or the boundary-layer bypass duct. Best efficiencies were measured, however, with installations that had vanes in the diffuser and in the duct outlet. The ratio of duct inlet velocity to the stream velocity was shown to be the most important parameter affecting the duct performance; a value of this parameter of about 0.6 was shown to be a good design value for the duct with or without vanes and 0.35 was a good value for the installation with the boundary-layer bypass. At values somewhat below 0.6 and 0.35, separation occurred ahead of the duct and, at higher values, there was some tendency for the duct losses to increase.

## INTRODUCTION

An investigation has been conducted in the NACA full-scale tunnel of engine-charge-air and cooling-air ducts located at several positions on the fuselage and in the wing of a model of a pursuit airplane. The results of the investigation relating to carburetor-air ducts on the top of the fuselage and to cooling-air ducts in the wing have been reported in references 1 and 2. In the present report, results are given for tests of a cooling duct installed on the bottom of the fuselage with the inlet behind the leading edge of the wing. This installation is designated a rear underslung fuselage duct.

The tests were directed toward the development of a duct having the following desirable characteristics:

- (1) Maximum conversion of the total pressure ahead of the duct to total pressure ahead of the heat exchanger
- (2) Satisfactory regulation of air-flow quantity over the range of airplane flight conditions
- (3) Low duct drag, particularly in the high-speed flight condition
- (4) High critical speed

A single basic duct configuration was tested with several modified inlets and outlets. In order to investigate methods of preventing boundary-layer separation, vanes were added in the diffuser and outlet sections of the duct and a boundary-layer bypass duct was installed. The resistance of an orifice plate simulating a heat exchanger was varied over a wide range of values to represent different types of cooler.

An investigation was made of the effects of inlet-velocity ratio and airplane angle of attack on the duct characteristics. In order to investigate the effects of propeller slipstream on the flow into the duct, tests were made with the propeller removed and with the propeller operating at thrust coefficients simulating high-speed and climbing flight. Critical speeds for the various duct installations were estimated for different

rates of air flow through the duct inlet by means of pressure-distribution measurements along the duct inlet lips and the duct-fuselage fillet.

# SYMBOLS

$C_L$	lift coefficient
$\Delta C_D$	increment of drag coefficient due to duct
$\Delta C_{D_i}$	calculated increment of internal-drag coefficient
$\Delta C_{D_e}$	increment of drag coefficient due to external drag ( $\Delta C_D - \Delta C_{D_i}$ )
$C_m$	pitching-moment coefficient
$T_o$	thrust coefficient ( $T/\rho V_o^2 D^2$ )
$\Delta D$	increment of drag due to duct
$p/q_o$	surface static-pressure coefficient
$\Delta p/q_o$	pressure-drop coefficient
$p$	static pressure (referenced to atmospheric pressure)
$q$	dynamic pressure
$\Delta p$	pressure drop across orifice plate
$H$	total pressure (referenced to atmospheric pressure)
$\Delta H$	loss in total pressure
$Q$	quantity rate of flow
$Q/V_o$	air-flow parameter
$V_i/V_o$	inlet-velocity ratio
$u$	local velocity
$T$	propeller thrust

- $V/nD$  advance-diameter ratio
- $\eta$  duct efficiency ( $Q\Delta p/\Delta V_0$ )
- $\alpha$  angle of attack of thrust axis relative to free-stream direction
- $\beta$  propeller blade setting at 0.75 radius
- $D$  propeller diameter
- $A$  duct area
- $S$  wing area

Subscripts denote average conditions:

- 0 in free stream
- 1 in duct inlet
- 2 at front face of orifice plate
- 3 in outlet of main duct
- 4 in outlet of boundary-layer bypass duct
- 5 below trailing edge of outlet guide vane

#### APPARATUS AND TESTS

A description of the NACA full-scale tunnel and the equipment used for the tests is given in reference 3. The model is shown mounted in the test section in figures 1 and 2, and a three-view drawing is given in figure 3. The model was equipped with a Curtiss-Wright controllable-pitch propeller that was driven by an electric motor. The propeller had 614C1.5-24 blades, which were fitted with the metal cuffs shown in figure 4.

The general arrangement and the principal dimensions of the basic duct installation and the modifications are shown in figures 5 and 6. The duct varied in cross section from a segment of a circle at the inlet to a circle at the orifice plate and to a crescent at the outlet. The

variation of the diffuser cross-sectional area with distance from the inlet is shown in figure 7. The three vane arrangements tested were:

- (1) A horizontal and a vertical vane in the inlet that divided the duct at the orifice plate into quadrants
- (2) A horizontal outlet vane that extended from the rear face of the orifice plate almost to the outlet.
- (3) A combination of the inlet and outlet vanes.

For some of the tests with vanes, the duct inlet was extended forward 5 inches and reduced in area from 1.10 square feet to 0.91 square foot. Figures 8 and 9 are photographs of the ducts installed on the model and disassembled. Sections through the duct inlet lips on the center line of the duct and through the duct-fuselage fillet at the inlets are given in figure 10.

For the tests in which the bypass was installed, the upper surface of the duct was lowered  $1\frac{1}{2}$  inches at the inlet and the contour of the outlet section was modified. The sections of the bypass duct were rectangular at the inlet and approximately crescent shape above the orifice plate; the area of the inlet section was approximately one-third the area above the orifice plate.

An aluminum orifice plate with holes  $3/4$ -inch in diameter (fig. 9(a)) was used to represent the heat exchangers. In order to simulate different types of heat exchanger, the pressure drop across the resistance plate was varied by plugging some of the holes in accordance with the technique of reference 4.

Measurements of total pressure and velocity distribution were made 1 foot ahead of the duct inlet and at several stations within the duct and within the boundary-layer bypass to determine the thickness of the boundary layer, the duct losses, and the air-flow quantities. Static-pressure measurements on the duct inlet lip and on the duct-fuselage fillet were made to estimate the critical speed.

Tests with propeller operating to simulate high-speed and climbing flight were made to determine the effects of slipstream. The propeller blade angle at the 0.75 radius  $\beta$ , the advance-diameter ratio  $V/nD$  and the thrust coef-

efficient  $T_0$ , which were estimated for an airplane equipped with a 1600-horsepower engine, were calculated to be  $60^\circ$ , 2.96, and 0.02, respectively, at the high-speed lift coefficient of 0.1. In the climbing condition at a lift coefficient of 0.5, the calculated values of  $\beta$ ,  $V/nD$ , and  $T_0$  were  $40^\circ$ , 1.22, and 0.11, respectively. The test airspeeds were 63 miles per hour for the high-speed condition and 45 miles per hour for the climbing condition.

The effect of the various duct installations on the drag, the maximum lift, and the pitching moment of the model was ascertained by force tests. The drag of each duct installation was determined as the difference between the drag of the model without ducts (fig. 1) and the drag of the model with the various duct arrangements installed. The drag tests were made for values of the lift coefficient from -0.2 to 0.5 at a tunnel airspeed of 100 miles per hour. The effects of the ducts on the maximum lift and the pitching moments were determined from tests at a tunnel airspeed of 63 miles per hour.

## RESULTS AND DISCUSSION

The results of the tests are discussed in six sections. The first two sections treat the factors that affect the pressures ahead of and behind the heat exchanger. Included in these sections are discussions of the air-flow characteristics, the duct configurations, and the heat-exchanger characteristics. The pressures available for cooling, the drag of the ducting system, and the duct efficiency, which are the parameters for expressing duct performance, are discussed in the third and fourth sections. The effects of the various duct installations on maximum lift, pitching moments, and critical speeds are discussed in the final sections.

### Factors Affecting Pressures ahead of Heat Exchanger

Values of the total pressure at the face of the heat exchanger that are less than the total pressure of the air stream ahead of the duct may be attributed to losses which occur ahead of the duct inlet and in the duct diffuser. For the type of fuselage duct tested in this investigation, the boundary layer on the fuselage ahead of the

duct has been shown to be the most important factor determining the losses that occur ahead of the inlet and in the diffuser (reference 1). The boundary layer tends to separate from the fuselage surface ahead of the duct inlet; this tendency is greatly increased by the adverse pressure gradient that results from deceleration of the flow as it approaches the duct inlet. The lower the inlet velocity, the greater is the adverse pressure gradient and the stronger is the tendency toward separation. As a corollary, the thicker and more depleted the boundary layer, the greater is the tendency toward separation under slight adverse pressure gradients. The primary problem in obtaining high pressure recoveries at the face of the heat exchanger therefore becomes the control of the flow to avoid boundary-layer separation or the provision of a way to prevent the boundary layer from disturbing the flow in the entire duct. Separation may usually be avoided by correct choice of the duct inlet velocity, although guide vanes or a boundary-layer bypass may be necessary for thick boundary layers (reference 5).

Air flow into duct.—As previously discussed, the air flow into a rear underslung fuselage duct is seriously affected by the fuselage boundary layer ahead of the duct. Measurements of total and static pressures (fig. 11) showed that, for the propeller-removed condition at  $\alpha = 0.2^\circ$ , the thickness of the boundary layer was  $1\frac{1}{4}$  inches at the center line of the fuselage 1 foot ahead of the inlet of the rear underslung fuselage duct and decreased approximately  $1/4$  inch for each increase of  $5^\circ$  in angle of attack.

The separation of the flow at the duct inlet that results from the boundary layer is shown by the velocity profiles of figure 12 for several values of  $V_1/V_0$ . At the low inlet-velocity ratios, the separation is accompanied by flow reversals that are indicated by the negative values of velocity adjacent to the fuselage. The existence of flow reversals was verified by tuft observations. The extent of the area of flow separation was reduced as the value of the inlet-velocity ratio was increased and, at  $V_1/V_0 = 0.61$ , the flow entered the duct inlet smoothly.

Increasing the angle of attack of the fuselage results in a similar improvement of the flow into the inlet. A narrower region of separation at angles of attack of



4.8° and 10.4° (fig. 13) results from the decrease in the boundary-layer thickness (fig. 11) and from the smaller adverse pressure gradient immediately ahead of the duct inlet.

The dependence of the flow separation at the duct inlet on the resistance of the heat exchanger was investigated by varying the pressure drop across the resistance plate  $\Delta p/q_0$  from 4.0 to 46.5. The tests were made with low inlet-velocity ratios, and flow separation and reversals occurred in all cases (fig. 14).

The elimination of separation ahead of the duct inlet not only reduces the losses before the cooling air enters the duct inlet but also enables the duct diffuser to operate at a higher efficiency. The improvement in the flow condition at the inlet which occurred when  $\alpha$  was increased from 0.2° to 10.4° (fig. 13), increased the average total pressure at the face of the orifice plate from  $0.69q_0$  to  $0.84q_0$  (fig. 15(a)). The average total pressure of  $0.69q_0$  at the orifice plate for the low angle of attack ( $\alpha = 0.2^\circ$ ) is considerably lower than would be calculated from the losses that occurred ahead of the inlet — an indication that further flow breakdown and energy dissipation occurred in the diffuser.

The effects of varying the inlet-velocity ratio on the total pressure at the face of the orifice plate are shown in figure 16 for tests with vanes installed in the diffuser and with the propeller removed. At low angle of attack, that is, at high-speed attitude, the pressure at the plate increases with the value of  $V_1/V_0$  and a maximum is indicated above the highest test condition,  $V_1/V_0 = 0.61$ . At the high angles of attack,  $\alpha = 4.8^\circ$  and  $10.4^\circ$ , the maximum pressure recovery is realized at lower values of  $V_1/V_0$  and the losses in total pressure, which occur particularly at low values of  $V_1/V_0$ , are much smaller than for angles of attack less than  $4.8^\circ$ . Beyond an inlet-velocity ratio of 0.60, the total pressures at the plate below the horizontal vane began to decrease owing to increased skin-friction losses.

The data obtained with different pressure drops across the orifice plate (figs. 16 and 17) show that the

pressure recovery is highest for the plates with the greatest resistance; the rate of increase of pressure recovery with increasing  $V_1/V_0$ , however, is about the same in all cases.

Guide vanes.— In order to decrease the losses in the diffuser that result from the flow breakdown which occurred with partly separated inlet flows, several guide-vane installations were investigated. The installation of vanes on the horizontal and the vertical center lines of the duct diffuser (fig. 5) increased the average total pressure at the face of the orifice plate  $0.09q_0$  at  $\alpha = 0.2^\circ$  and  $0.04q_0$  at  $\alpha = 10.4^\circ$  (fig. 15(b)). With this arrangement, the separated flow was confined to the half of the diffuser above the horizontal vane and the total pressure below the vane averaged about  $0.95q_0$  for all angles of attack. Above the vane, however, the total pressure at the plate varied with angle of attack from about  $0.61q_0$  at  $\alpha = 0.2^\circ$  to  $0.81q_0$  at  $\alpha = 10.4^\circ$ . The same effect is shown by the results of other tests in figure 18.

Because the static pressures behind the upper and the lower halves of the orifice plate are about the same, the high total pressure in the lower half of the plate caused a large fraction of the air to flow through this area. This phenomenon had been observed previously in tests of ducts with inlet vanes and a method of overcoming this difficulty was developed (reference 5).

Vanes were added in the duct outlet to restrict the flow of air through the lower half of the duct and to divert it through the upper half adjacent to the fuselage. The part of the flow that passed through the upper half of the duct for various outlet-vane arrangements is shown in figure 19. The flow may be evenly divided in the diffuser by correct outlet-vane location, as in test 3.

The attainment of larger flows through the upper than through the lower half of the diffuser results in increased total pressures at the face of the heat exchanger (fig. 20). For duct installations with inlet and outlet vanes, the total pressure at low angles of attack was about 13 percent higher than for the duct with-

out vanes and about 8 percent higher than for the duct with only inlet vanes. With only an outlet vane, the flow in the upper and in the lower halves of the duct could be regulated (test 7, fig. 19); however, the total pressure at the face of the radiator was only  $0.03q_0$  higher than for the duct without vanes.

When the inlet-velocity ratio is low - for example, when  $V_1/V_0$  ranges from 0.35 to 0.40 and when extensive flow separation occurs at the duct inlet - full correction of the duct flow by means of the outlet vane may require considerable detail investigation. An example of the effect of incorrect outlet-vane setting on the division of the flow in a duct of this type is shown in test 5 (fig. 19). Reducing the inlet area and increasing the inlet-velocity ratio from 0.41 to 0.60 (test 6, fig. 19) provided a much more uniform flow. A method of calculating outlet-vane locations is outlined in reference 5.

Boundary-layer bypass. - As an alternate method of eliminating the pressure losses due to boundary-layer separation, a separate duct was provided for bypassing the fuselage boundary layer around the heat exchanger (fig. 6). With this arrangement, the air entered the cooling duct inlet at free-stream total pressure and the flow reversals usually observed at low inlet velocities did not occur. Because the difficulties with the flow through the inlet were eliminated and no initial boundary layer existed on the upper surface of the duct, the duct diffuser performed efficiently and total pressures as high as  $0.97q_0$  were measured at the face of the orifice plate (figs. 21 and 22). The total-pressure recoveries were dependent both on the location of the nose of the dividing vane and on the division of flow between the bypass and the main duct (table I).

The highest pressures were obtained with the nose of the dividing vane slightly behind the duct inlet (tests 10 to 13, figs. 21 and 22 and table I), although good results were also obtained with the nose of the vane in the plane of the inlet (tests 8 and 9, fig. 21 and table I). When the vane was extended 4 inches ahead of the duct entrance, the average total pressures at the plate decreased about  $0.06q_0$  (tests 3 and 5, fig. 21 and table I) although the same flow through the boundary-layer bypass was maintained.

A value of  $Q/V_0 = 0.08$  in the secondary passage was sufficient to remove the boundary layer completely at  $V_1/V_0 = 0.3$  for the entire duct entrance (test 10, fig. 21(d) and table I). It appears likely that a smaller bypass flow may have sufficed inasmuch as  $H_2/q_0 = 0.93$  was measured in test 8 (table I) with  $Q/V_0 = 0.03$  for the bypass.

Propeller operation.— The effects of the propeller slipstream on the fuselage boundary-layer profiles and on the inlet velocity distributions are shown in figures 11(b), 23, and 24. At  $T_0 = 0.2$ , propeller operation had a negligible effect both on the boundary-layer characteristics (fig. 11(b)) and on the inlet velocity distribution (fig. 23). Operation of the propeller in the climbing condition at  $T_0 = 0.11$ , however, increased the thickness of the boundary layer about  $3/8$  inch (fig. 11(b)).

As a result of the increased total pressure in the slipstream, the average total pressures at the face of the orifice plate increased both in the high-speed and in the climbing conditions, as shown in figure 25 for the arrangement with vanes in the diffuser. In the climbing condition and with flaps installed on the duct outlet, the increases in total pressure due to propeller operation were about  $0.30q_0$  and average total pressures at the orifice plate of about  $1.15q_0$  were measured at inlet-velocity ratios ranging from 0.60 to 0.90. Below these values of  $V_1/V_0$ , the pressures at the plate were lower because of inlet losses. Average total pressures as high as  $1.30q_0$  were measured at the section of the plate below the horizontal guide vane (figs. 26(c) and 26(d)). Average total pressures of this magnitude may be obtained over the entire radiator by the installation of a boundary-layer bypass.

In simulated climb, the propeller slipstream reduced the symmetry of the pressure patterns at the face of the orifice plate above the horizontal vane (figs. 26(c) and 26(d)). Slightly lower pressures were measured on the right-hand than on the left-hand side of the plate owing to asymmetrical slipstream effects.

### Factors Affecting Pressures behind Heat Exchanger

The total pressure at the duct outlet is dependent upon the total-pressure losses that occur ahead of the duct inlet, the losses that occur within the diffuser, and the pressure drop that results from the air flow through the heat exchanger. The outlet static pressure is a function of the external static pressure near the outlet and of the shape of the outlet section of the duct. The external static pressure in the region of the outlet opening is determined by outlet-flap deflection, angle of attack of the model, and propeller-operating conditions.

The shape of the outlet section of the duct affects the outlet static pressure through its influence on the contraction of the exhausting air stream and through its effect on the angle at which the air is discharged into the main stream. If the outlet section is too short and the angle of convergence too high, the jet of air leaving the duct continues to contract in cross section and to increase in velocity for some distance downstream and the static pressure does not reach a value equal to that of the free stream until some distance behind the outlet opening. If the flow is discharged at an angle to the external stream, an effective thickening of the body occurs behind the outlet opening. The magnitude of this thickening is dependent upon the angle-of-flow discharge with reference to the external stream and upon the total pressure at the outlet. As a result of this effective thickening of the body, the velocity of the external stream over this part of the body increases and the external static pressure correspondingly decreases.

Outlet configuration.— The outlet openings tested (fig. 5) were representative of present design practice. The larger exits B and C were formed from exit A by progressively cutting back the lower surface of the duct at the outlet. Because no modifications were made in the contours of the upper surface of the outlet section, this cutting back of the lower surface caused the flow to discharge from outlet C at a greater angle relative to the external stream than from outlets A or B.

The results of the tests show that an approximately linear relationship exists between the total and the static pressure at the outlet (figs. 27 to 29). When no

outlet flaps were installed, the static pressures at the outlet opening were always positive and increased linearly with the outlet total pressures. The rate of change of outlet static pressure with outlet total pressure was greatest for the largest exit 0.

A comparison of the curves of figures 27 to 29 shows that the vanes and the boundary-layer bypass also affect the outlet static pressures because of their influence on the characteristics of the flow in the outlet section of the duct. No rule for the prediction of any of these effects could be established, however, because of the many variables involved.

An example of the effect of the flow through the boundary-layer bypass on the velocity distribution at the duct outlet is shown in figure 30. At the top of the duct exit, there is a region of low velocity that resulted from the bypass flow which is depleted in total pressure. As the flow through the bypass is decreased (fig. 30) or as the angle of attack of the model is increased (fig. 31), this area of low velocity becomes smaller and finally disappears. Figure 32, which shows typical velocity distributions observed in most cases, is included for comparison. The air quantities computed from the outlet velocity distributions are given in figures 33 and 34 and in table I.

With the installation of outlet flaps set at  $45^\circ$ , the static pressures at the outlet openings were decreased to about  $-0.20q_0$  for outlet B and to  $-0.30q_0$  for outlet 0 and the dependency of the static pressure upon the outlet total pressure was practically eliminated (fig. 27). In figure 33, it is shown that the installation of a flap on outlet B increased the flow through

the duct by  $0.20 \frac{Q}{V_0}$  at  $\Delta p/q_2 = 10.9$ , by  $0.16 \frac{Q}{V_0}$  at  $\Delta p/q_2 = 19.6$ , but by only  $0.08 \frac{Q}{V_0}$  at  $\Delta p/q_2 = 46.5$ . A sample of the velocity distribution at the duct outlet with flaps installed is given in figure 35.

Propeller operation.— Operation of the propeller in the high-speed condition had little effect on the average outlet static pressure (fig. 27) and on the air-flow quantity (fig. 33). In the climbing condition, with flaps

installed on outlet B, propeller operation decreased the average outlet static pressure by  $0.10q_0$  (fig. 27) and increased the flow through the duct by  $Q/V_0 = 0.09$  (approx.) at pressure-drop coefficients of 10.9 and 19.6. Typical velocity distributions obtained at outlet B with the propeller operating are shown for the high-speed condition in figure 36 and for the climbing condition in figure 37.

### Pressures Available for Cooling

The pressure available for cooling is defined as the difference between the total pressure at the face of the heat exchanger  $H_2$  and the static pressure at the duct outlet  $p_3$  and may be expressed nondimensionally as

$$\frac{H_2 - p_3}{q_0} . \quad \text{The effect of changes in duct configuration and}$$

air-flow characteristics on these quantities have been discussed in previous sections and the resulting cooling pressures are presented in figures 38 and 39, and in table I.

Increases in pressure available for cooling were obtained by increasing the pressure drop across the orifice plate either by varying the resistance of the plate or by varying the air flow through the duct (fig. 38). At a pressure-drop coefficient 10.9, average cooling pressures of  $1.01q_0$  at an angle of attack of  $0.2^\circ$  and  $1.11q_0$  at an angle of attack of  $10.4^\circ$  were measured for the duct with vanes in the diffuser and with flaps installed on outlet B. The pressures available for cooling increased in all instances with the angle of attack of the model.

In figure 39 is shown the increase in average pressure available for cooling, which resulted from the higher total pressure obtained at the face of the orifice plate by the installation of guide vanes in the diffuser. The addition of an outlet vane to the duct with outlet B had no effect (fig. 39) because the small increase in total pressure ahead of the plate (fig. 20) was compensated for by a corresponding increase in the outlet static pressure. With the outlet area reduced from 0.91 to 0.50 square foot (outlet B to outlet A), however, the addition of an outlet vane increased the cooling pressures by about  $0.05q_0$  (figs. 38 and 39).

The highest pressures available for cooling were obtained for the duct with the boundary-layer bypass. At inlet-velocity ratios of about 0.33, cooling pressures as high as  $0.68q_0$  were measured for some of the best bypass arrangements (table I) as compared with the highest value of  $0.59q_0$  obtained for the high-speed condition by the use of guide vanes (fig. 39). At an inlet-velocity ratio of about 0.50, the pressures available for cooling decreased slightly and were approximately equal to those measured for the arrangement with guide vanes. When the total pressure at the face of the orifice plate decreased, the cooling pressure also decreased and, for the case in which there was no flow through the bypass and the total pressure at the orifice plate was  $0.71q_0$  (test 2, table I), the measured cooling pressure was only  $0.48q_0$ .

Operating the propeller increased the pressures available for cooling about  $0.02q_0$  to  $0.05q_0$  in the high-speed condition and about  $0.40q_0$  in the climbing condition with outlet flaps installed (fig. 38). For the arrangement with vanes in the diffuser, maximum pressures available for cooling that ranged from  $1.42q_0$  to  $1.51q_0$  were measured in the climbing condition and were indicative of very good outlet-flap effectiveness.

### Drag and Duct Efficiency

Total drag due to duct installation.— A summary of the total drag of the various installations investigated is presented in figure 40 and in tables I and II. The increment of drag due to the duct system  $\Delta C_D$  is the difference between the drag of the model without the duct and the drag of the model with the various duct arrangements installed. The drag due to the internal and the external flow are included in this increment.

At  $\Delta p/q_2 = 10.9$ , at  $Q/V_0 = 0.51$ , and at  $C_L = 0.1$ , the increment of total duct drag without vanes or boundary-layer bypass was 0.0020. This value was not materially changed by the installation of inlet vanes (table II). With both the inlet and the outlet vanes, the drag increment was 0.0016 at  $Q/V_0 = 0.54$  and 0.0012 at  $Q/V_0 = 0.37$ . These values were the lowest total-drag coefficients measured for any of the duct installations. With vanes in the diffuser, increasing the air-flow quantity or the pressure-drop coefficient increased the increment of total



These values were the lowest total-drag coefficients measured for any of the duct installations. With vanes in the diffuser, increasing the air-flow quantity or the pressure-drop coefficient increased the increment of total drag (fig. 40). For the range of values of  $\Delta p/q_p$  and  $Q/V_o$

tested, the increment of total-drag coefficient varied from 0.0018 at  $\Delta p/q_p = 10.9$  and  $Q/V_o = 0.30$  to 0.0024 at  $\Delta p/q_p = 19.6$  and  $Q/V_o = 0.49$ . The drag of the installation with the boundary-layer bypass generally exceeded that of the optimum vane arrangement by from 17 to 33 percent at  $Q/V_o = 0.35$  (approx.) and by from 25 to 56 percent at  $Q/V_o = 0.55$  (tables I and II).

Duct internal-drag coefficient.— In addition to the total drag, figure 40 and tables I and II show the increment of internal-drag coefficient calculated from the expression

$$\Delta C_{D_i} = \frac{2Q}{SV_o} \left( \frac{\sqrt{H_1} - \sqrt{H_3}}{\sqrt{H_o}} \right)$$

which was derived from the momentum loss of an incompressible fluid flowing through the system. At  $\Delta p/q_p = 10.9$ ,

at  $Q/V_o = 0.51$ , and at  $C_L = 0.1$ , the internal-drag coefficient was 0.0009 for the duct without vanes or bypass (table II). The addition of vanes in the diffuser alone increased the internal-drag coefficient to 0.0011, but the addition of inlet and outlet vanes together or the addition of an outlet vane alone decreased the coefficient to about 0.0008, although the flow was also decreased by the addition of the outlet vane alone. When the flow for the fully vaned installation was decreased to  $Q/V_o = 0.37$ , the increment of internal-drag coefficient was reduced to 0.0002. An increase in the air-flow quantity or in the pressure-drop coefficient rapidly increased the internal-drag coefficient (fig. 40).

Duct external-drag coefficient.— The duct external-drag coefficient, which is equal to the difference between the total- and the internal-drag coefficients, was 0.0011 for the installation without vanes and varied between 0.0008 and 0.0010 for the duct with the various vane arrangements at  $\Delta p/q_p = 10.9$  and at  $Q/V_o = 0.50$  (approx.) (table II). With vanes in the diffuser, the external-drag coefficient varied from 0.0019 with the

inlet and the outlet sealed to 0.0005 at  $\Delta p/q_2 = 19.6$  and 10.9 and  $Q/V_0 = 0.49$  and 0.59, respectively, (fig. 40). The high external drag measured with small air quantities is attributed to flow separation at the duct-fuselage fillet. The addition of a bypass to the installation without vanes resulted in external-drag coefficients that were 0.0004 to 0.0010 higher than those obtained for the vaned installations at the same values of  $\Delta p/q_2$  and  $Q/V_0$  (tables I and II). Tufts indicated that the flow at the duct fuselage fillet with the bypass installed generally was not smooth.

Duct efficiency.— The duct efficiency is defined as the ratio of useful power expended in forcing air through the orifice plate to the total power required to overcome the drag due to the duct; that is,

$$\eta = \frac{Q\Delta p}{\Delta p V_0}$$

In accordance with this definition, only the air flowing through the resistance plate was considered to do any useful work for the tests with the boundary-layer bypass installed.

For  $\Delta p/q_2 = 10.9$  and  $Q/V_0 = 0.51$ , the duct efficiency of the installation without vanes or bypass was 0.42 (table II). Owing to the poor flow distribution between the upper and lower sections of the duct, the use of inlet vanes alone decreased the duct efficiency to 0.33. The use of both inlet and outlet vanes, however, increased the efficiency to about 0.65 with both the original and the modified inlets. These efficiencies were the highest measured for any of the duct arrangements. The relatively low duct efficiency of 0.28 obtained for the fully vaned duct at  $V_1/V_0 = 0.34$  was the result of high external drag (table II), which usually occurs with low air flows (fig. 40).

For the duct with the vanes in the diffuser, the duct efficiency increased rapidly as either the air-flow quantity or the pressure-drop coefficient was increased; the lowest duct efficiency was about 0.10 for  $\Delta p/q_2 = 10.9$  and  $Q/V_0 = 0.30$  and the highest were 0.56 and 0.57 at  $\Delta p/q_2 = 19.6$  and 10.9 and  $Q/V_0 = 0.49$  and

0.59, respectively, (fig. 41). The efficiency of the duct with the boundary-layer bypass ranged from 0.06 to 0.09 at  $Q/V_0 = 0.35$  (approx.) and from 0.09 to 0.13 at  $Q/V_0 = 0.55$  (table I). It is believed that higher efficiencies can be attained while high pressure recoveries are still maintained by simultaneously decreasing the inlet area of the boundary-layer bypass and the air-flow quantity instead of by restricting the flow through the bypass alone.

#### Maximum Lift and Pitching Moments

The installation of the duct system had no effect on the maximum lift but increased the negative slope of the pitching-moment curve. An analysis of the results of figure 42 indicates that the increments of pitching-moment coefficient due to the duct are greater than can be estimated from the drag of the duct alone.

#### Critical Speed

By the method of reference 6, the critical speeds of the duct inlet were estimated from pressure-distribution measurements on the surface of the inlet lip and the duct-fuselage fillet at a tunnel airspeed of 63 miles per hour. The maximum negative pressures were extrapolated to higher Mach numbers as in figure 43, and the critical speeds were found from the intersection of the extrapolated pressure curves with the curve of Mach number for the local speed of sound.

At the high-speed angle of attack of  $0.2^\circ$ , the highest critical Mach numbers calculated for the duct inlet lip and for the duct-fuselage fillet were 0.55 and 0.49, respectively; these values correspond to sea-level critical speeds of 420 and 374 miles per hour. These critical speeds were undesirably low and indicated that modifications in the shape of the inlet lip and the fillet were desirable. As shown in reference 1, these modifications should include increases in the camber and the thickness of the inlet lip and the duct-fuselage fillet to provide a more uniform pressure distribution.

The critical speeds of the duct inlet decreased with the inlet-velocity ratio. The reductions in critical speed are indicated in figures 44 and 45 by the increased

maximum negative pressures at the low values of  $V_1/V_0$ .

For the duct-fuselage fillet, the peak negative pressure increased from  $-1.78q_0$  to  $-2.34q_0$  for a variation in the inlet-velocity ratio from 0.53 to 0.37; this result corresponds to a decrease in critical Mach number from 0.49 to 0.44.

The pressure distributions varied with changes in angle of attack of the model (figs. 46 to 48); reductions in peak negative pressures of  $0.55q_0$  to  $0.60q_0$  on the inlet lip and of  $0.35q_0$  to  $0.80q_0$  on the duct-fuselage fillet were measured when the angle of attack was increased from  $0.2^\circ$  to  $10.4^\circ$ . These reductions in peak negative pressures with increases in angle of attack are attributed principally to the fact that the duct inlet is located on the lower surface of the wing. As the angle of attack of the airplane is increased, the static pressure beneath the wing is increased and, for the same mass flow of air through the duct inlet, the air enters the duct at a higher velocity relative to the flow in the region of the duct inlet. The angles of attack of the inlet lip and of the duct-fuselage fillet, which are determined by the inlet-velocity ratio (reference 1), are decreased and the induced velocities over the surfaces are reduced. At an inlet-velocity ratio of 0.40, an increase in the angle of attack from  $0.2^\circ$  to  $10.4^\circ$  increased the sea-level critical speed of the duct-fuselage fillet from 350 to 374 miles per hour and the critical speed of the inlet lip from 412 to 496 miles per hour.

Operation of the propeller in the high-speed condition had little effect on the inlet-lip pressures but increased the negative pressures at the fillet about  $0.40q_0$  at an inlet velocity ratio of 0.26 and  $0.30q_0$  at an inlet-velocity ratio of 0.44 (fig. 49). As in the propeller-removed tests, separation was present at the duct-fuselage fillet at low inlet-velocity ratios (fig. 50).

#### SUMMARY OF RESULTS

The results of the general investigation of rear underslung fuselage ducts reported herein are summarized as follows:

1. The ratio of the duct inlet velocity to the stream velocity was the most important parameter affecting the performance of rear underslung fuselage ducts. An inlet-velocity ratio of about 0.6 was found to be a good design value for such an installation with or without vanes and a value of 0.35 was permissible for the duct with the boundary-layer bypass.

2. Because of the thickness of the boundary layer at the inlet of rear underslung fuselage ducts, serious losses in total pressure ahead of the heat exchanger occurred when no vanes nor boundary-layer bypass was used.

3. Lowest drags and highest duct efficiencies in combination with good pressure recoveries ahead of the heat exchanger were measured for the rear underslung fuselage duct with both inlet and outlet vanes. The use of either inlet or outlet vanes alone did not greatly improve the over-all duct performance.

4. Best total pressure recoveries, but generally higher drag and lower duct efficiencies, were measured for the duct arrangement with the boundary-layer bypass.

5. Propeller operation increased the total pressures at the face of the heat exchanger. In the high-speed condition (at a thrust coefficient  $T_c$  of 0.02), the increases in total pressure ahead of the heat exchanger were small; whereas, in the climbing condition (at  $T_c = 0.11$ ), average increases of about  $0.30q_0$  (where  $q_0$  is the free-stream dynamic pressure) were measured.

6. The static pressures at the duct outlet were positive for the installations without outlet flaps. The addition of outlet flaps reduced the static pressures to as low as  $-0.30q_0$  with the propeller removed and to as low as  $-0.40q_0$  with the propeller operating in the climbing condition.

7. The positive values of the outlet static pressures were reduced by discharging the cooling air parallel to the external stream and by decreasing the angle of convergence of the outlet section of the duct.

8. Owing to the insufficient amount of camber and thickness at the duct-fuselage fillet and at the inlet

lip, the critical speed of the duct installation was undesirably low. The value of the critical speed increased with increases in the inlet-velocity ratio and in the angle of attack of the model.

Langley Memorial Aeronautical Laboratory,  
National Advisory Committee for Aeronautics,  
Langley Field, Va.

#### REFERENCES

1. Nelson, W. J., and Czarnecki, K. R.: Wind-Tunnel Investigation of Carburetor-Air Inlets. NACA ARR, Feb. 1942.
2. Nelson, W. J., and Czarnecki, K. R.: Wind-Tunnel Investigation of Wing Ducts on a Single-Engine Pursuit Airplane. NACA ARR No. 3J13, 1943.
3. DeFrance, Smith J.: The N.A.C.A. Full-Scale Wind Tunnel. NACA Rep. No. 459, 1933.
4. Czarnecki, K. R.: Pressure-Drop Characteristics of Orifice Plates Used to Simulate Radiators. NACA ARR, March 1942.
5. Katzoff, S.: The Design of Cooling Ducts with Special Reference to the Boundary Layer at the Inlet. NACA ACR, Dec. 1940.
6. von Kármán, Th.: Compressibility Effects in Aerodynamics. Jour. Aero. Sci., vol. 8, no. 9, July 1941, pp. 337-356.

TABLE I  
SUMMARY OF DATA FOR DUCT  
INSTALLATION WITH BOUNDARY-LAYER BYPASS  
[Nominal pressure-drop coefficient = 10.9]

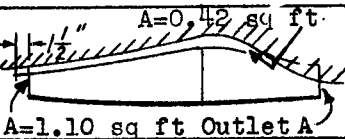
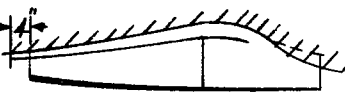
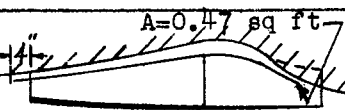
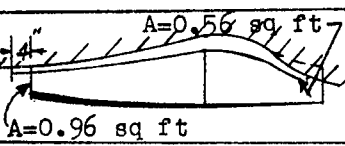
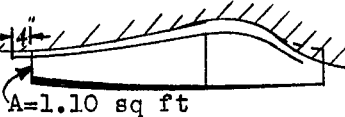
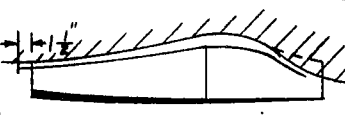
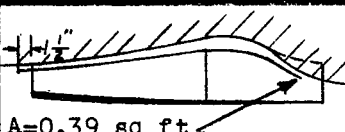
Test	Configuration	$\alpha$	$Q/V_0$		$V_1/V_0$ Entire set-up	$H_2/q_0$	$H_2-P_3/q_0$	Increment of drag coefficient at $C_L = 0.1$			$\eta$
			Entire set-up	Cooling duct				$\Delta C_D$	$\Delta C_{D1}$	$\Delta C_{D2}$	
1		0.2	--	--	--	0.71	--	--	--	--	--
		4.8	--	--	--	.79	--	--	--	--	--
2		0.2	0.27	0.27	0.25	.71	0.48	--	0.0006	--	--
		4.8	.30	.30	.27	.77	.53	--	--	--	--
3		0.2	0.35	0.25	0.32	0.88	0.62	--	0.0002	--	--
		4.8	.36	.23	.33	.89	.63	--	--	--	--
4		0.2	0.34	0.23	0.35	0.89	0.62	--	0.0002	--	--
		4.8	.36	.23	.33	.93	.65	0.0016	0.0001	0.0015	0.06
5		10.4	.36	.22	.33	.94	.65	--	--	--	--
		4.8	.37	.25	.34	.97	.68	0.0014	0.0002	0.0012	0.09
6		0.2	0.35	0.27	0.32	0.95	0.68	--	--	--	--
		4.8	.35	.29	.34	.92	.69	--	--	--	--
7		0.2	0.34	0.29	0.33	0.87	0.59	--	0.0002	--	--
		4.8	.35	.29	.34	.92	.69	--	--	--	--

TABLE I (Continued)

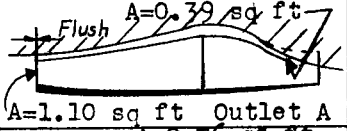
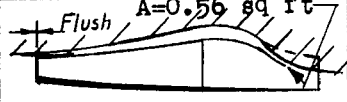
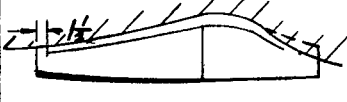

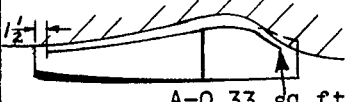
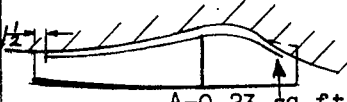

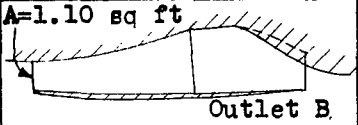
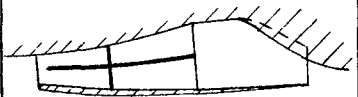
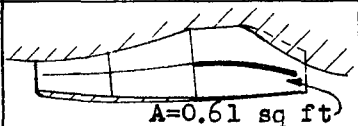
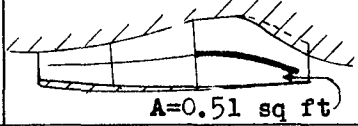
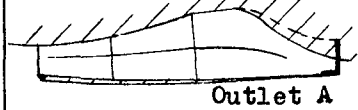
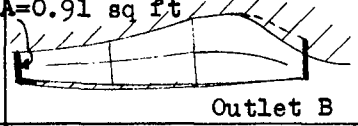
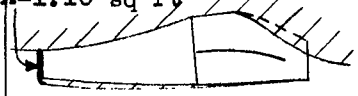
Test	Configuration	$\alpha$	$Q/V_0$		$V_1/V_0$ Entire set-up	$H_2/q_0$	$H_2-p_3/q_0$	Increment of drag coefficient at $C_L = 0.1$			$\eta$
			Entire set-up	Cooling duct				$\Delta C_D$	$\Delta C_{D_1}$	$\Delta C_{D_e}$	
8		0.2	0.35	0.32	0.33	0.93	0.63	--	0.0002	--	--
		4.8	.36	.30	.34	.95	.66	--	--	--	--
9		0.2	0.36	0.27	0.32	0.95	0.65	--	0.0001	--	--
		4.8	.37	.26	.33	.95	.69	--	--	--	--
10		0.2	0.36	0.28	0.31	0.96	0.68	0.0016	0.0001	0.0015	0.10
		4.8	.37	.25	.32	.97	.69	--	--	--	--
11		0.2	0.55	0.32	0.50	0.97	0.59	0.0020	0.0008	0.0012	--
		4.8	.56	.30	.51	.96	.63	--	--	--	--
12		0.2	0.56	0.38	0.51	0.97	0.64	0.0025	0.0007	0.0018	0.13
		4.8	.55	.35	.50	.97	.63	--	--	--	--
13		0.2	--	--	--	0.94	--	0.0023	--	--	--
		4.8	--	--	--	.95	--	--	--	--	--
14		0.2	0.52	0.37	0.47	0.89	0.58	0.0022	0.0009	0.0013	0.13
		4.8	.51	.32	.46	.87	.56	--	--	--	--



TABLE II  
SUMMARY OF DRAG DATA  
FOR VARIOUS GUIDE-VANE ARRANGEMENTS  
[Nominal pressure-drop coefficient = 10.9]

Test	Configuration	Air-flow parameter, $Q/V_0$	Inlet- velocity ratio, $V_1/V_0$	Increment of drag coefficient, $C_L = 0.1$			Duct efficiency, $\eta$
				$\Delta C_D$	$\Delta C_{D1}$	$\Delta C_{D0}$	
1	 A=1.10 sq ft Outlet B	0.51	0.46	0.0020	0.0009	0.0011	0.42
2	 A=0.61 sq ft	.47	.42	.0021	.0011	.0010	.33
3	 A=0.61 sq ft	.53	.48	--	.0007	--	--
4	 A=0.51 sq ft	.54	.49	.0016	.0008	.0008	.65
5	 Outlet A	.37	.34	.0012	.0002	.0010	.28
6	 A=0.91 sq ft Outlet B	.54	.60	.0016	.0007	.0009	.66
7	 A=1.10 sq ft	.49	.45	--	.0008	--	--

NACA

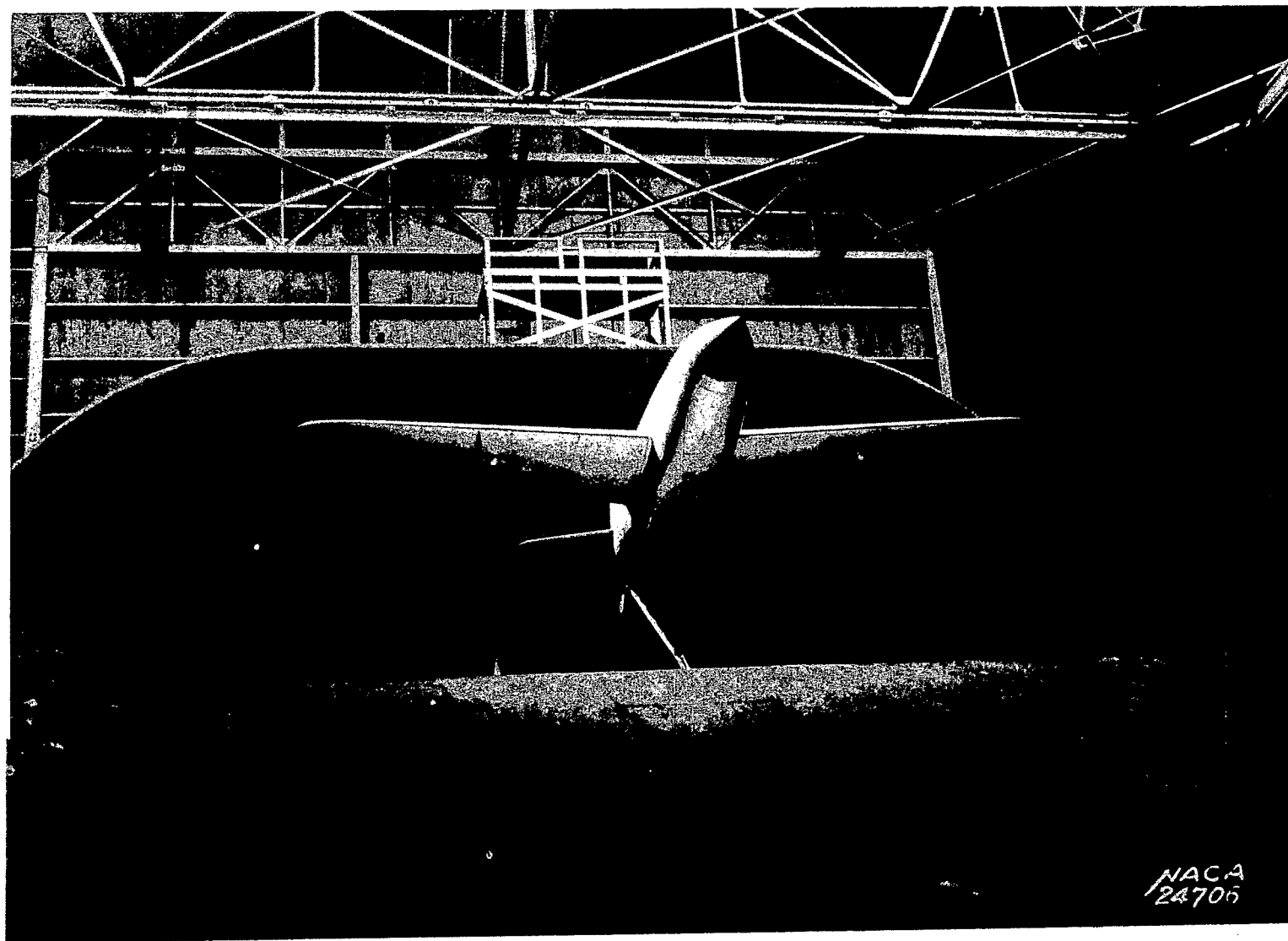


Fig. 1

Figure 1.- Model in basic condition as mounted in the NACA full-scale tunnel.

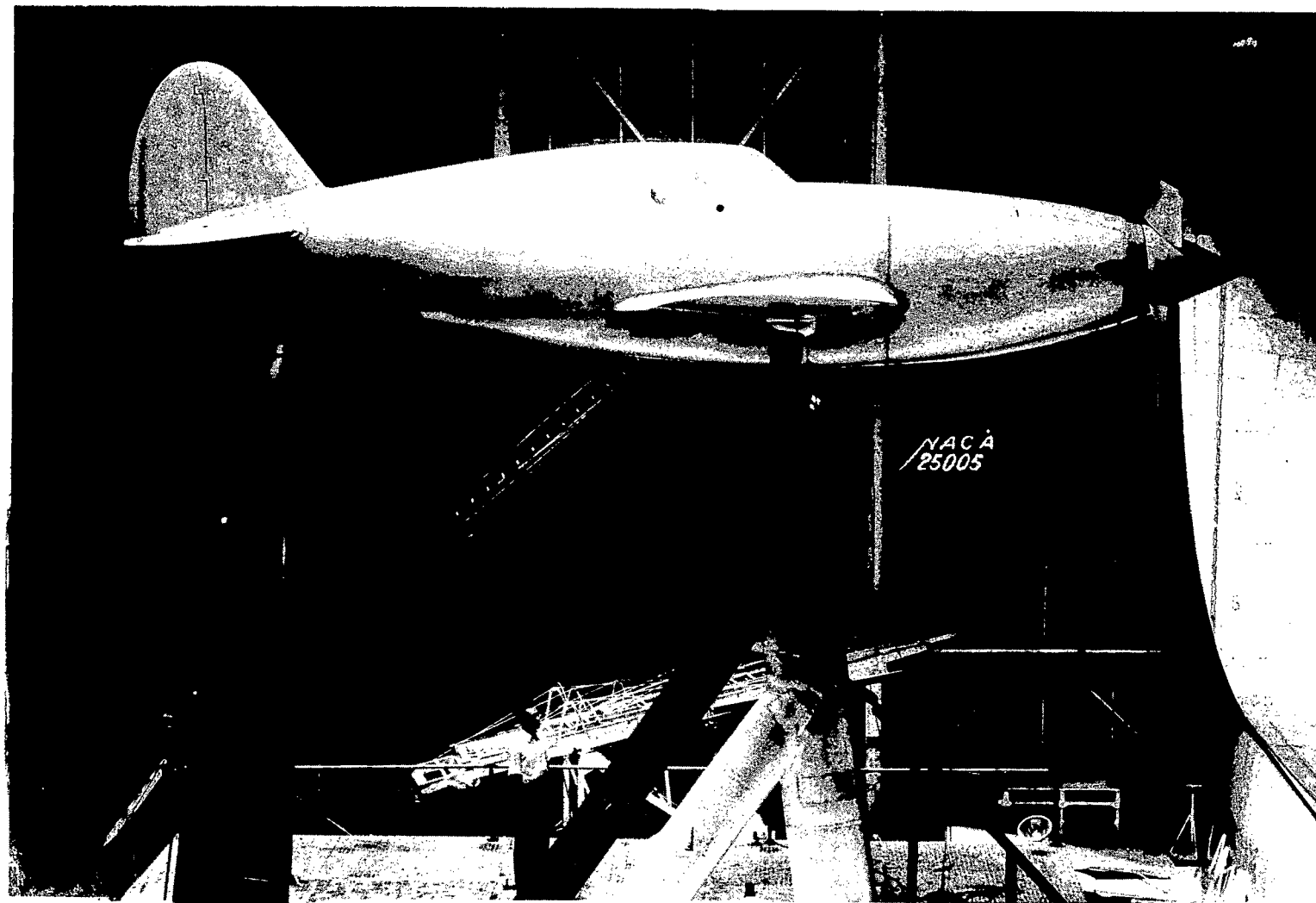


Figure 2.- Side view of model as mounted in the NACA full-scale tunnel.

NACA

Fig. 2

NACA

Fig. 3

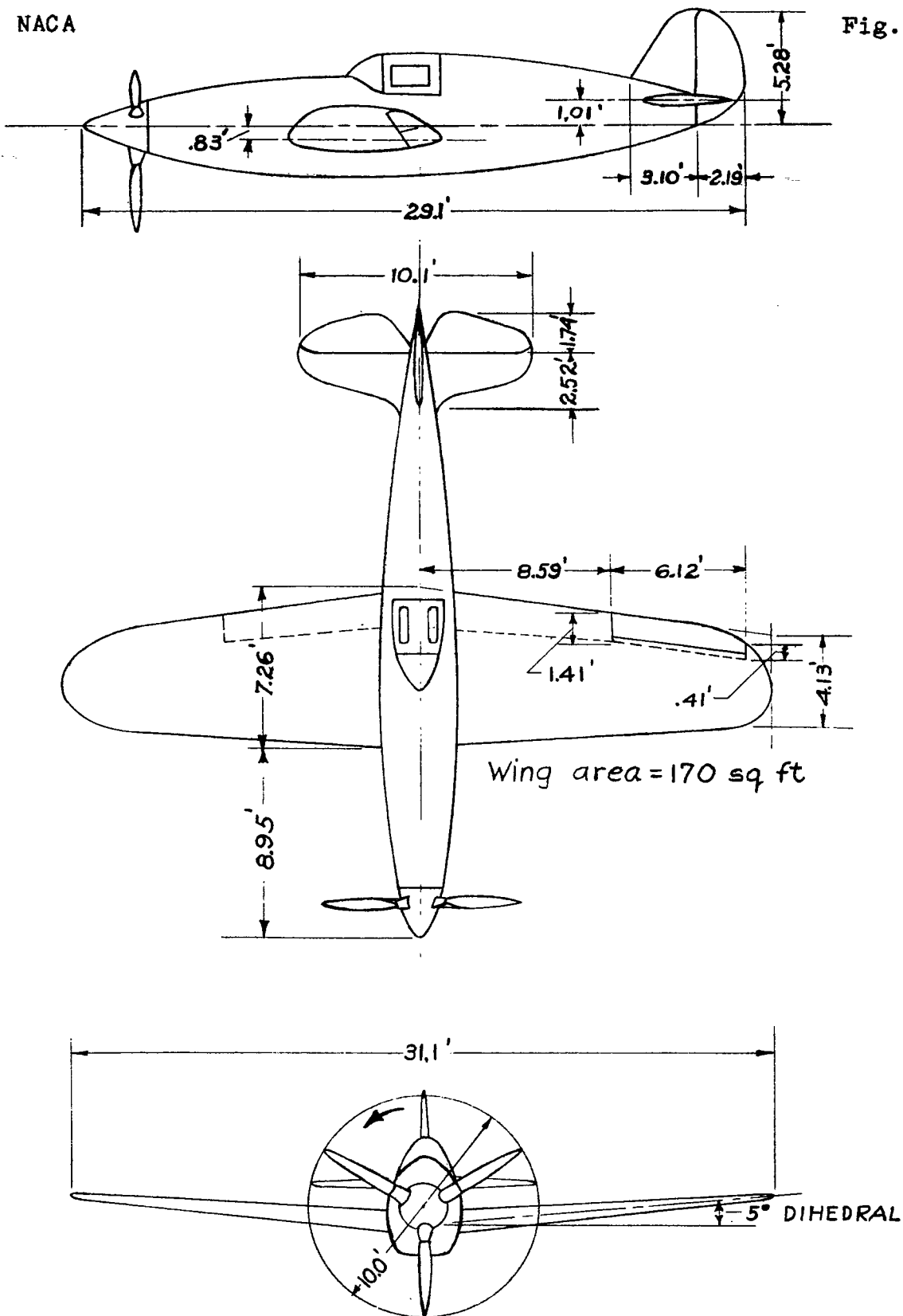


Figure 3.- General arrangement of model.

Section A

x	y <sub>U</sub>	y <sub>L</sub>
0	0	0
0.116	0.280	0.250
.232	.390	.315
.463	.535	.405
.694	.645	.465
.925	.745	.510
1.487	.890	.565
1.850	.990	.595
2.315	1.065	.600
2.775	1.110	.595
3.700	1.135	.575
4.625	1.095	.540
5.560	1.000	.465
6.475	.840	.385
7.410	.625	.280
8.330	.360	.165
9.250	0	0
R <sub>L.E.</sub> = 0.335		
R <sub>T.E.</sub> = 0.058		

Section B

x	y <sub>U</sub> =y <sub>L</sub>
0	0
0.194	0.430
.388	.625
.775	.930
1.163	1.160
1.550	1.340
2.330	1.635
3.100	1.845
3.880	2.000
4.650	2.110
6.200	2.190
7.750	2.100
9.300	1.840
10.850	1.465
12.400	1.025
13.950	.535
15.500	0
R <sub>L.E.</sub> = 0.520	
R <sub>T.E.</sub> = 0	

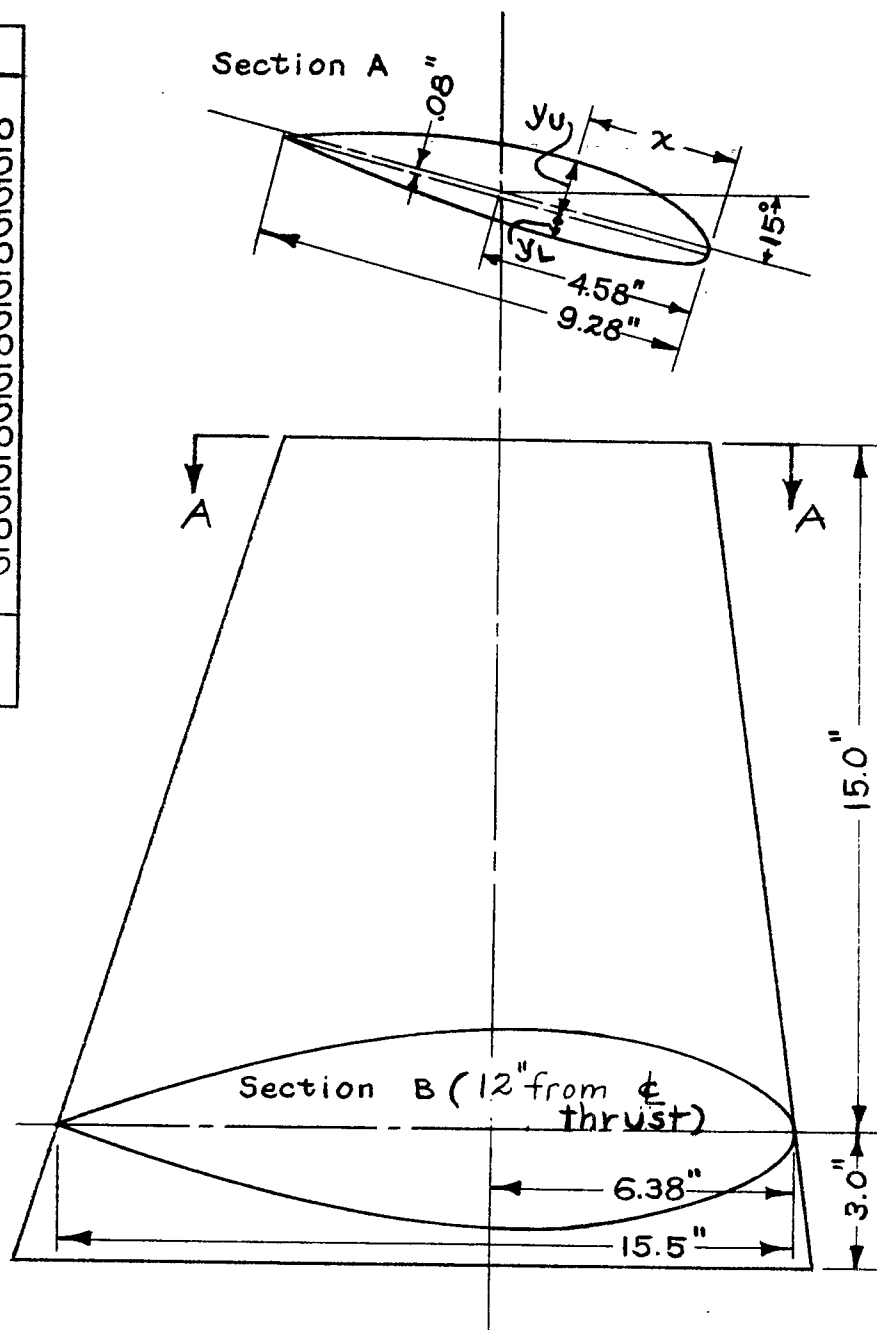
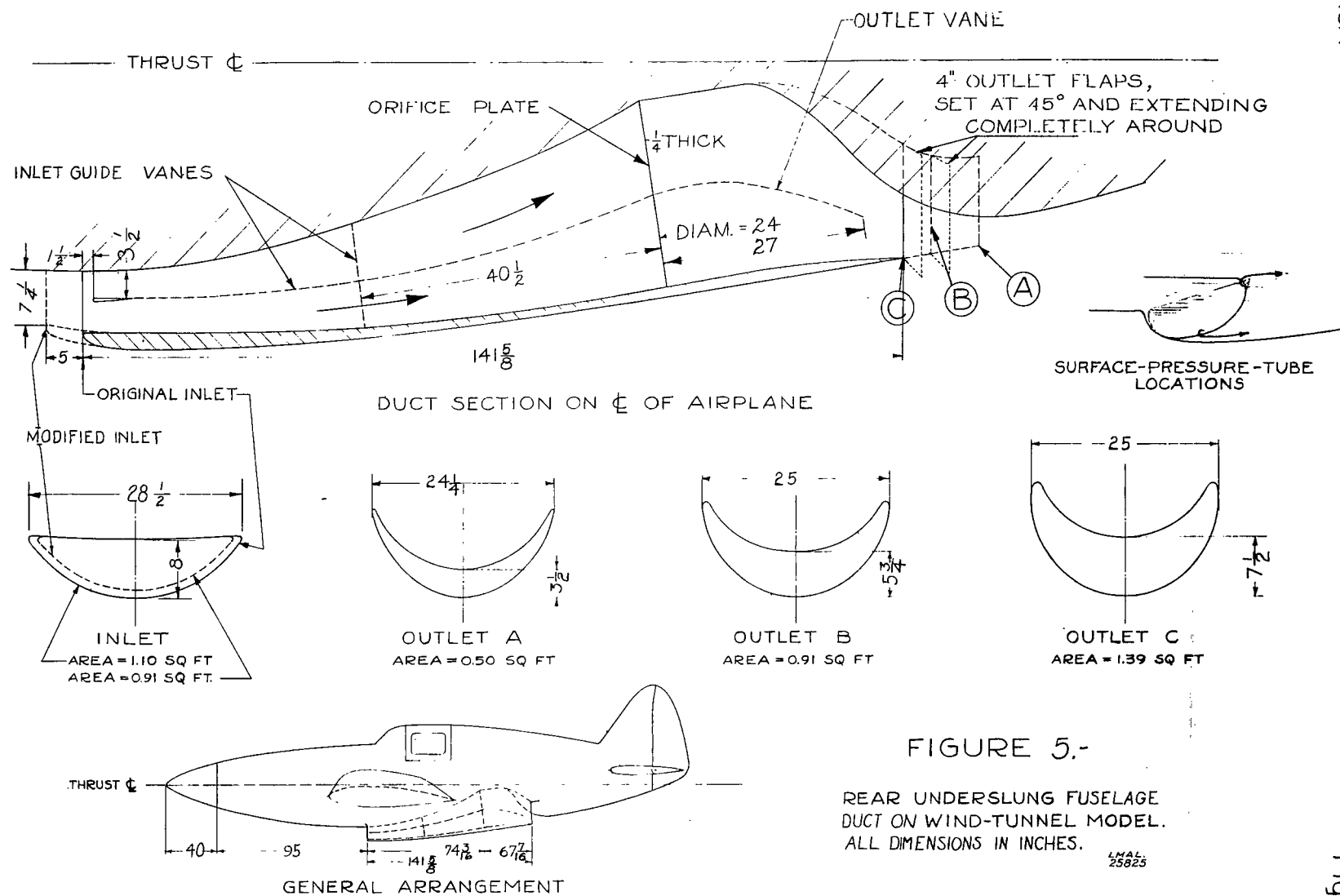


Figure 4. - Dimensions of propeller cuff.



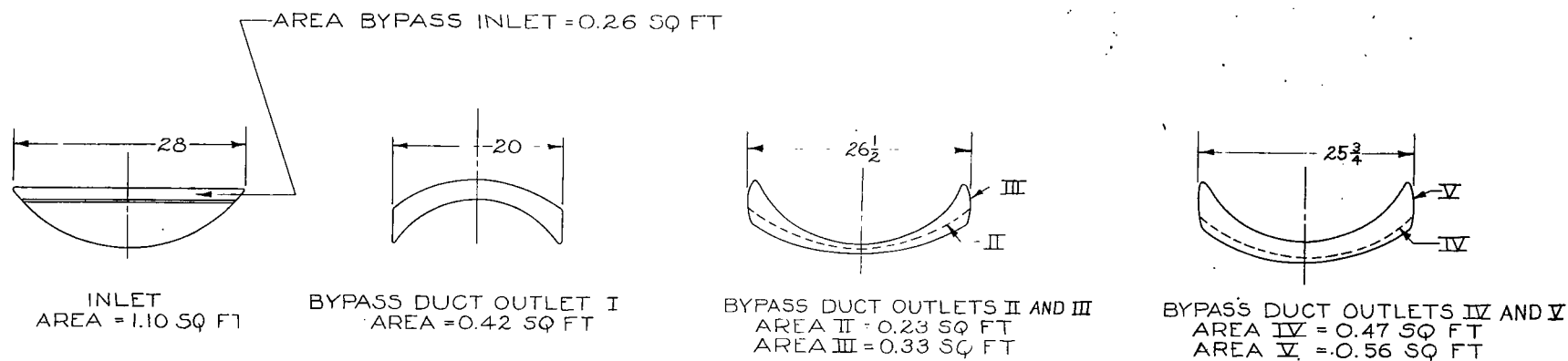
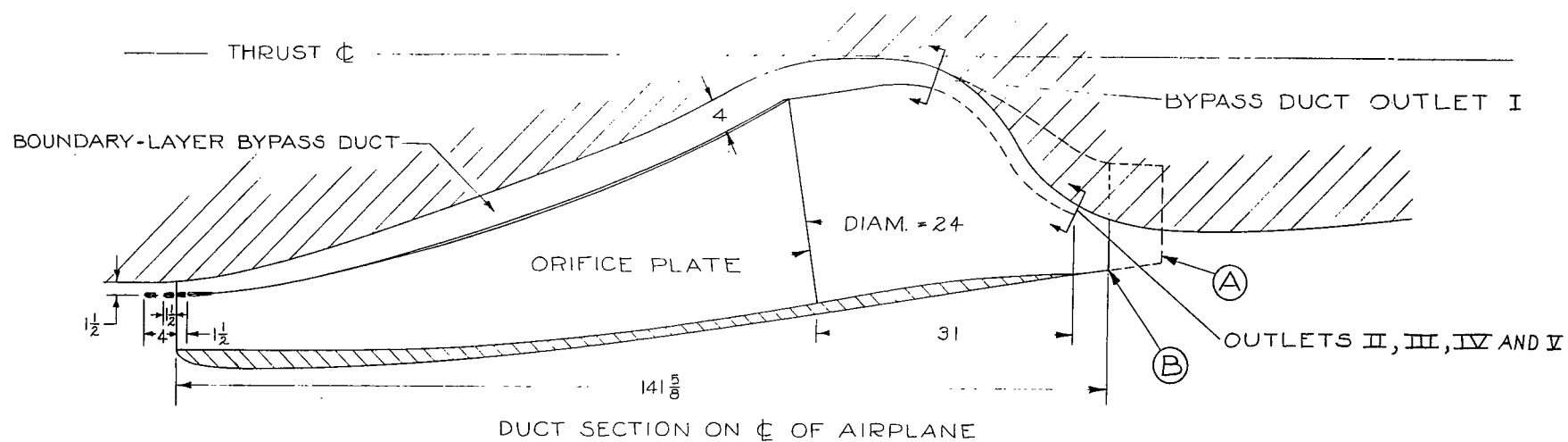


FIGURE 6.- REAR UNDERSLUNG INSTALLATION WITH BOUNDARY-LAYER BYPASS. ALL DIMENSIONS IN INCHES.

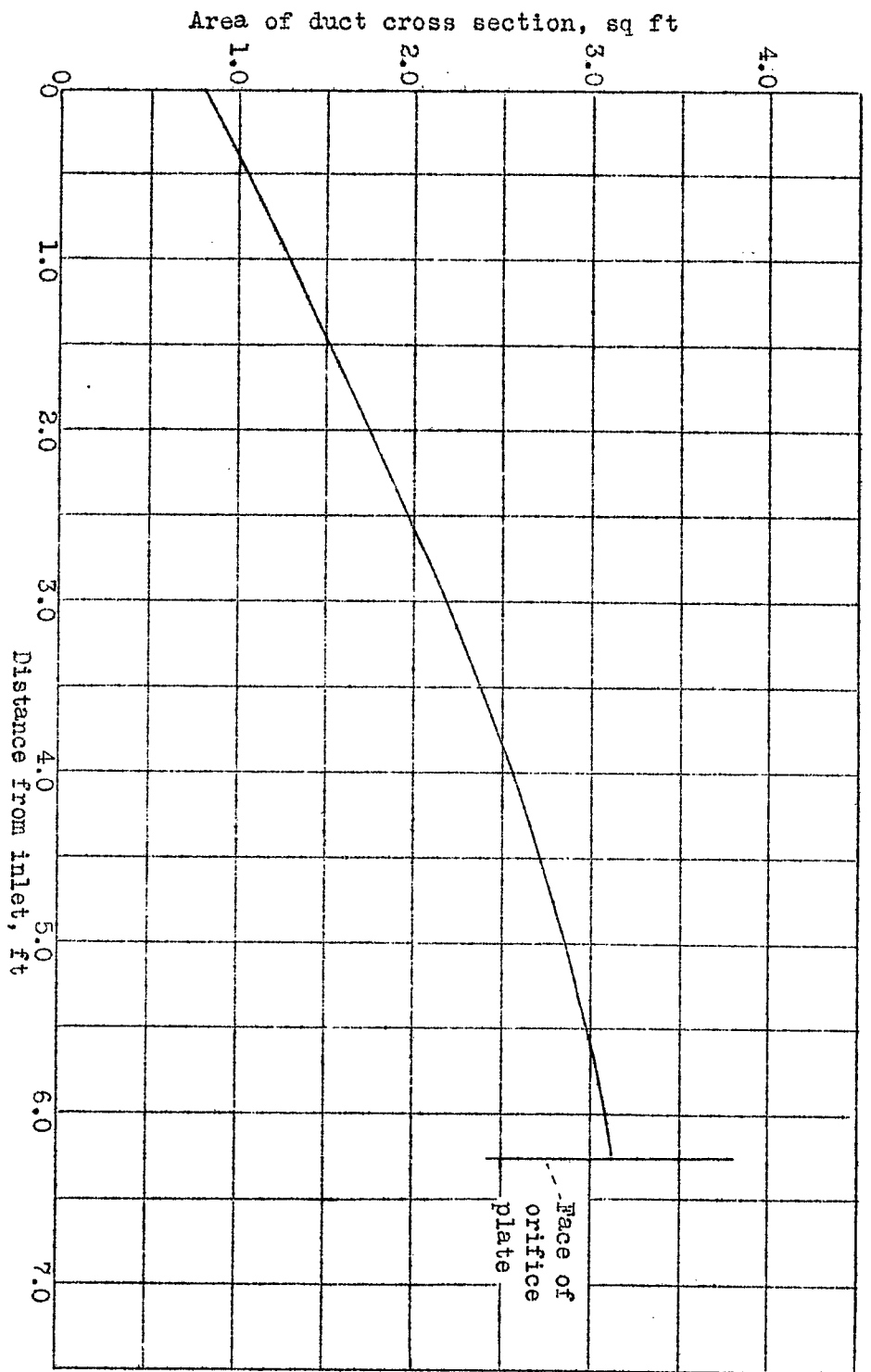
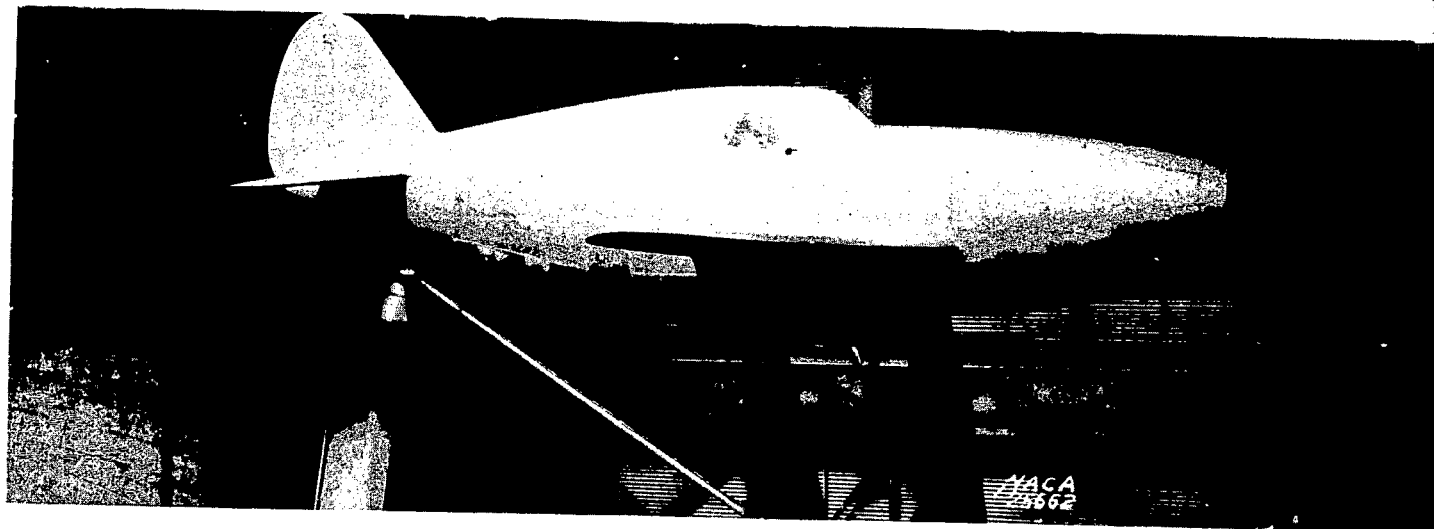


Figure 7.- Variation of diffuser cross-sectional area with distance from inlet.

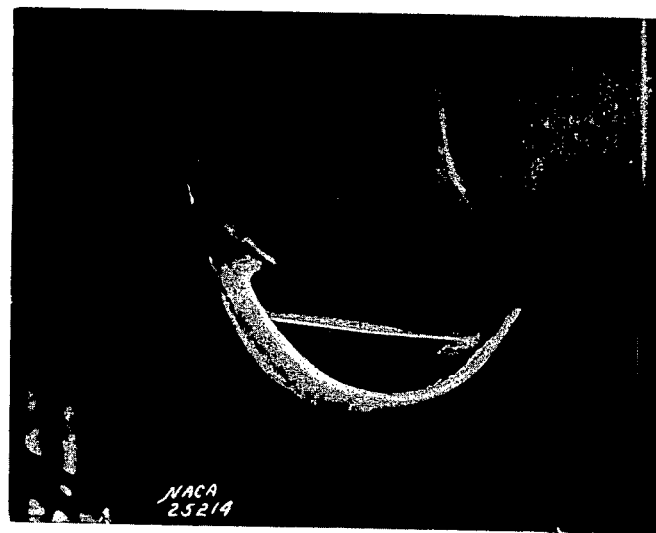




(a) As installed on model.



(b) Outlet C.

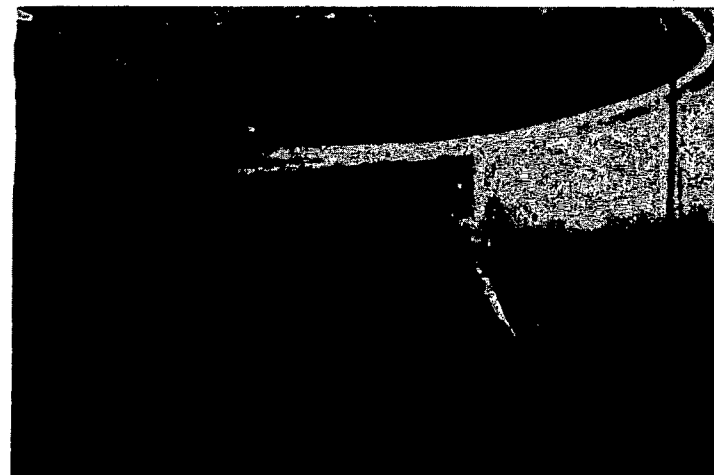


(c) Original inlet.

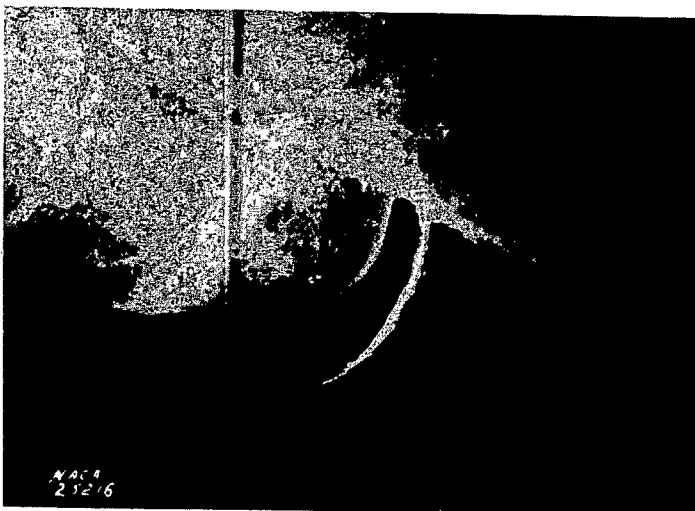
Figure 8.- General and detail views of rear underslung fuselage duct.



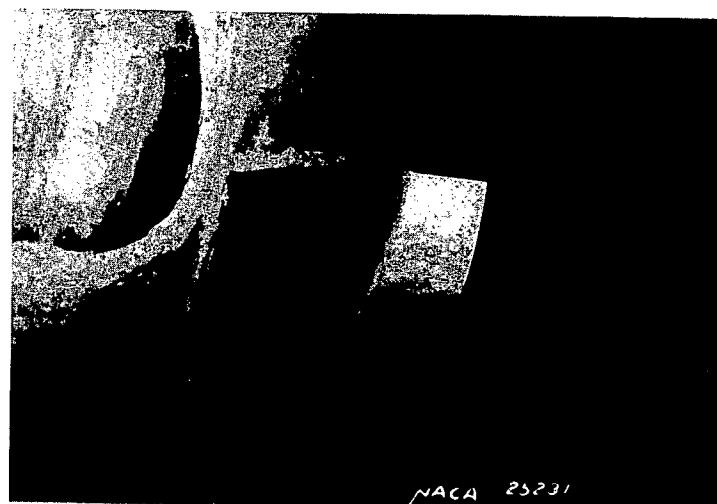
(a) Internal duct system and orifice plate



(b) Inlet seal.

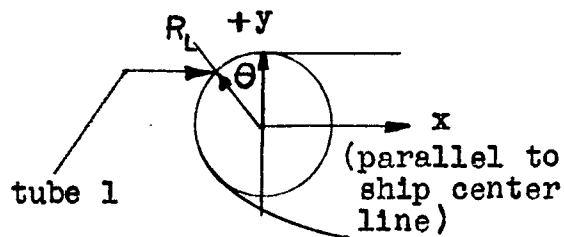


(c) Outlet A.



(d) Flap on outlet C.

Figure 9.- Typical details of duct installation.



Station $x$ , in.	Ordinate, $y$ , in.					
	A		B		C	
	Upper	Lower	Upper	Lower	Upper	Lower
0	0.37	-0.46	0.37	-0.80	0.37	-0.55
.25	.45	-.61	.40	-1.08	.37	-.79
.50	.48	-.75	.42	-1.30	.32	-.95
.75	.50	-.84	.44	-1.47	.26	-1.08
1.00	.50	-.93	.44	-1.61	.20	-1.21
1.25	.50	-1.01	.45	-1.72	.14	-1.34
1.50	.50	-1.09	.45	-1.81	.09	-1.45
1.75	.50	-1.16	.44	-1.90	.04	-1.55
2.00	.50	-1.23	.44	-1.95	-.01	-1.64
2.50	.50	-1.34		-2.04	-.10	-1.82
3.00	.50	-1.43		-2.12	-.18	-1.98
3.50		-1.51		-2.18	-.25	-2.12
4.00		-1.57		-2.23	-.32	-2.25
4.50		-1.62		-2.29	-.37	-2.34
5.00		-1.66		-2.35	-.43	-2.43
6.00		-1.71		-2.42	-.51	-2.59
7.00		-1.75		-2.52	-.58	-2.71
8.00		-1.80		-2.61	-.64	-2.80
9.00		-1.82		-2.69	-.70	-2.87
10.00		-1.84		-2.78	-.74	-2.94
12.00		-1.84		-2.91		-3.04
14.00		-1.82		-3.05		-3.11
16.00		-1.80		-3.21		-3.14
$R_L$ , in.	0.37		0.37		0.37	
$\theta$ , deg	20		30		—	

(See figure 5 for position of sections)

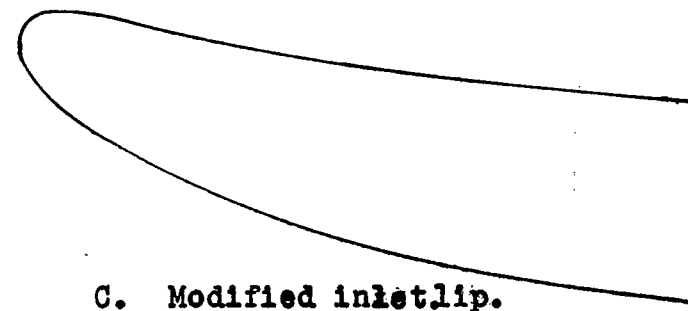
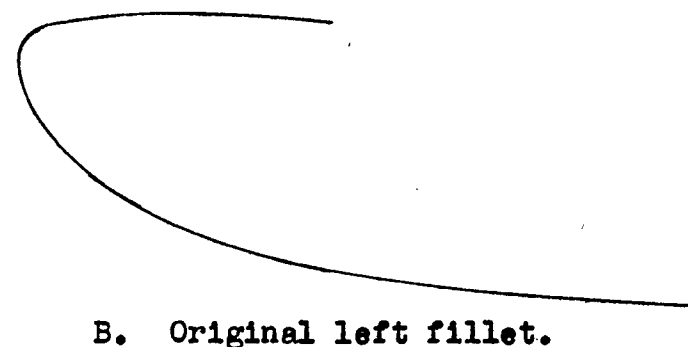
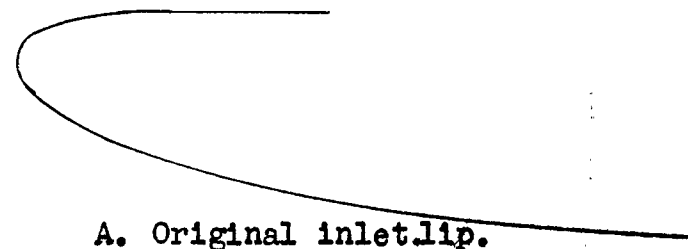


Figure 10.- Sections through inlet lips on center line of duct and through duct-fuselage fillet.

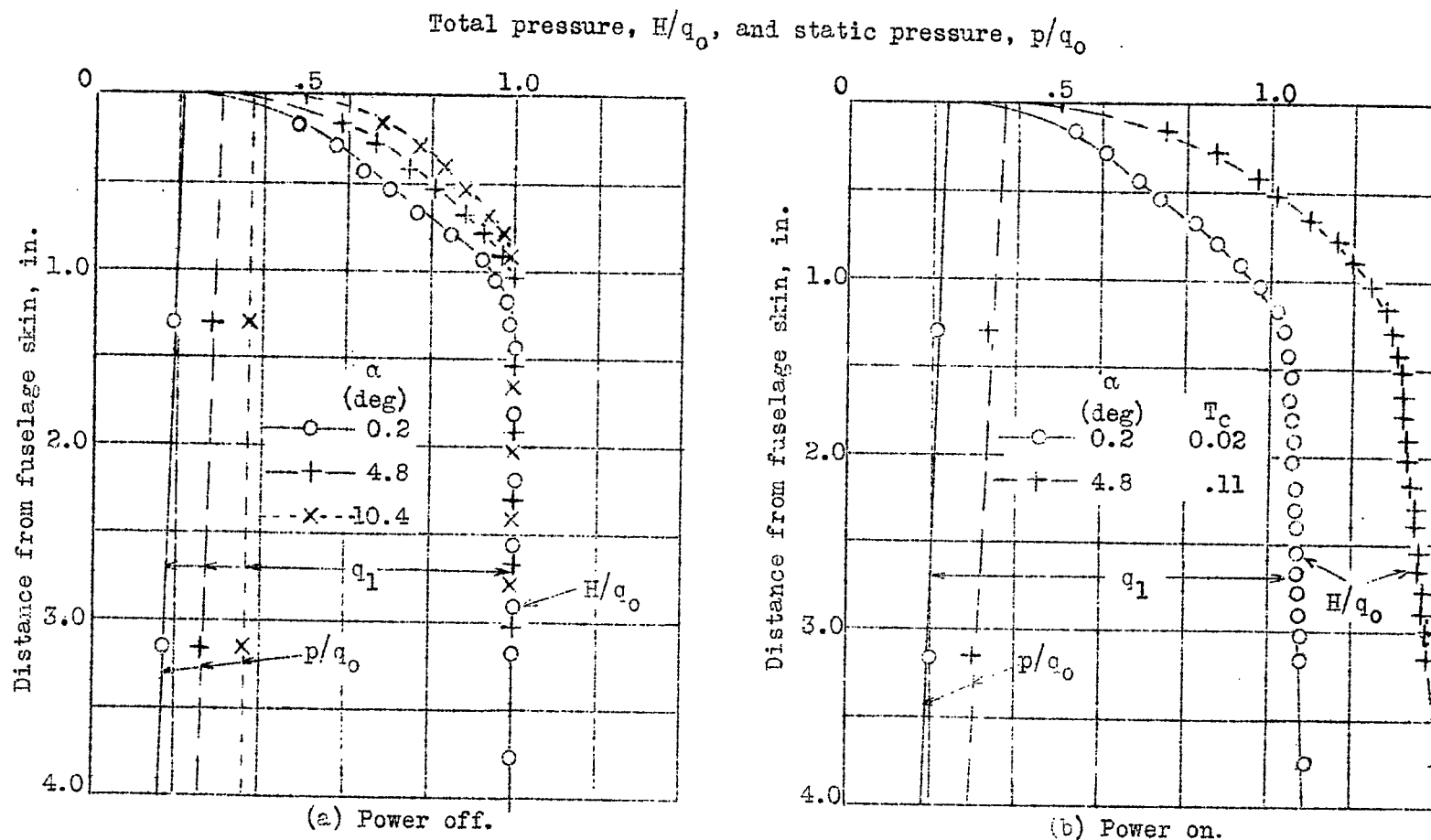


Figure 11.- Total-and static-pressure profiles 1 foot ahead of duct inlet.  $\Delta p/q_2$ , 19.6; outlet C; inlet guide vanes in.

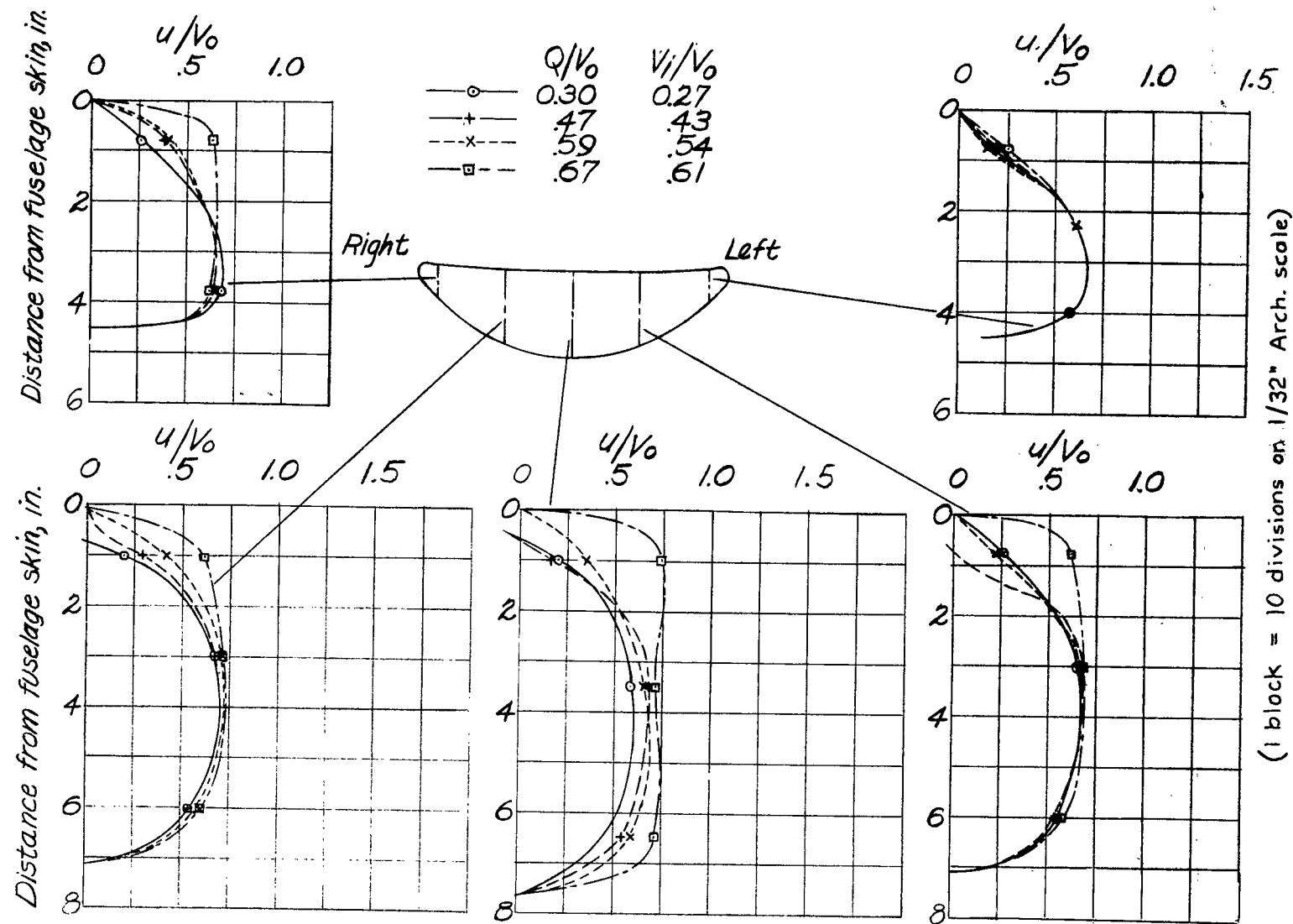


Figure 12.-Effect of  $V_1/V_0$  on inlet velocity distribution. Power off;  
 $\alpha$ ,  $0.2^\circ$ ;  $\Delta p/q_2$ , 10.9; inlet guide vanes in.

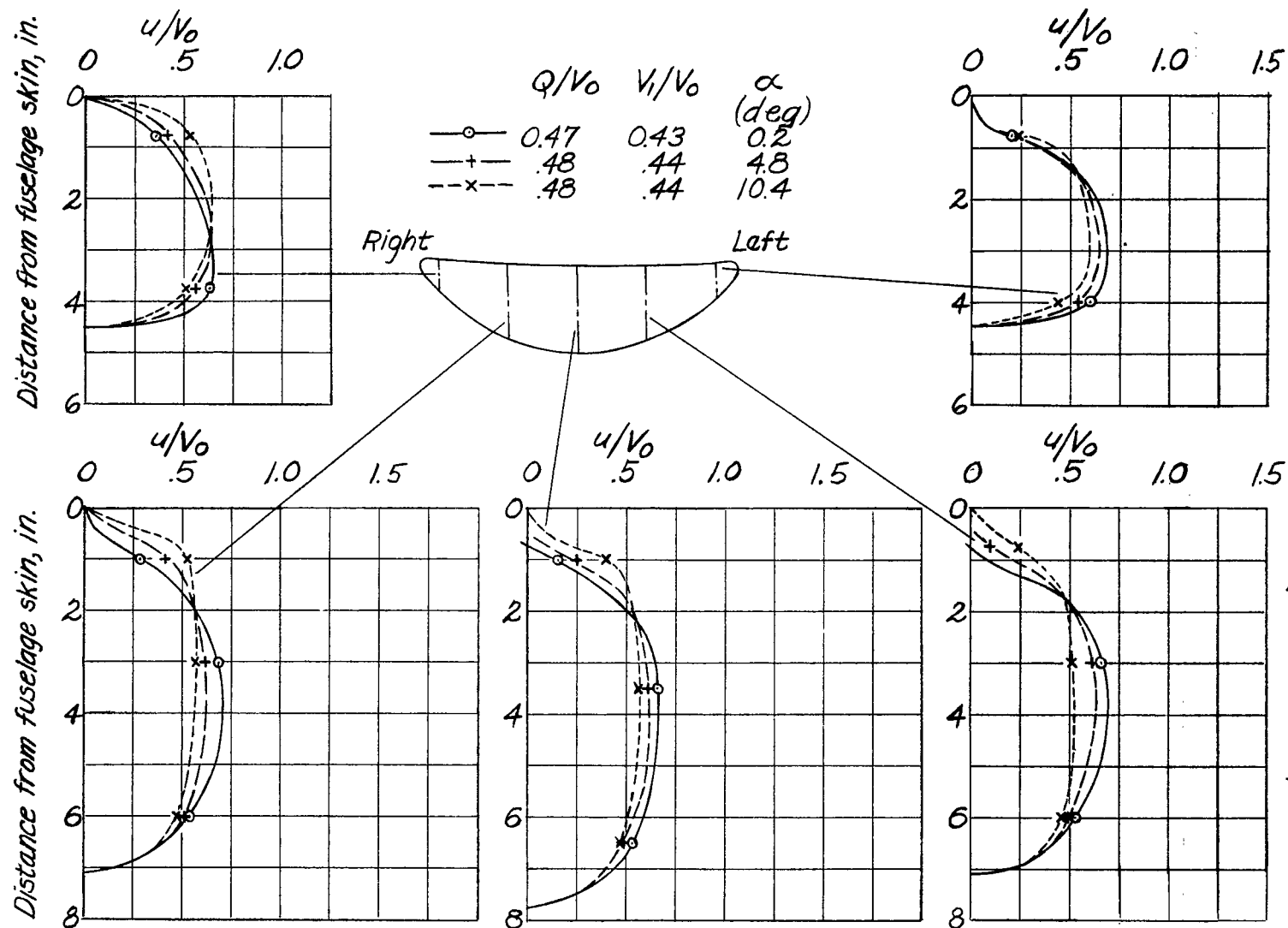


Figure 13.- Effect of angle of attack on inlet velocity distribution. Power off;  $\Delta p/q_2$ , 10.9; outlet B; inlet guide vanes in.

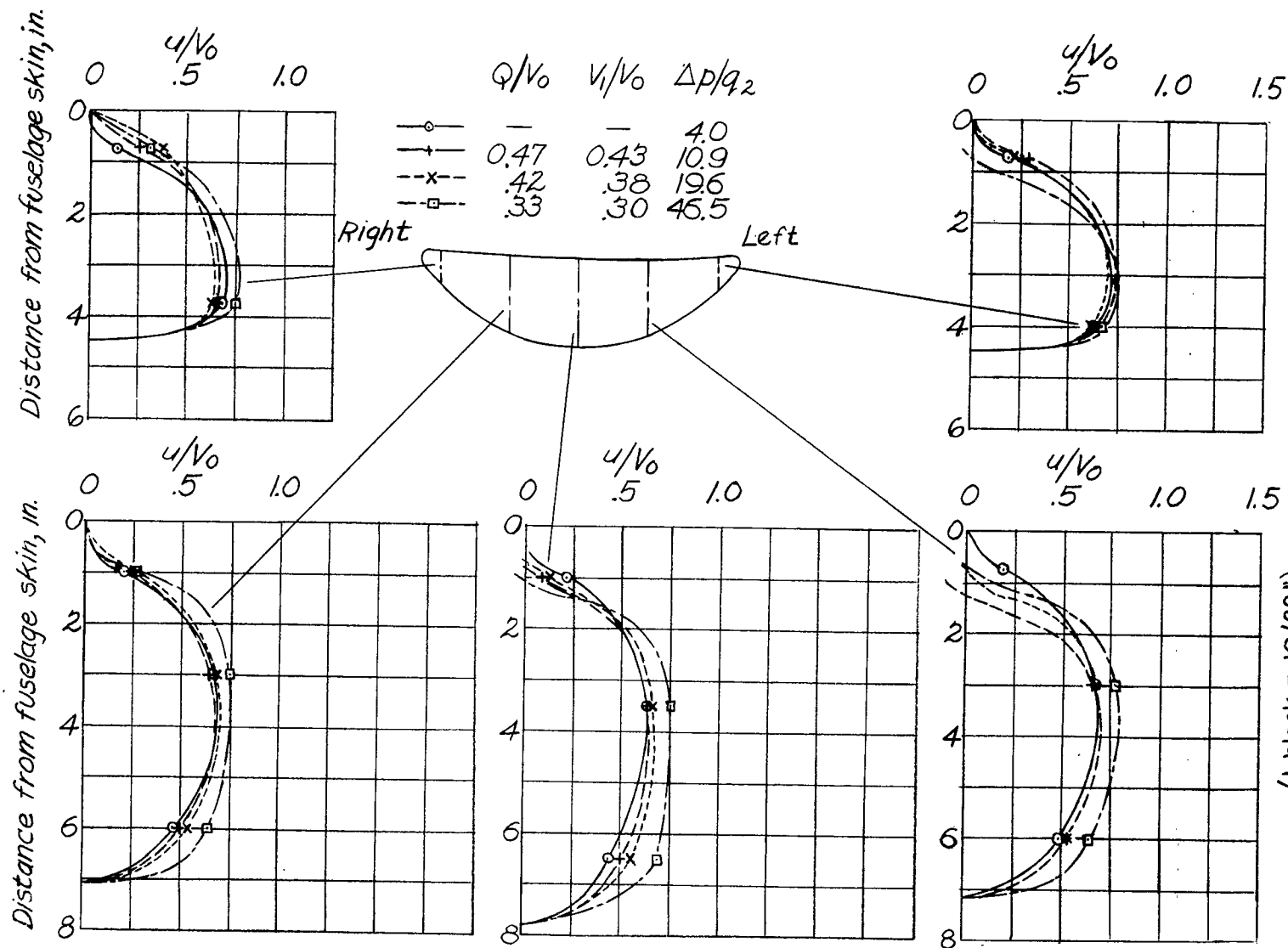


Figure 14.- Effect of  $\Delta p/q_2$  on inlet velocity distribution. Power off;  $\alpha$ , 0.2°; outlet  $B$ ; inlet guide vanes in.

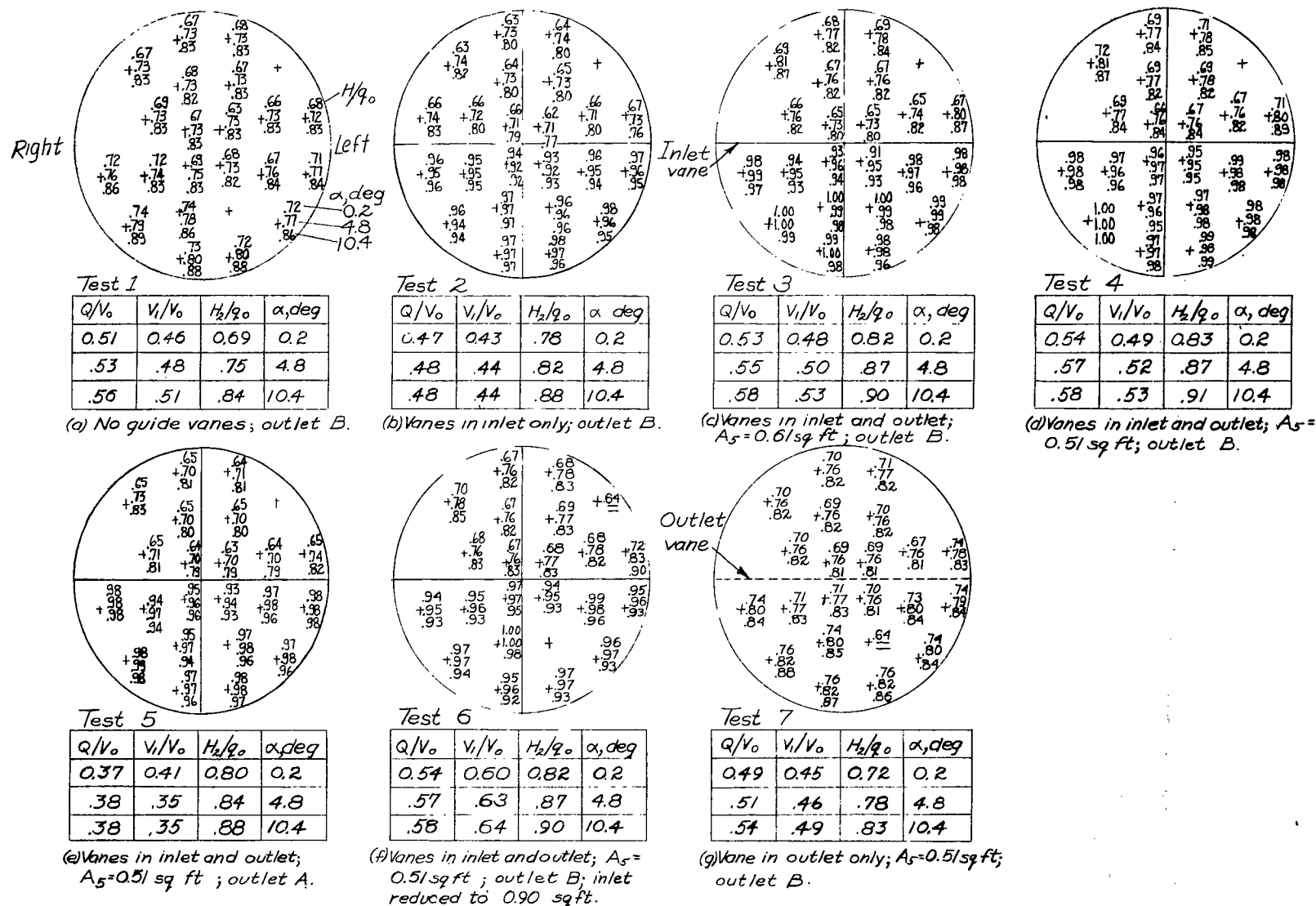


Figure 15. - Summary of pressure distribution at orifice plate for various guide-vane arrangements. Power off;  $\Delta p/p_2$ , 10.9; no outlet flaps. (Exact location of tube designated +.)



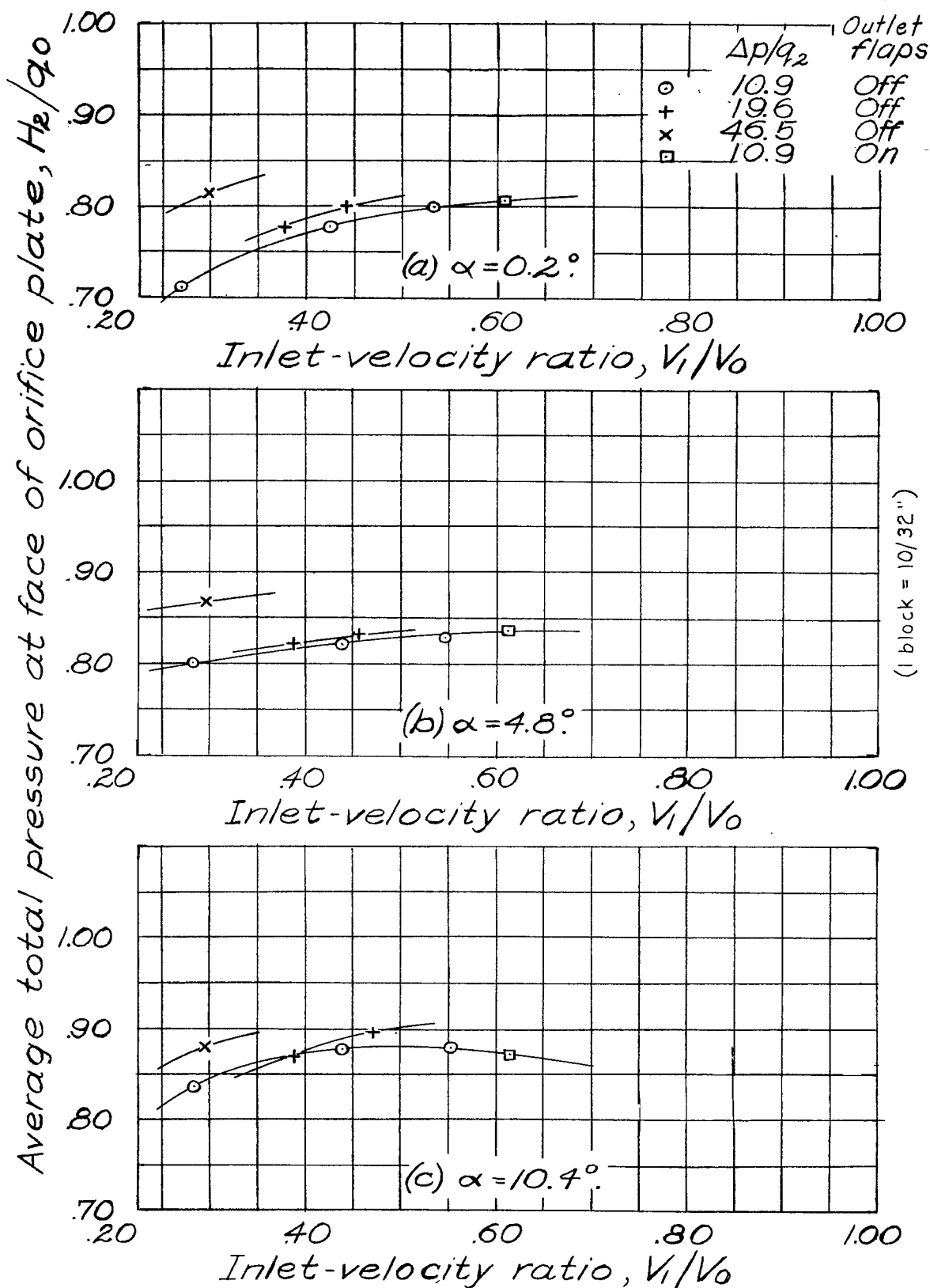


Figure 16.-Variation of average total pressure at face of orifice plate with  $V_i/V_0$ . Power off; inlet guide vanes in.

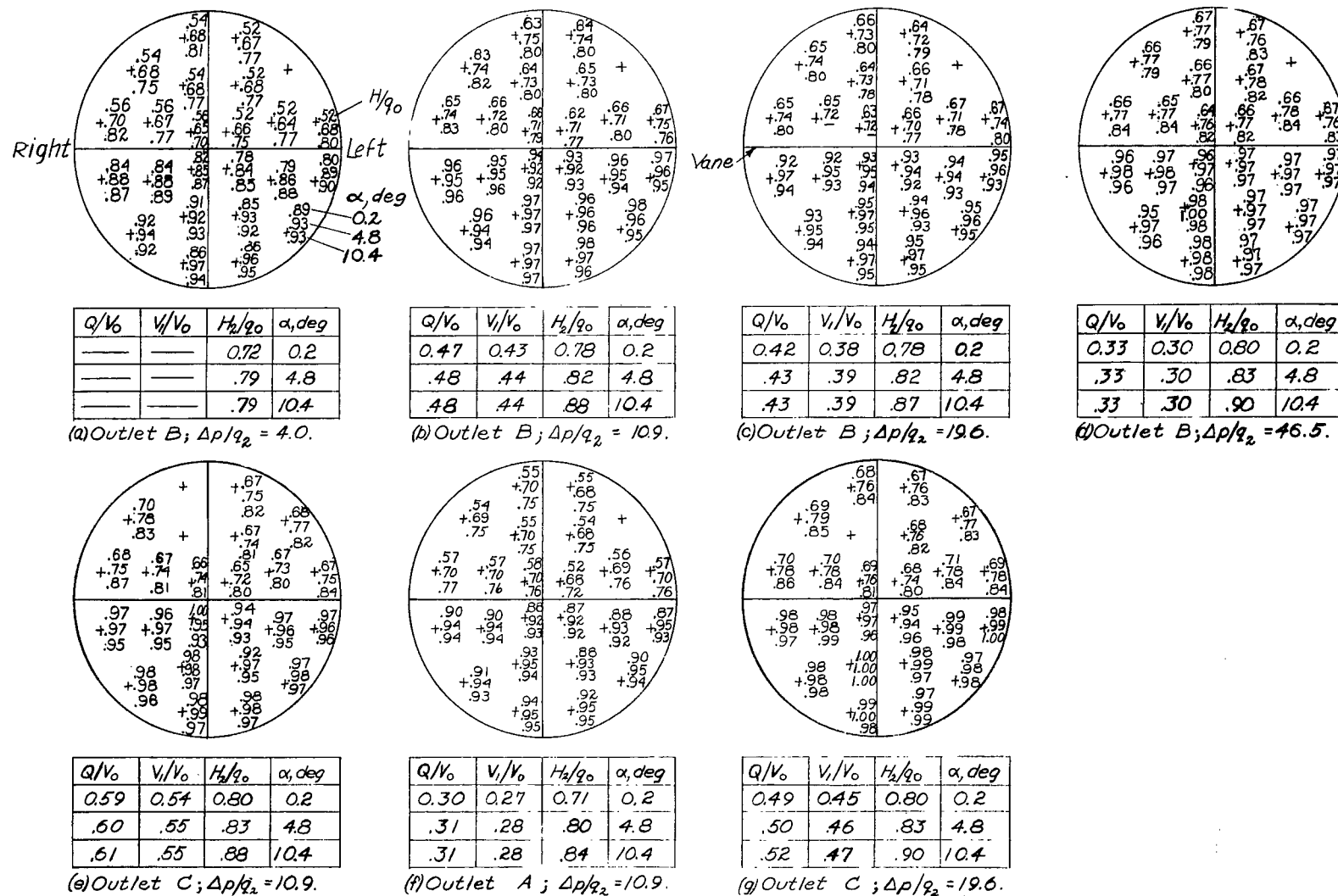


Figure 17.- Summary of pressure distributions at orifice plate for various angles of attack, air-flow quantities, and pressure-drop coefficients. Power off; no outlet flaps; inlet guide vanes in. (Exact location of tube designated +.)

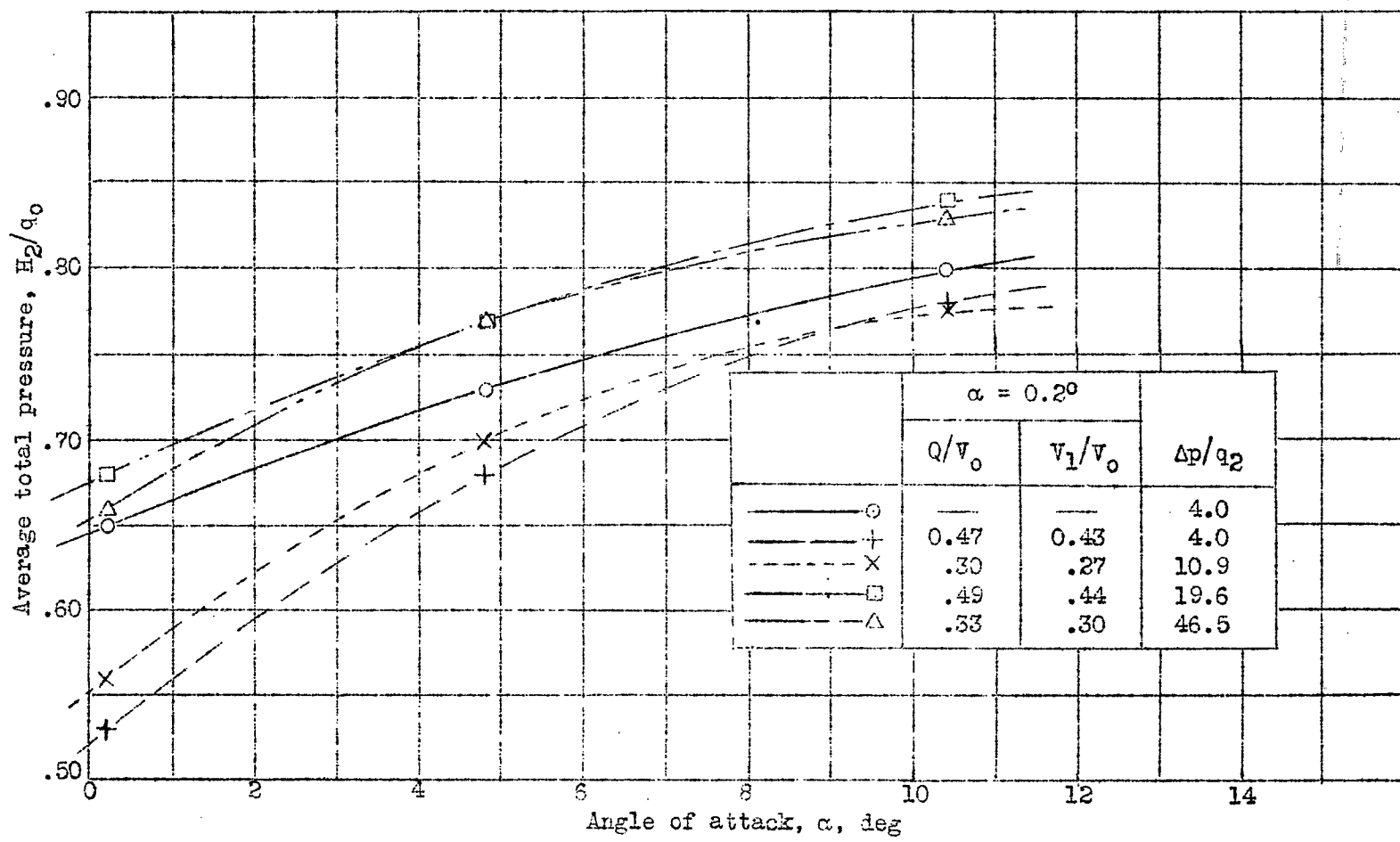
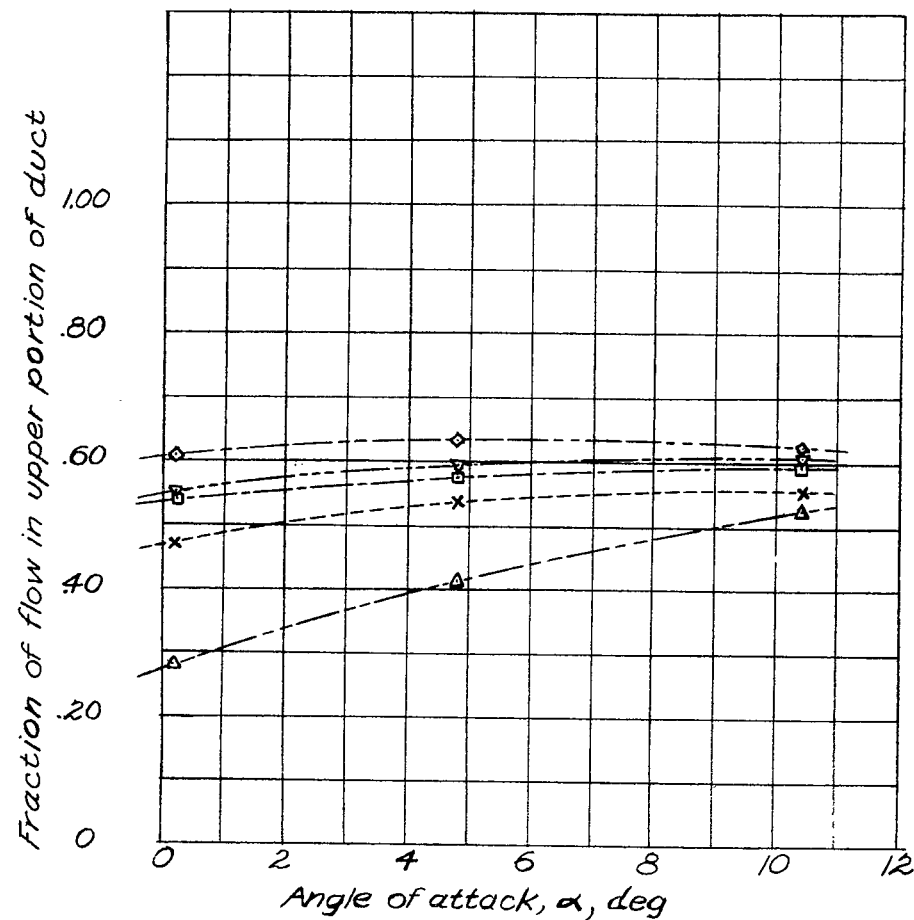


Figure 18.- Effect of angle of attack on average total pressure at orifice plate above horizontal guide vane. Power off; inlet guide vanes in.



(1 block = 10/30")

Test	Configuration	$V_1/V_0$ $\alpha = 0.2^\circ$
--x--3		0.48
--□--4		.49
--Δ--5		.34
--▽--6		.60
--◇--7		.45

Figure 19.-Effect of guide-vane arrangement on air-flow division between upper and lower portions of duct. Power off;  $\Delta p/q_x$ , 10.9.

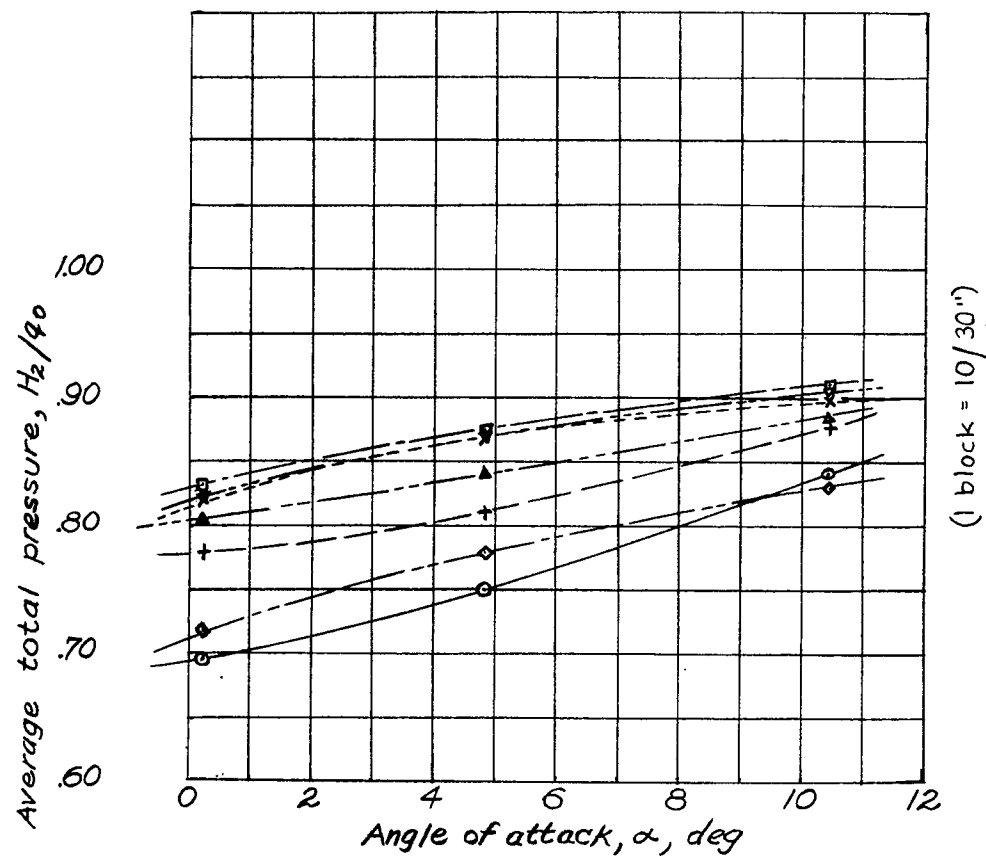


Figure 20.- Effect of guide-vane arrangement on total pressure at face of orifice plate. Power off;  $\Delta p/q_2$ , 10.9.

Test	Configuration	$V_1/V_0$ $\alpha = 0.2^\circ$
1		0.46
2		.42
3		.48
4		.49
5		.34
6		.60
7		.45

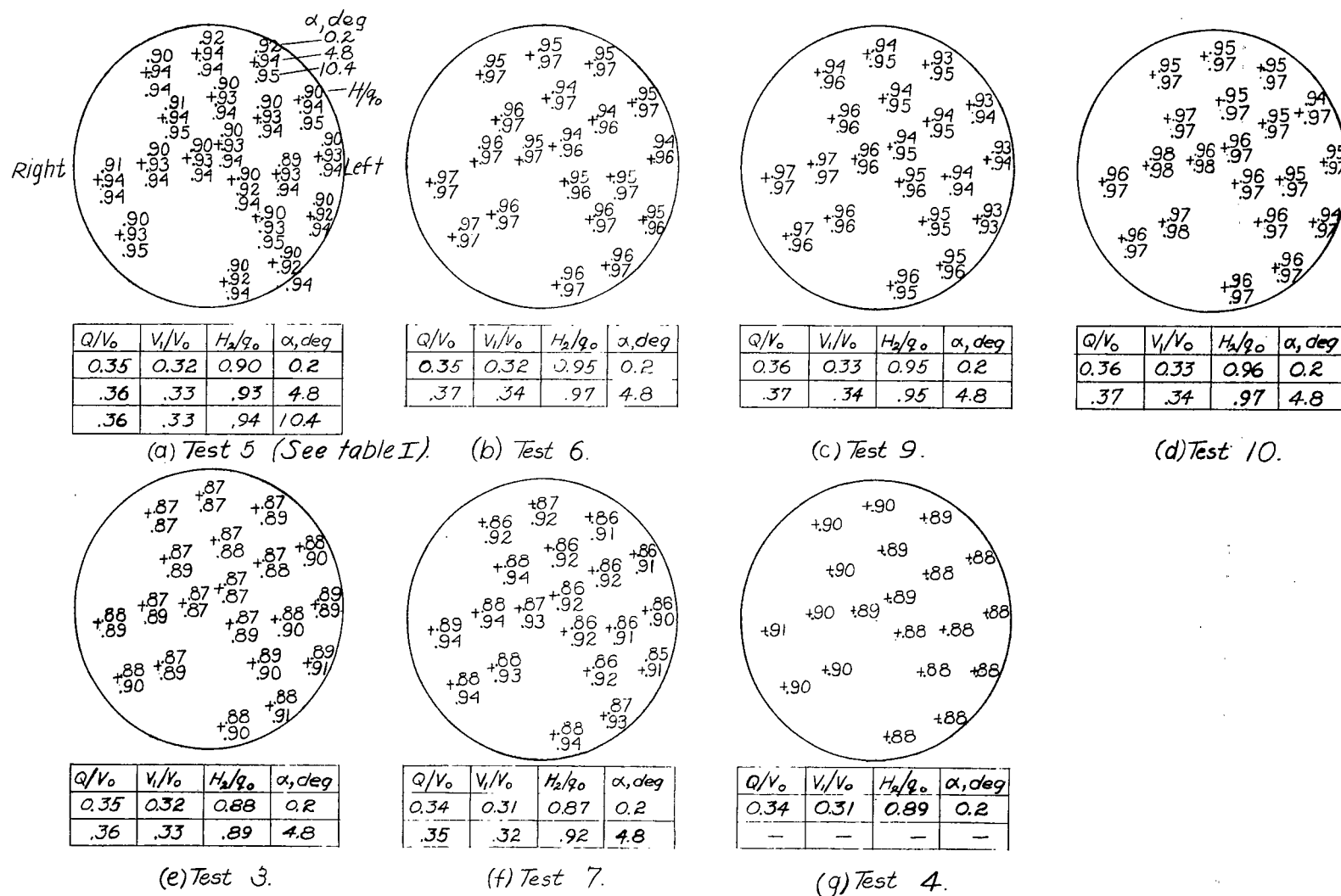
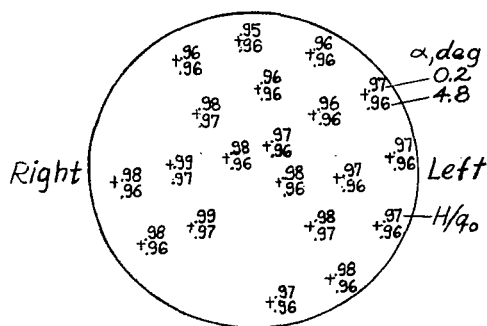
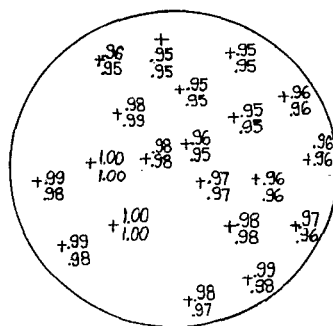


Figure 21: Summary of total-pressure distribution at orifice plate for installation with boundary-layer bypass duct. Power off;  $\Delta p/q_2, 10.9$ ; outlet B. (Exact location of tube designated +.)



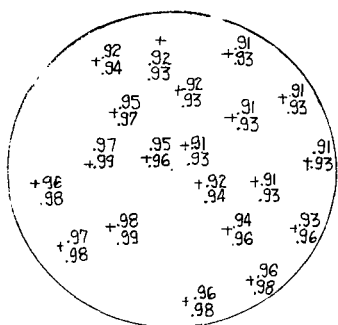
$Q/V_0$	$V_1/V_0$	$H_2/q_0$	$\alpha, \text{deg}$
0.55	0.50	0.97	0.2
.56	.51	.96	4.8

(a) Test 11.



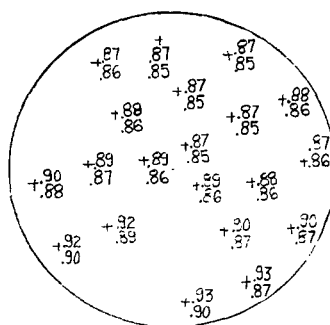
$Q/V_0$	$V_1/V_0$	$H_2/q_0$	$\alpha, \text{deg}$
0.56	0.51	0.97	0.2
.55	.50	.97	4.8

(b) Test 12.



$Q/V_0$	$V_1/V_0$	$H_2/q_0$	$\alpha, \text{deg}$
—	—	0.94	0.2
—	—	.95	4.8

(c) Test 13.



$Q/V_0$	$V_1/V_0$	$H_2/q_0$	$\alpha, \text{deg}$
0.52	0.47	0.89	0.2
.51	.46	.87	4.8

(d) Test 14.

Figure 22.—Summary of pressure distributions at orifice plate for installation with boundary-layer bypass duct. Power off;  $\Delta p/q_2, 10.9$ ; outlet B; no outlet flaps. (Exact location of tube designated +.)

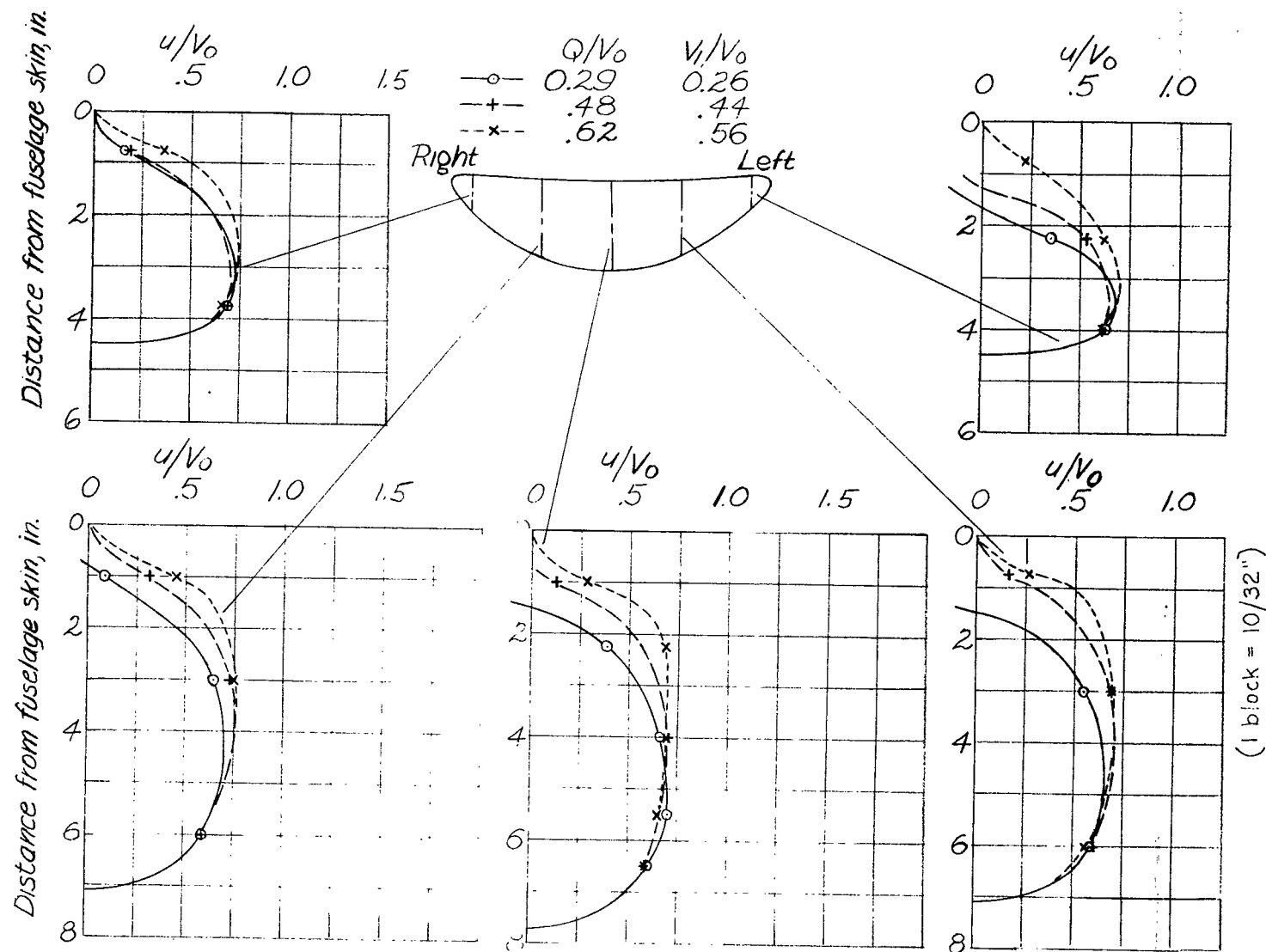


Figure 23.- Effect of  $V_1/V_0$  on inlet velocity distribution. Power on;  $\alpha$ ,  $0.2^\circ$ ;  $\beta$ ,  $60^\circ$ ;  $T_c$ , 0.02;  $\Delta p/q_2$ , 10.9; inlet guide vanes in.



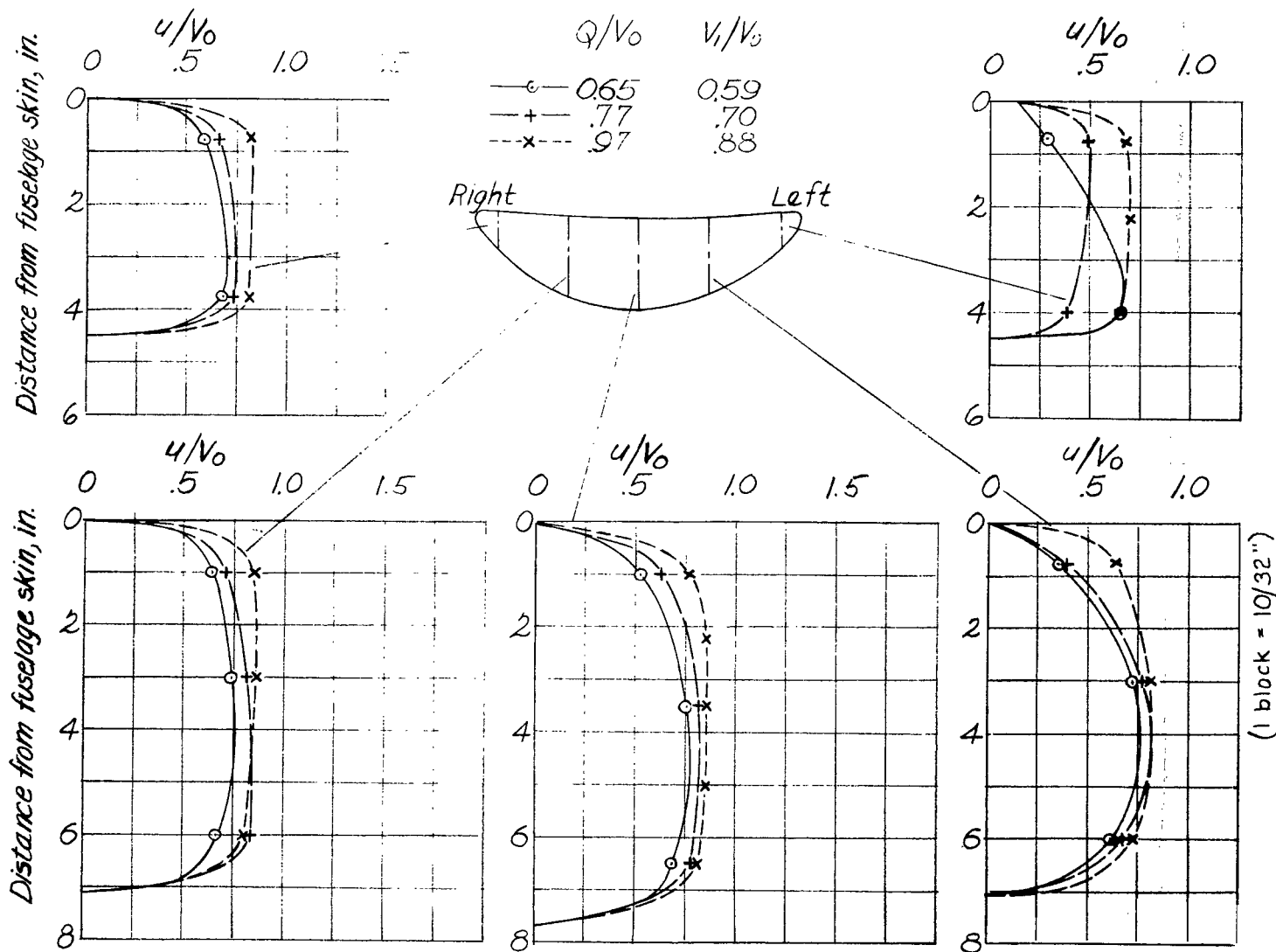


Figure 24- Effect of  $V_1/V_0$  on inlet velocity distribution. Power on;  $\alpha$ ,  $4.8^\circ$ ;  $\beta$ ,  $40^\circ$ ;  $T_c$ , 0.11;  $\Delta p/q_2$ , 10.9; inlet guide vanes in.

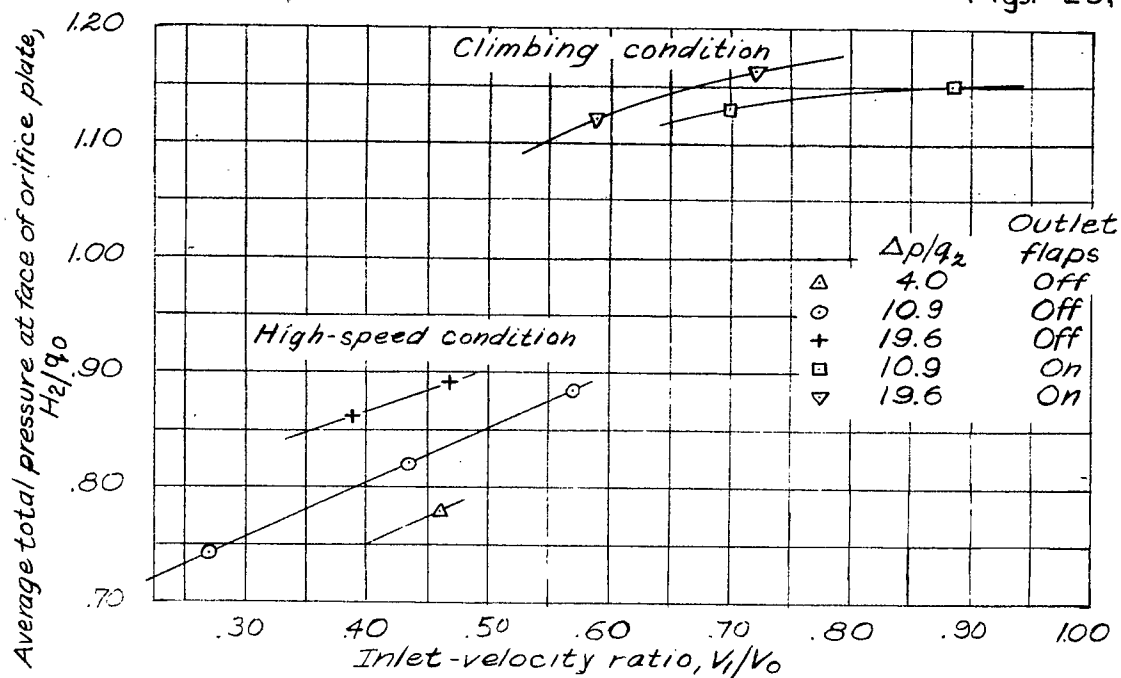


Figure 25.-Variation of average total pressure at face of orifice plate with  $V_1/V_0$ . High-speed condition:  $\alpha, 0.2^\circ$ ;  $\beta, 60^\circ$ ;  $T_c, 0.02$ . Climbing condition:  $\alpha, 40^\circ$ ;  $\beta, 40^\circ$ ;  $T_c, C.II$ . Guide vanes in inlet.

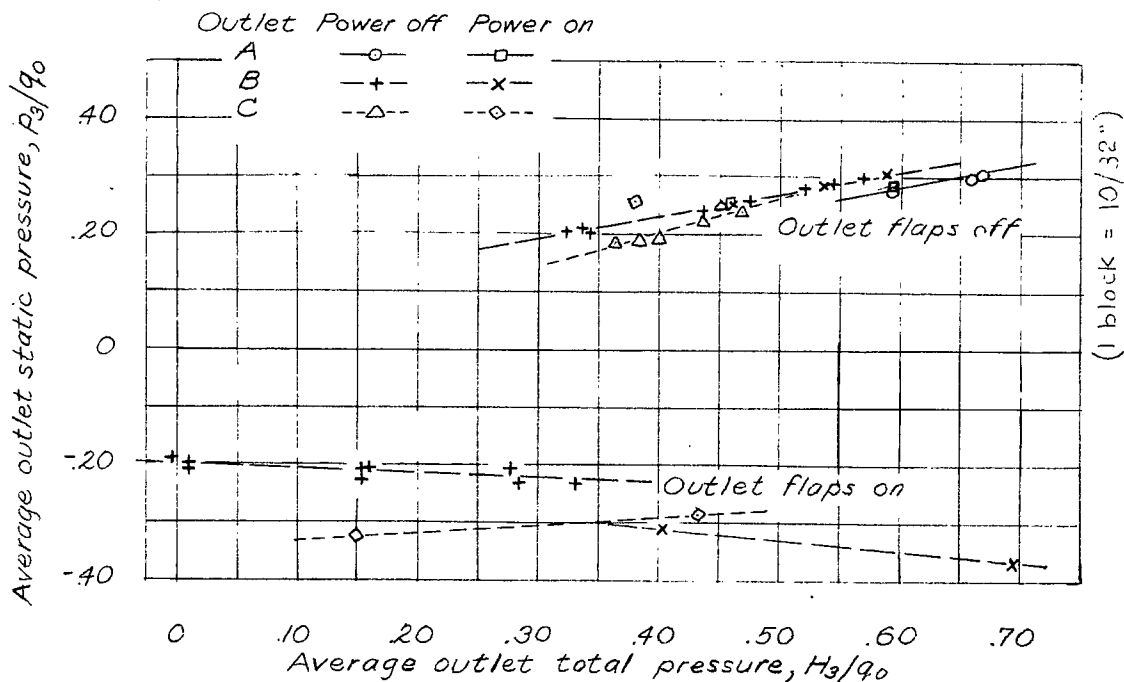
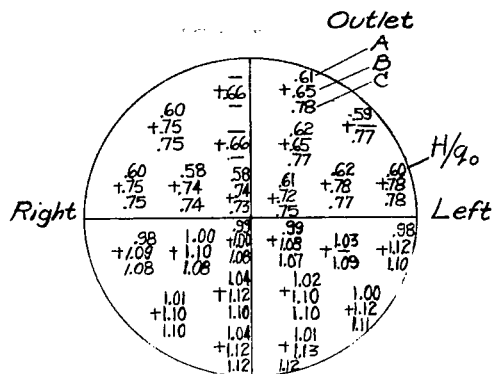
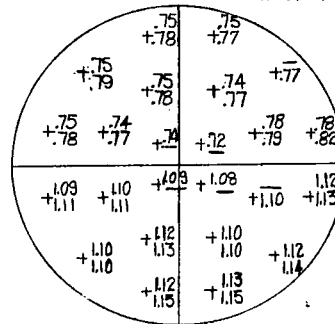


Figure 27.-Variation of outlet static pressure with outlet total pressure. Power off and power on; guide vanes in inlet.



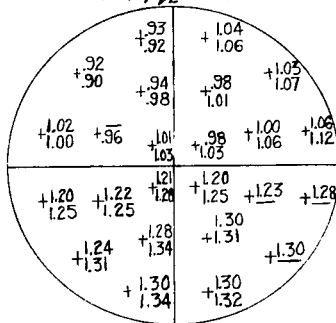
$Q/V_0$	$V_1/V_0$	$H_2/q_0$	Outlet
0.29	0.26	0.75	A
.48	.44	.82	B
.63	.57	.87	C

(a)  $\alpha = 0.2^\circ$ ;  $\Delta p/q_2 = 10.9$ ;  $\beta = 60^\circ$ ;  $T_c = 0.02$ ; no flaps.



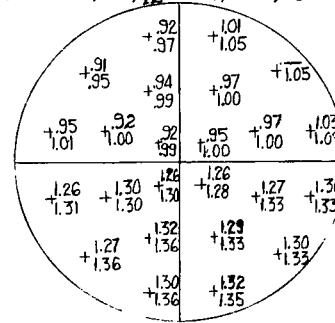
$Q/V_0$	$V_1/V_0$	$H_2/q_0$	Outlet
0.43	0.39	0.86	B
.54	.49	.88	C

(b)  $\alpha = 0.2^\circ$ ;  $\Delta p/q_2 = 19.6$ ;  $\beta = 60^\circ$ ;  $T_c = 0.02$ ; no flaps.



$Q/V_0$	$V_1/V_0$	$H_2/q_0$	Outlet
0.77	0.70	1.13	B
.97	.88	1.15	C

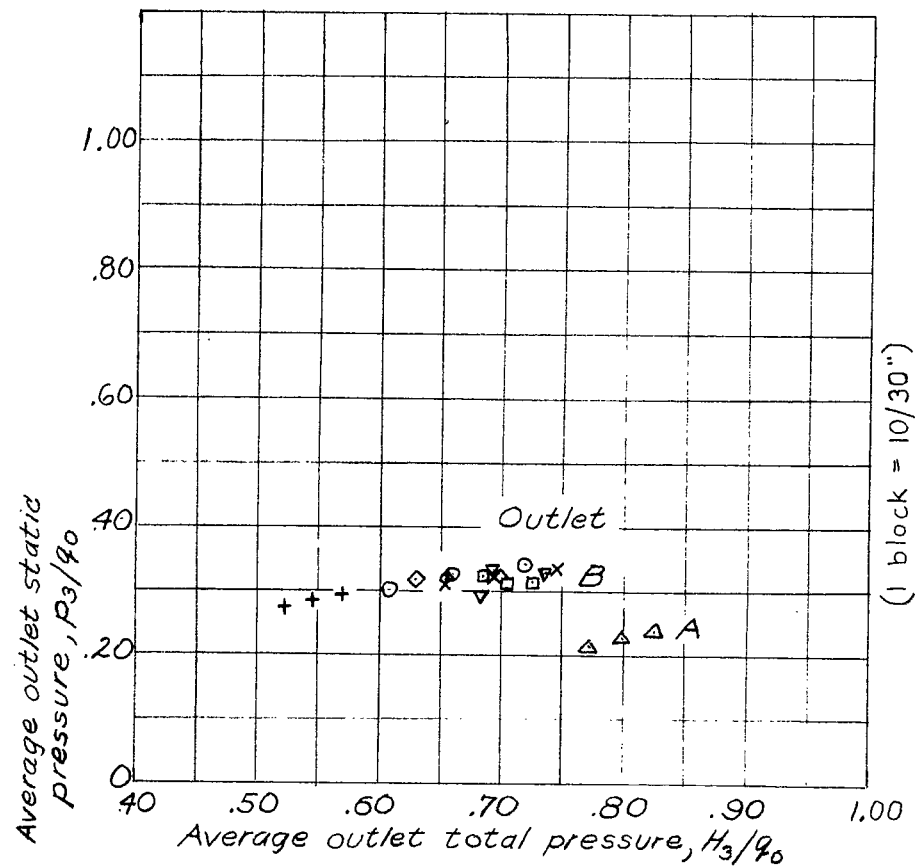
(c)  $\alpha = 4.8^\circ$ ;  $\Delta p/q_2 = 10.9$ ;  $\beta = 40^\circ$ ;  $T_c = 0.11$ ; flaps on.



$Q/V_0$	$V_1/V_0$	$H_2/q_0$	Outlet
0.65	0.59	1.12	B
.79	.72	1.16	C

(d)  $\alpha = 4.8^\circ$ ;  $\Delta p/q_2 = 49.6$ ;  $\beta = 40^\circ$ ;  $T_c = 0.11$ ; flaps on.

Figure 26.- Summary of pressure distributions at orifice plate for various pressure-drop coefficients. Power on; inlet guide vanes in. (Exact location of tube designated +.)



Test	Configuration	$V_1/V_0$ $\alpha = 0.2^\circ$
—○— 1		0.46
—+— 2		.42
--x-- 3		.48
—□— 4		.49
—△— 5		.34
—▽— 6		.60
—◇— 7		.45

Figure 28.- Variation of outlet static pressure with outlet total pressure for various guide-vane arrangements. Power off; no outlet flaps.

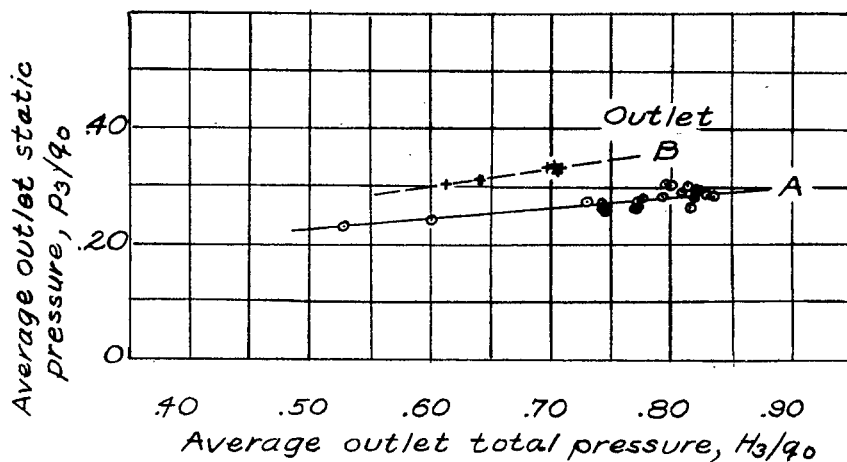


Figure 29.-Variation of outlet static pressure with outlet total pressure with boundary-layer bypass installed. Power off; no outlet flaps.

(1 block = 10/32")

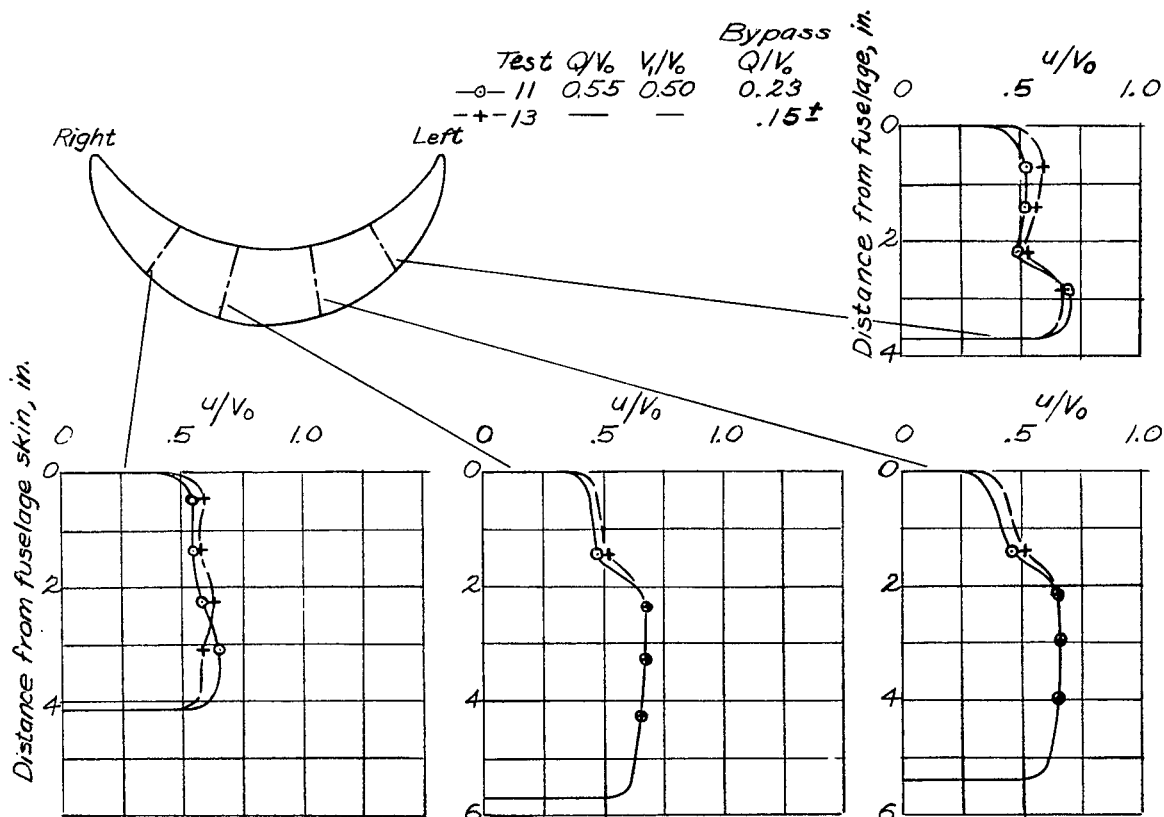


Figure 30.-Effect of flow through boundary-layer bypass on outlet velocity distribution. Power off;  $\alpha$ , 0.2;  $\Delta p/q_2$ , 10.9; outlet B.

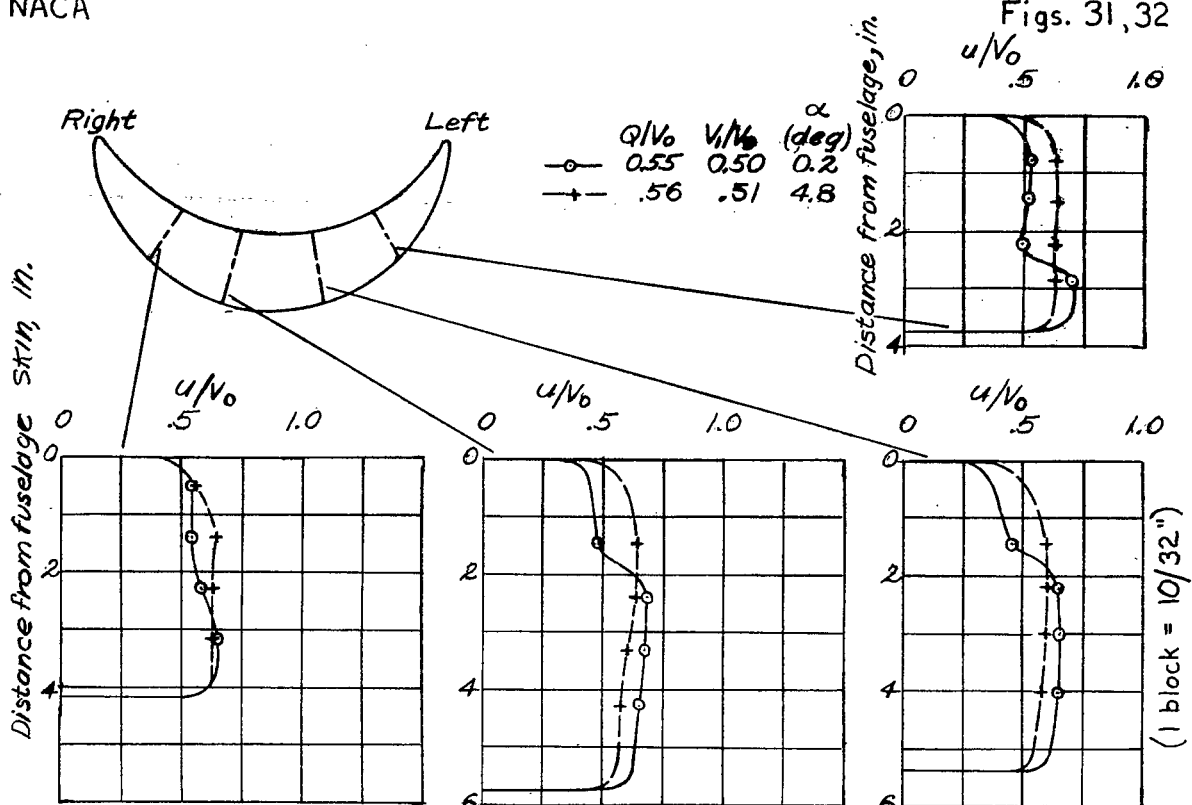


Figure 31.- Effect of angle of attack on outlet velocity distribution. Run 11; power off;  $\Delta p/q_2$ , 10.9; outlet B; boundary-layer bypass outlet V.

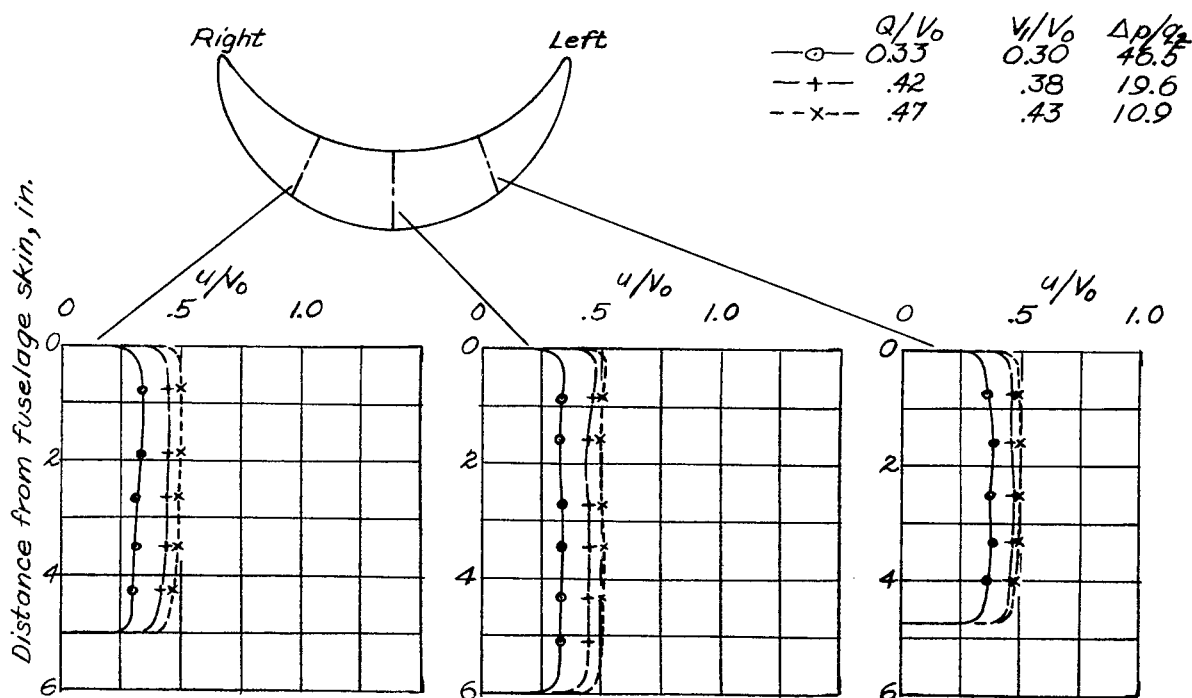


Figure 32.- Effect of  $Q/V_0$  on outlet velocity distribution. Power off;  $\alpha$ , 0.2; outlet B; outlet flaps off; inlet guide vanes in.

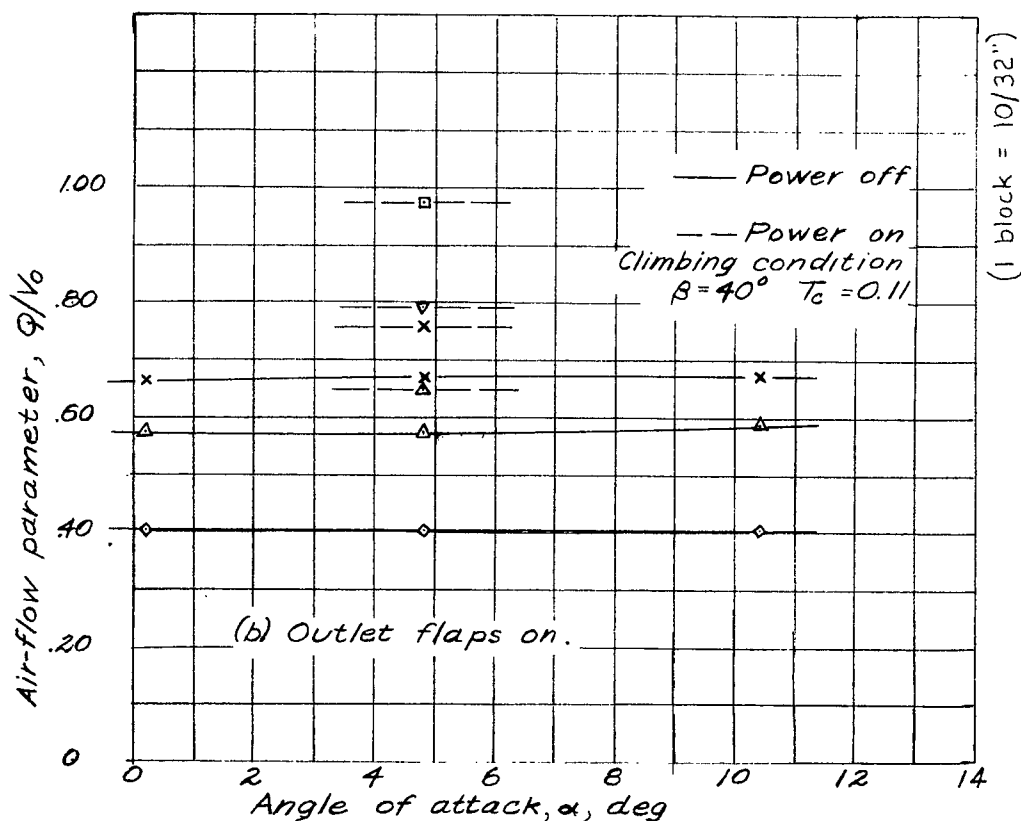
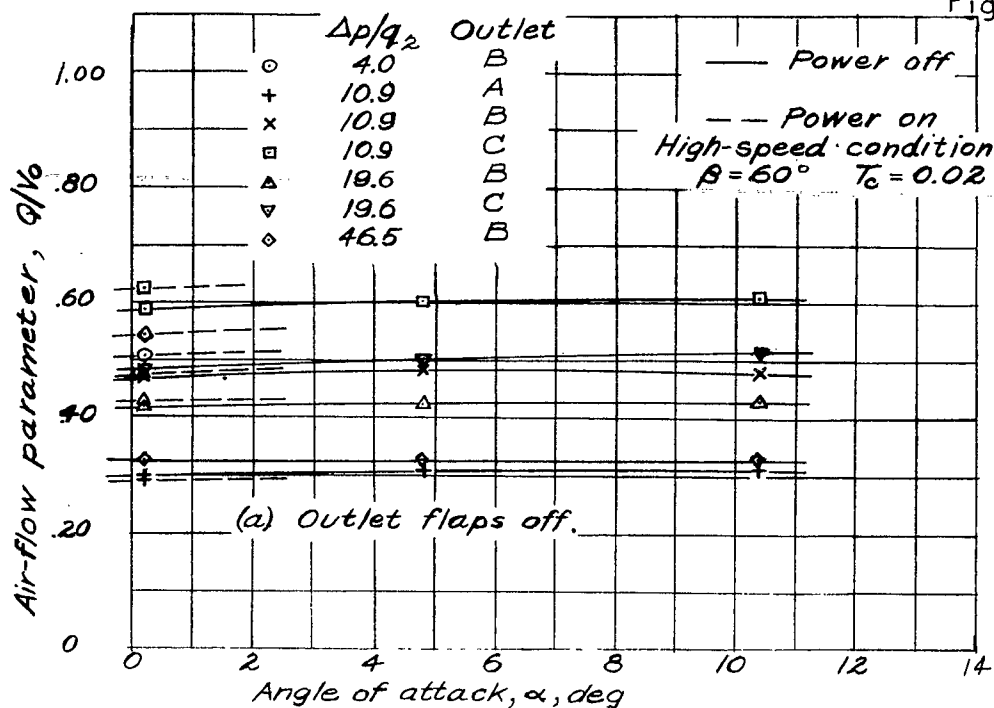
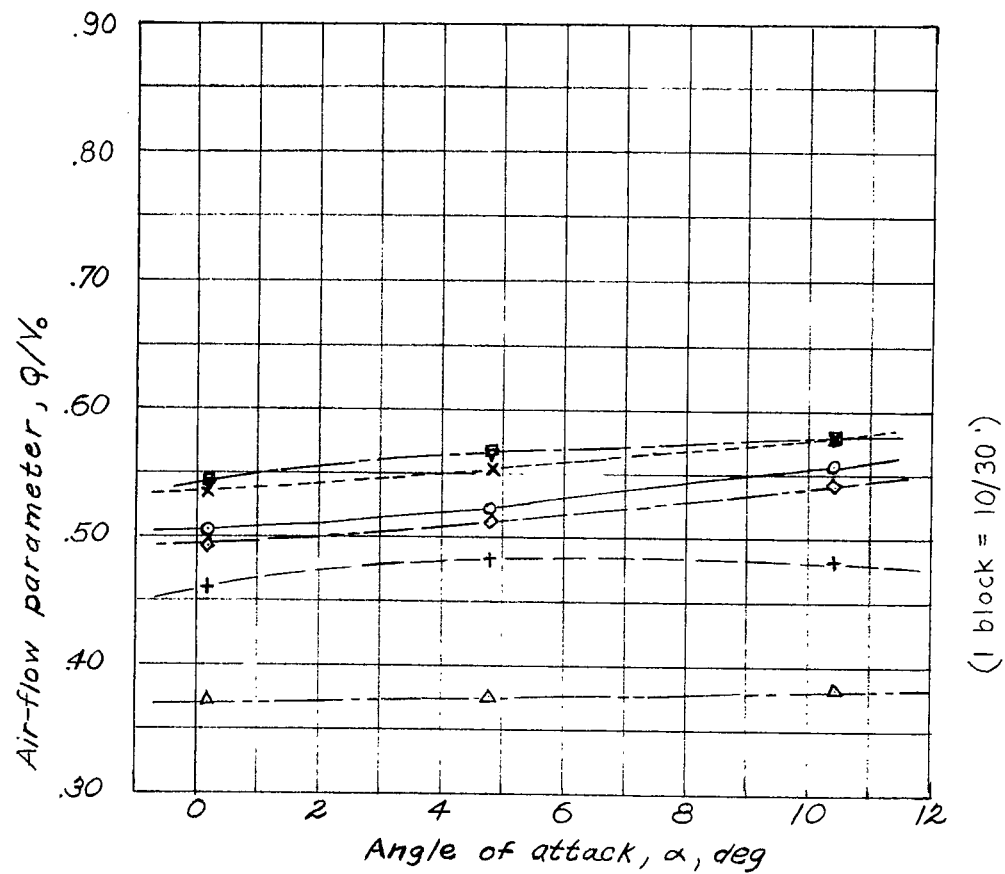


Figure 33.-Summary of air flows through duct. Power off and power on; inlet guide vanes in.



Run	Configuration	$V_1/V_0$ $\alpha = 0.2^\circ$
—○— 1		0.46
—+— 2		.42
--x-- 3		.48
—■— 4		.49
—△-- 5		.34
—▽-- 6		.60
—◇--- 7		.45

Figure 34.- Effect of guide-vane arrangement on  $q/V_0$ . Power off;  $\Delta p/q_2, 10.9$ .



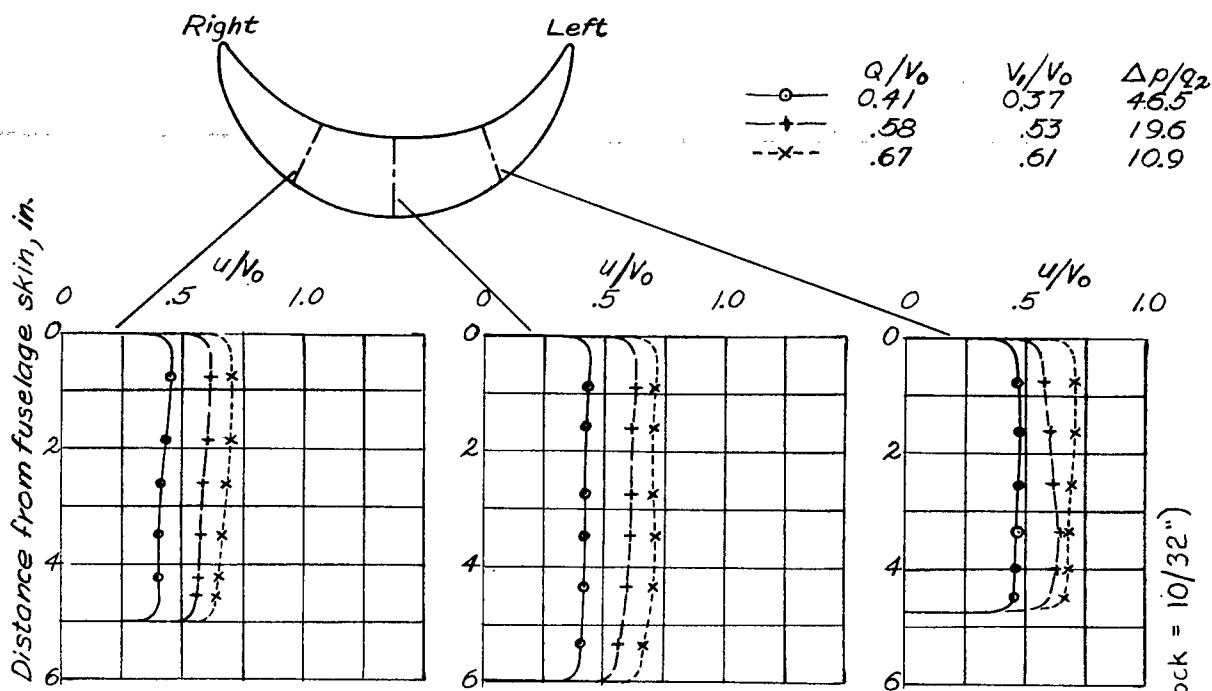


Figure 35.-Effect of  $Q/V_0$  on outlet velocity distribution. Power off;  $\alpha$ ,  $0.2^\circ$ ; outlet B; outlet flaps on; inlet guide vanes in.

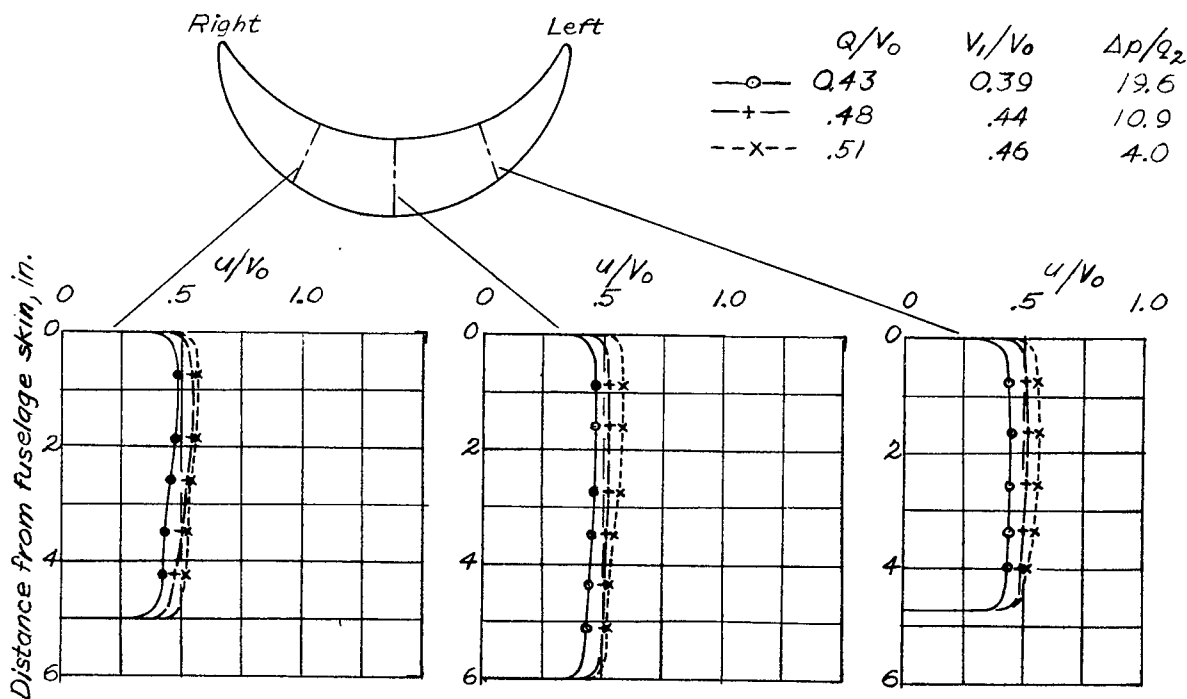


Figure 36.-Effect of  $Q/V_0$  on outlet velocity distribution. Power on; outlet B;  $\alpha$ ,  $0.2^\circ$ ;  $\beta$ ,  $60^\circ$ ;  $T_c$ , 0.02; inlet guide vanes in.

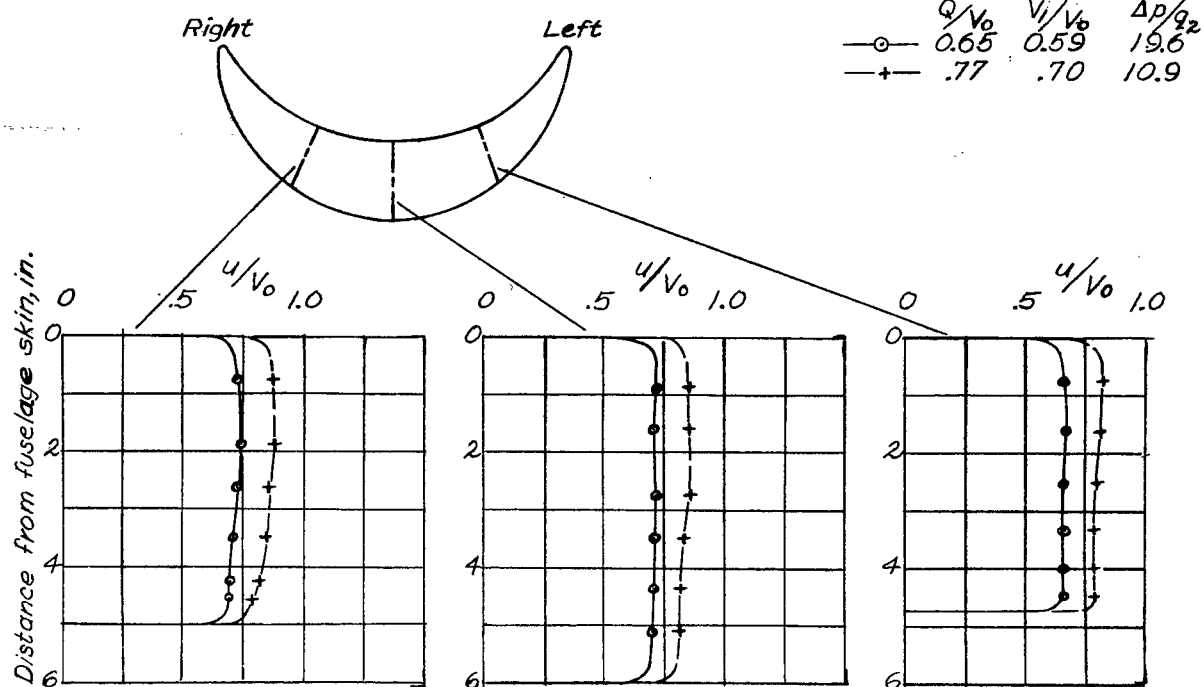


Figure 37.- Effect of  $Q/V_0$  on outlet velocity distribution. Power on; outlet B;  $\alpha$ ,  $4.8^\circ$ ;  $\beta$ ,  $40^\circ$ ;  $T_c$ , 0.11; outlet flaps on; inlet guide vanes in.

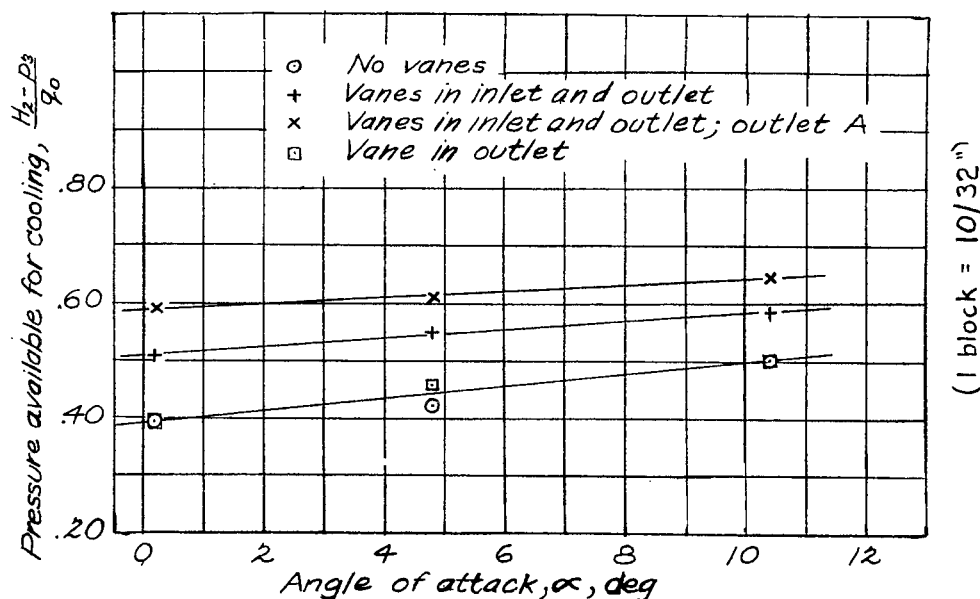


Figure 39.- Effect of vanes on pressures available for cooling at various angles of attack of the model. Power off;  $\Delta p/q_2$ , 10.9; outlet B except when specified.

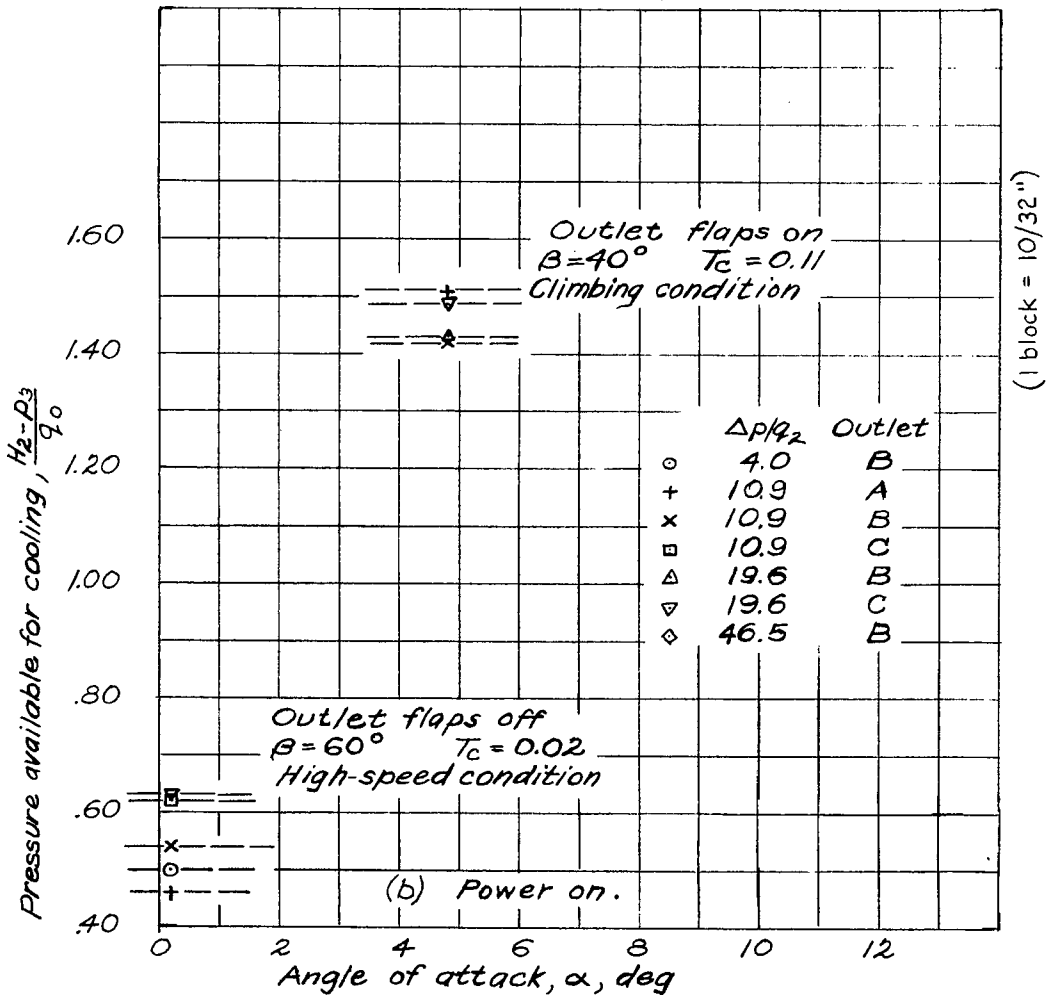
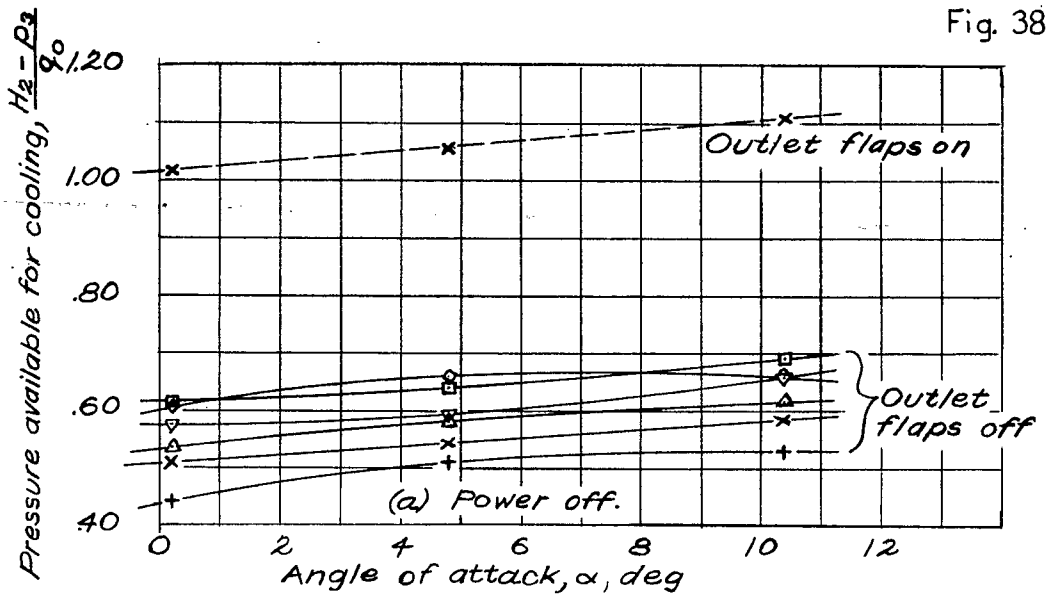


Figure 38 - Summary of pressures available for cooling.  
Power off and power on; inlet guide vanes in.

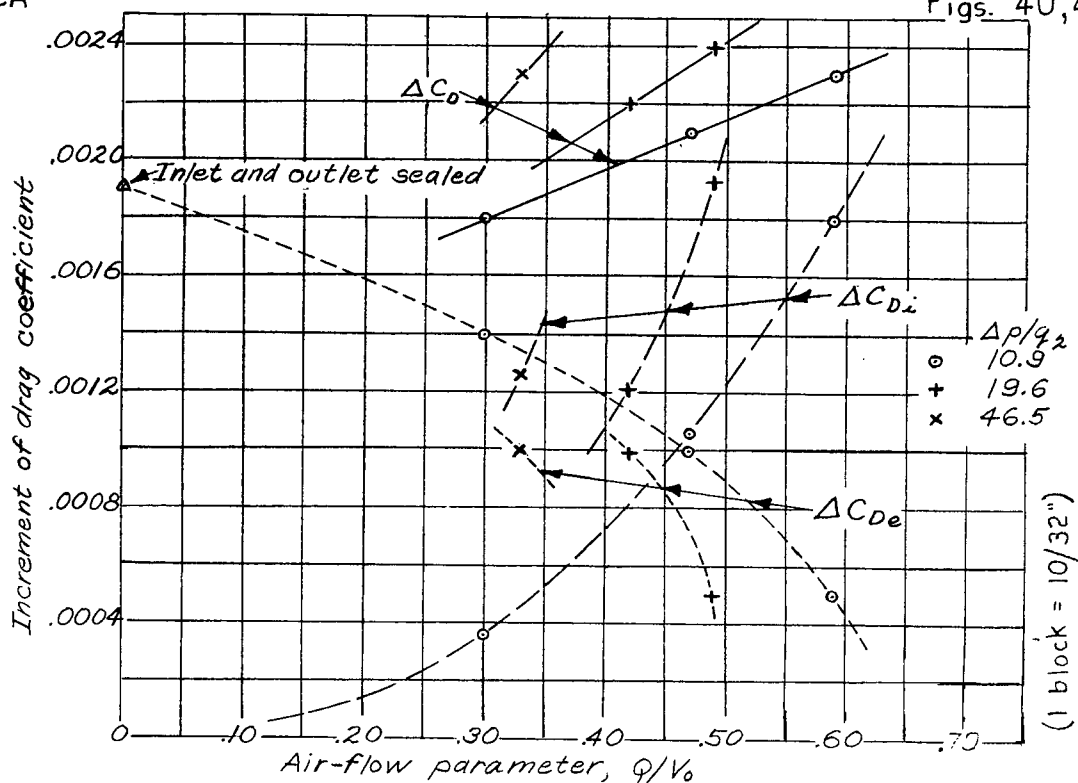


Figure 40.- Variation of increments of total, internal, and external drag coefficients with  $Q/V_0$ . Inlet guide vanes in.

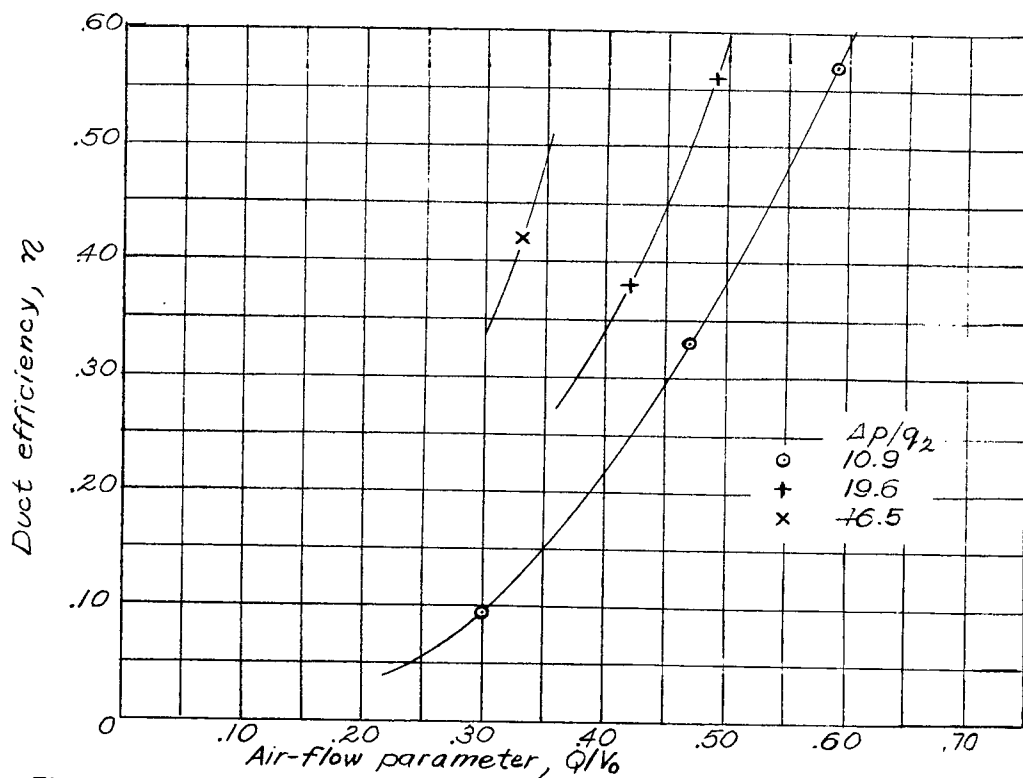
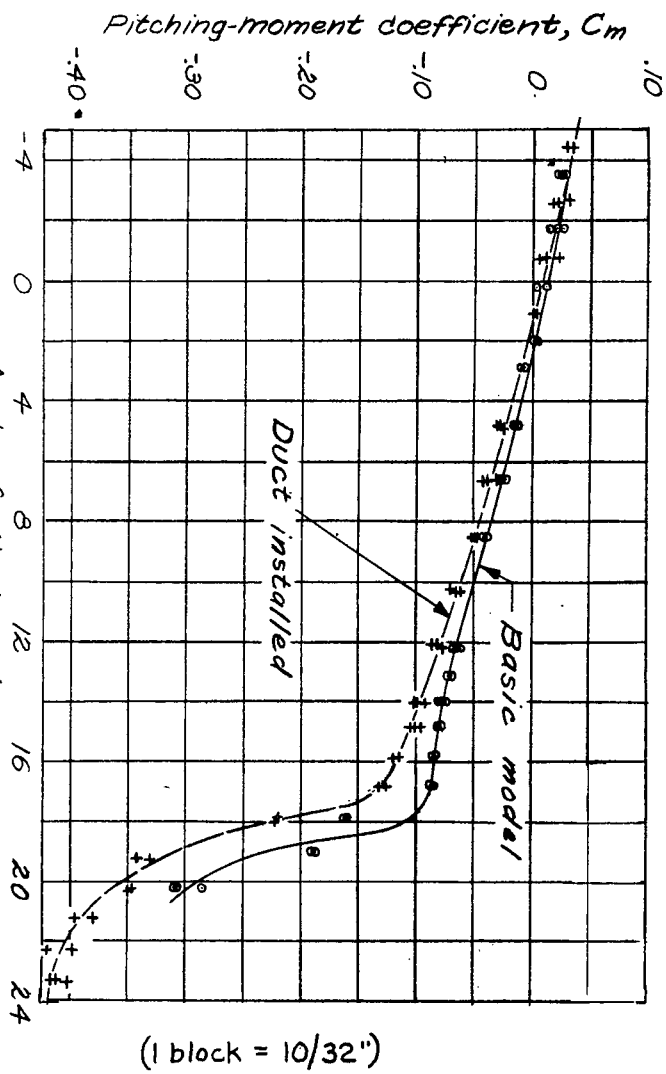


Figure 41.- Variation of duct efficiency with  $Q/V_0$ . Inlet guide vanes in.



Figs. 42, 43

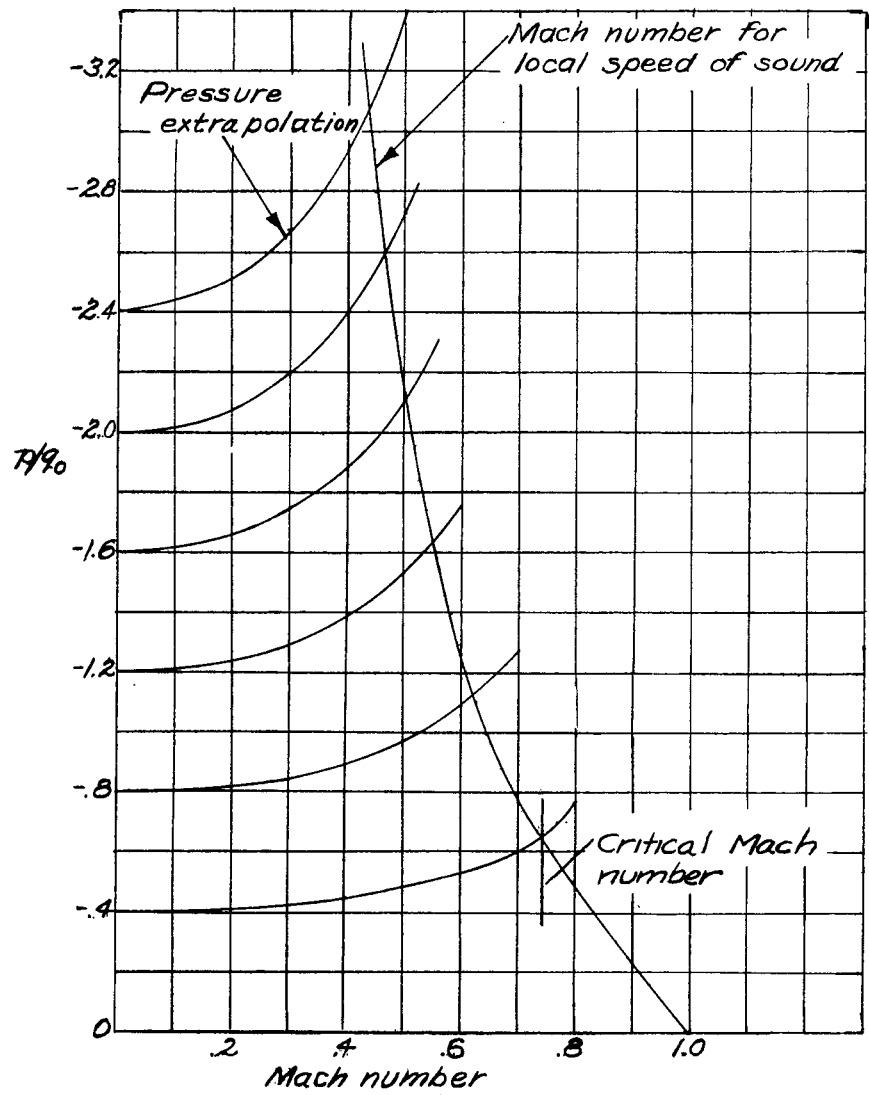


Figure 43: Pressure coefficient against Mach number for determining critical speed.

Fig. 44

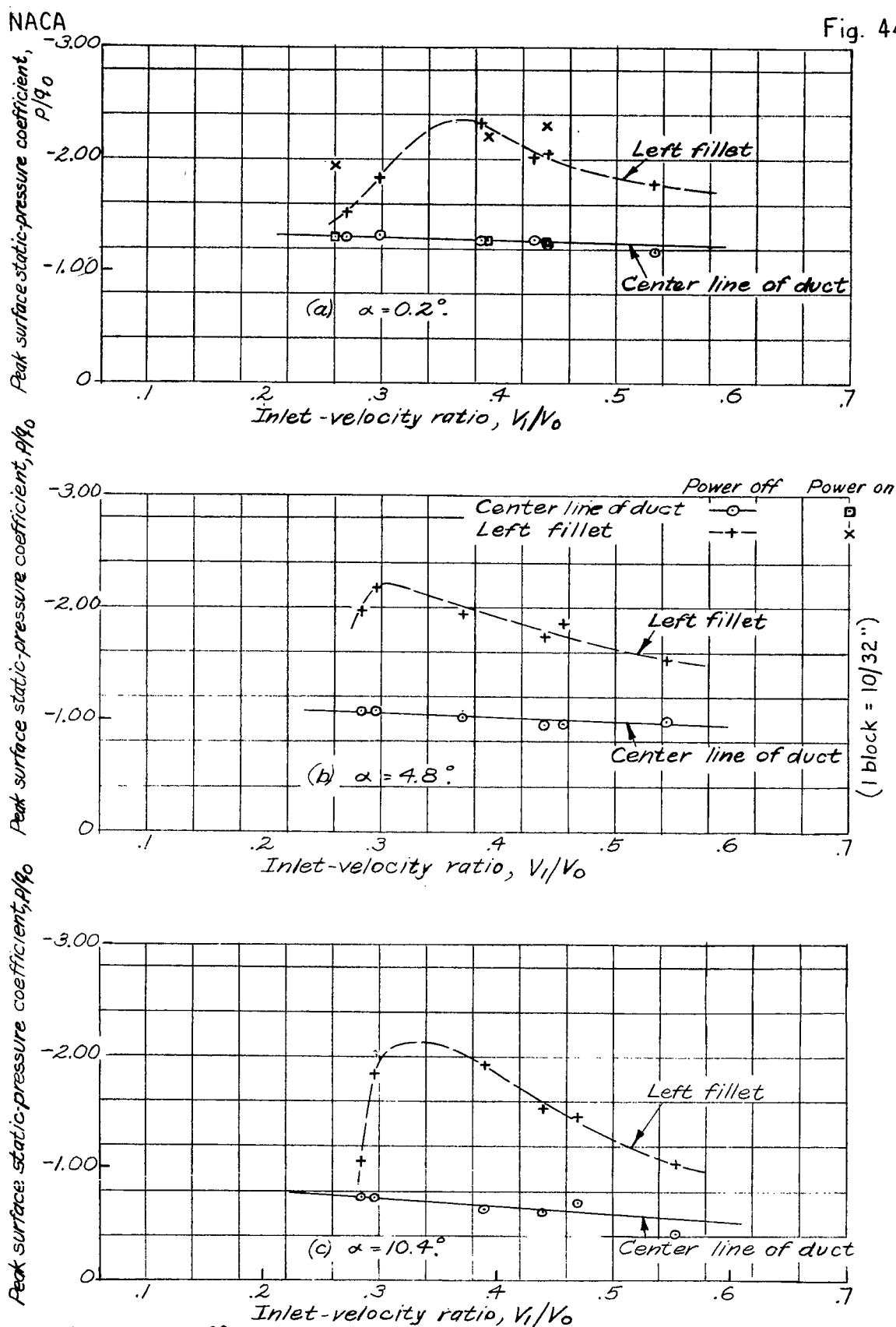


Figure 44.- Effect of inlet-velocity ratio on peak surface static-pressure coefficients. Inlet guide vanes in.

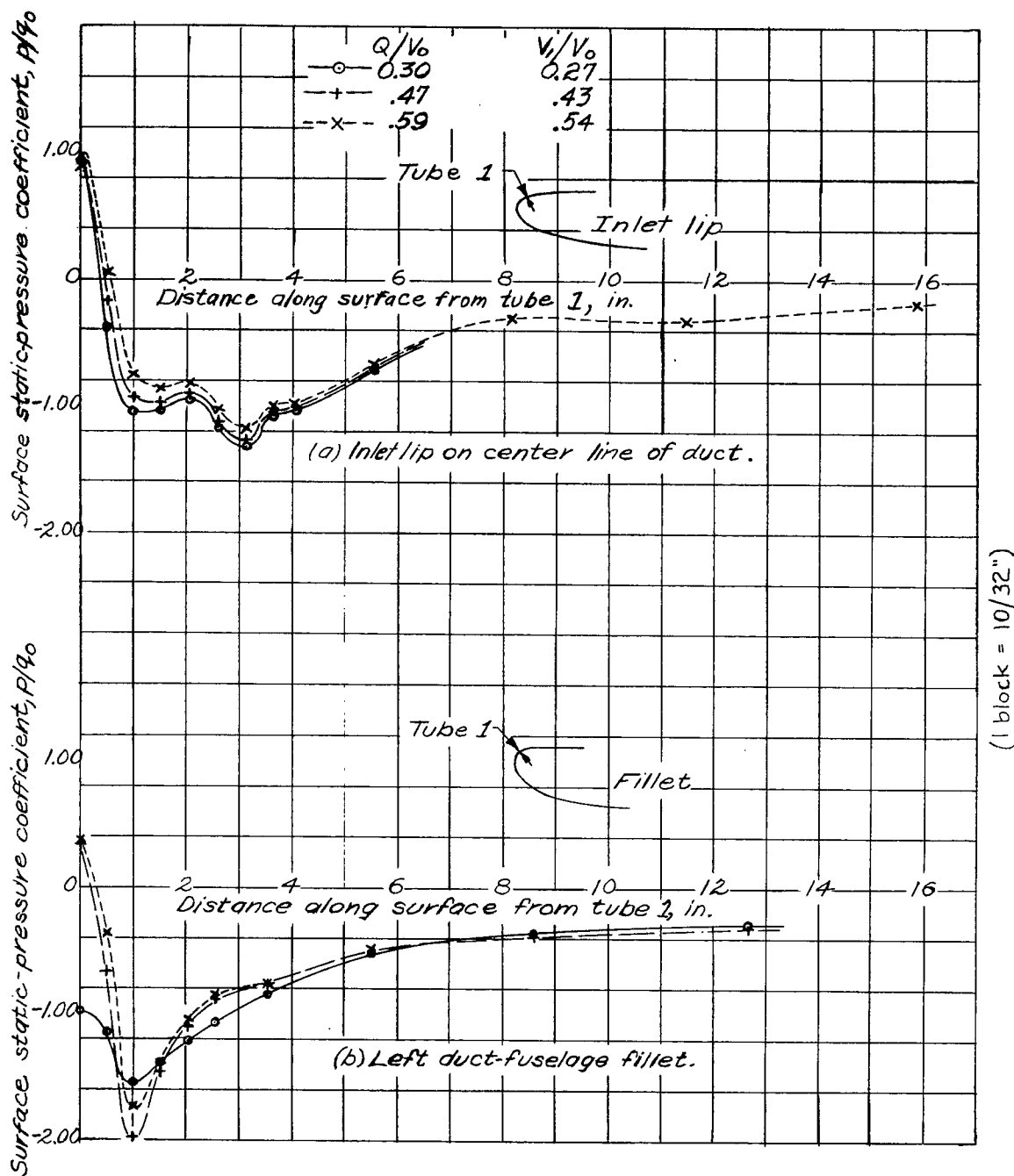


Figure 45.- Effect of  $V_1/V_0$  on surface pressure distribution. Power off;  $\alpha$ ,  $0.2^\circ$ ;  $\Delta p/q_2$ , 10.9; inlet guide vanes in; Mach number, 0.08.

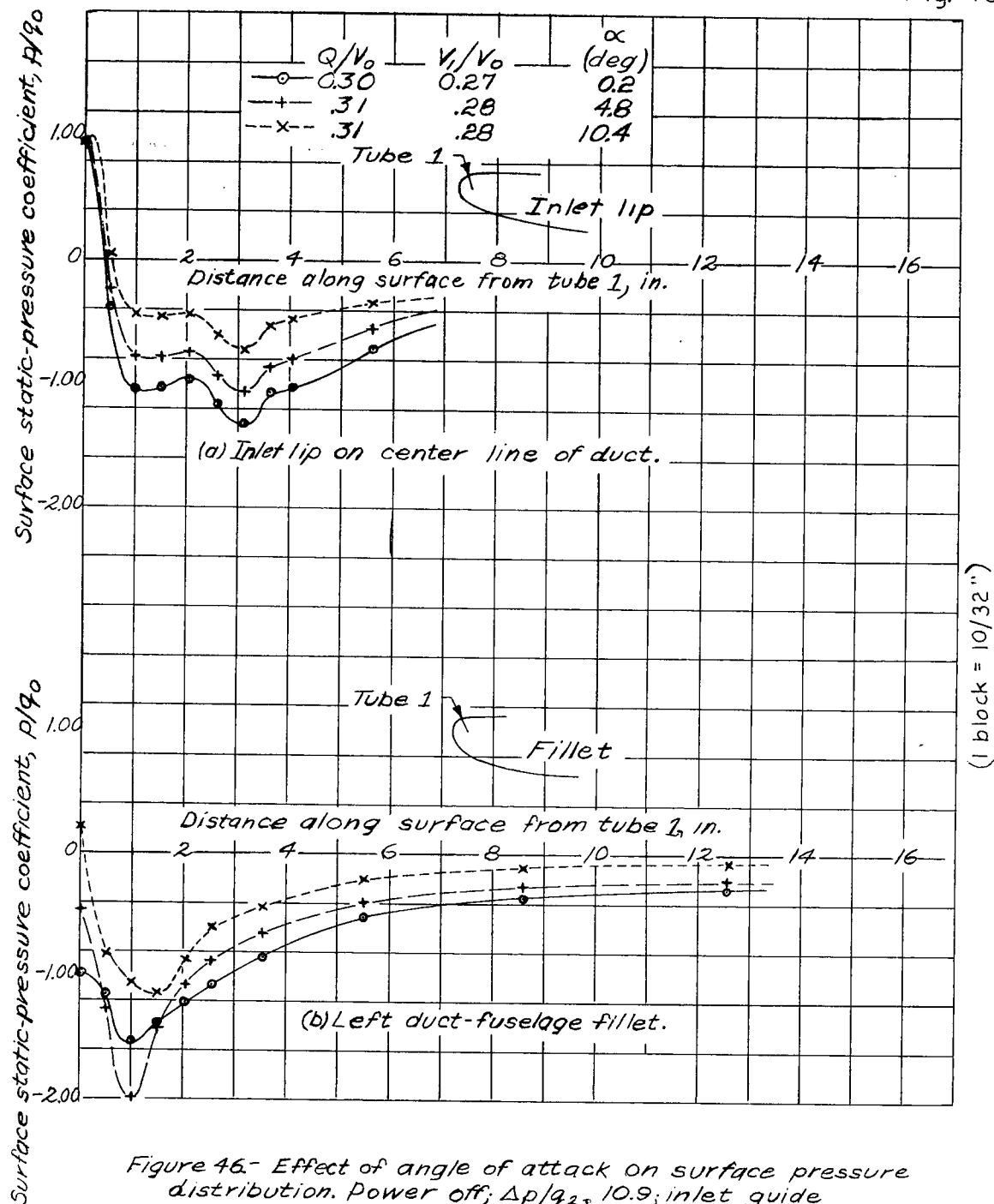


Figure 46.- Effect of angle of attack on surface pressure distribution. Power off;  $\Delta p/q_{25}$  10.9; inlet guide vanes in; Mach number, 0.08.



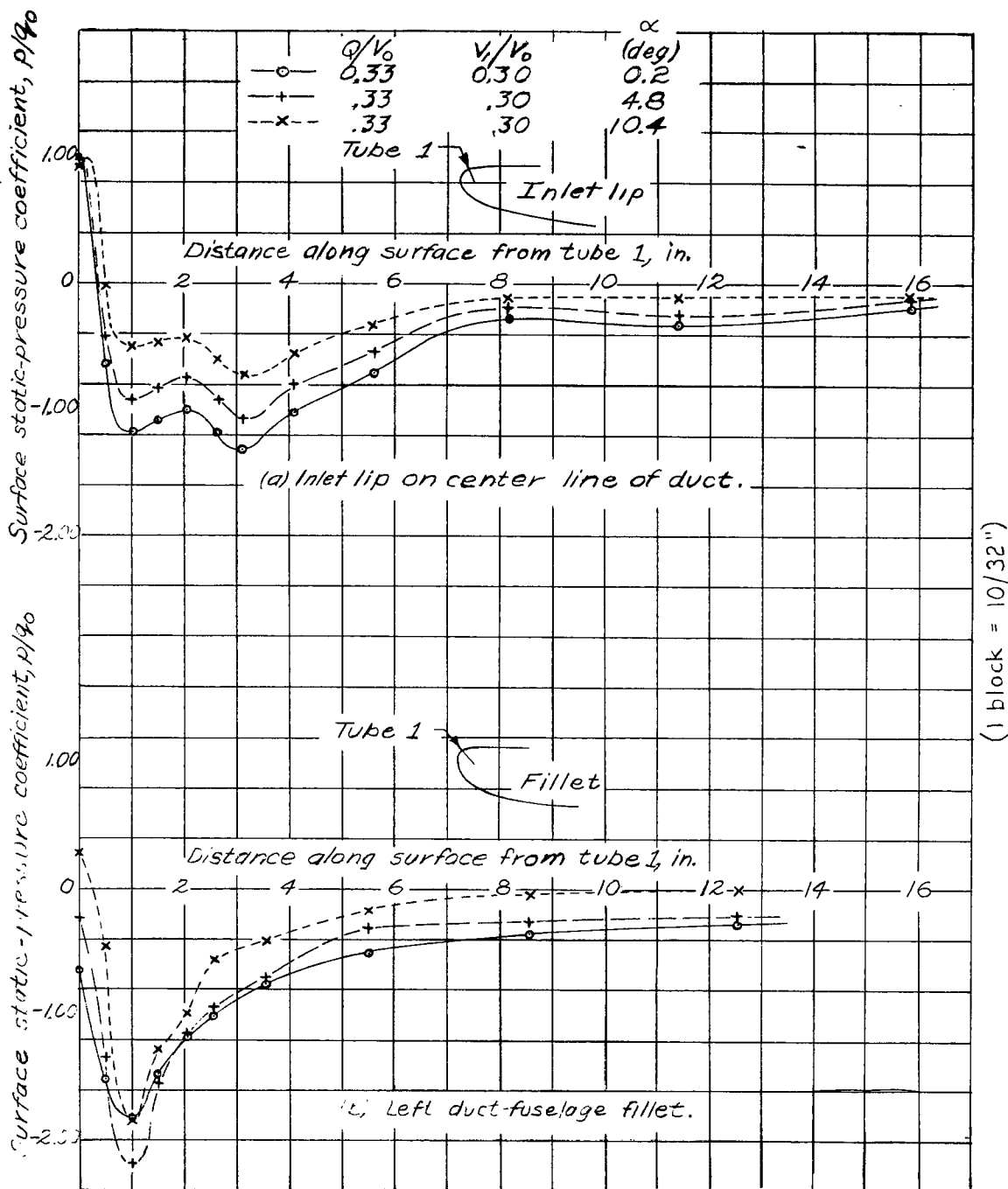


Figure 47.- Effect of angle of attack on surface pressure distribution Power off;  $\Delta p/q_{\infty}$ , 46.5; outlet B; inlet guide vanes in; Mach number, 0.08.

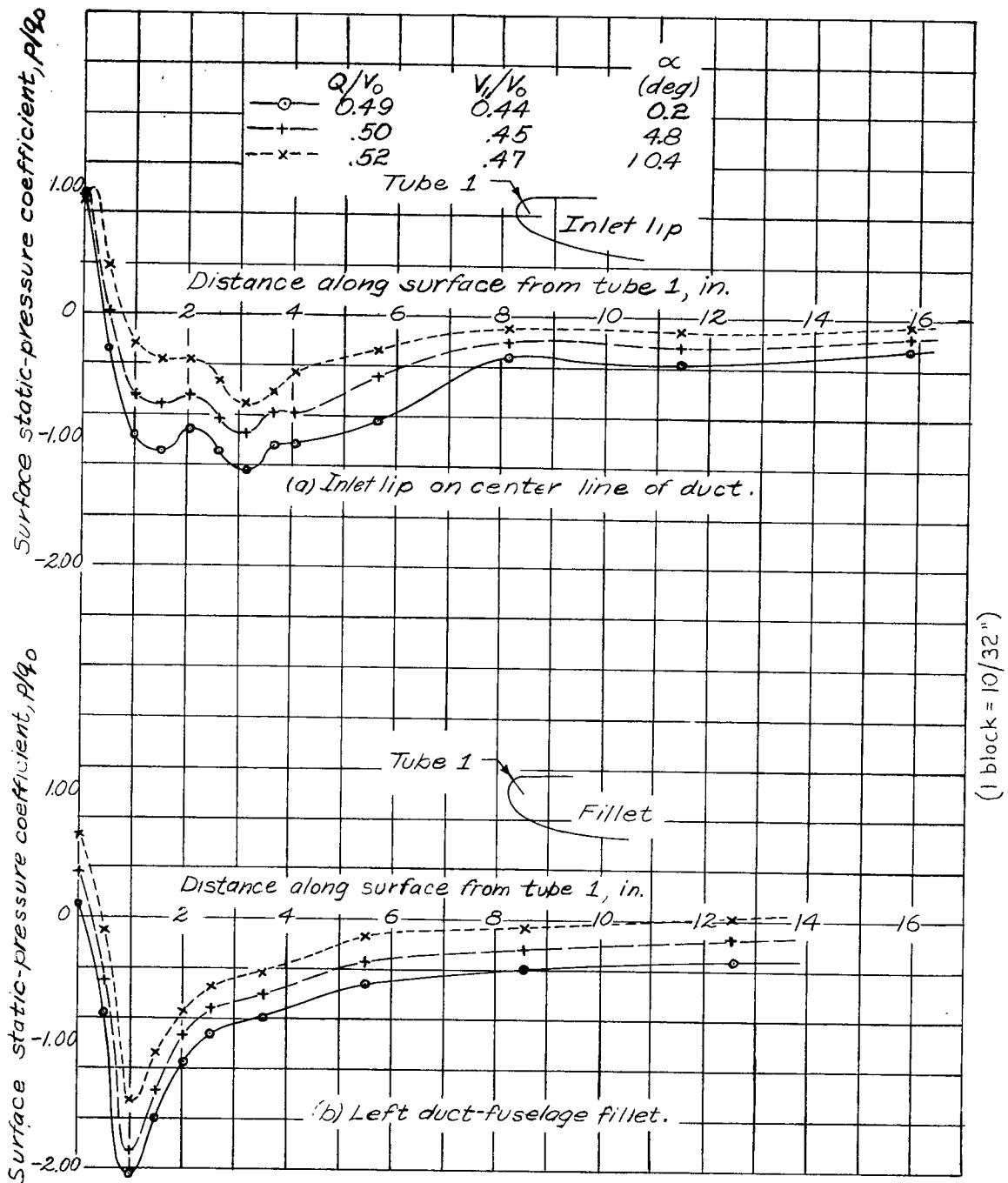


Figure 48.- Effect of angle of attack on surface pressure distribution. Power off;  $\Delta p/q_2$ , 19.5; outlet C; inlet guide vanes in; Mach number, 0.08.

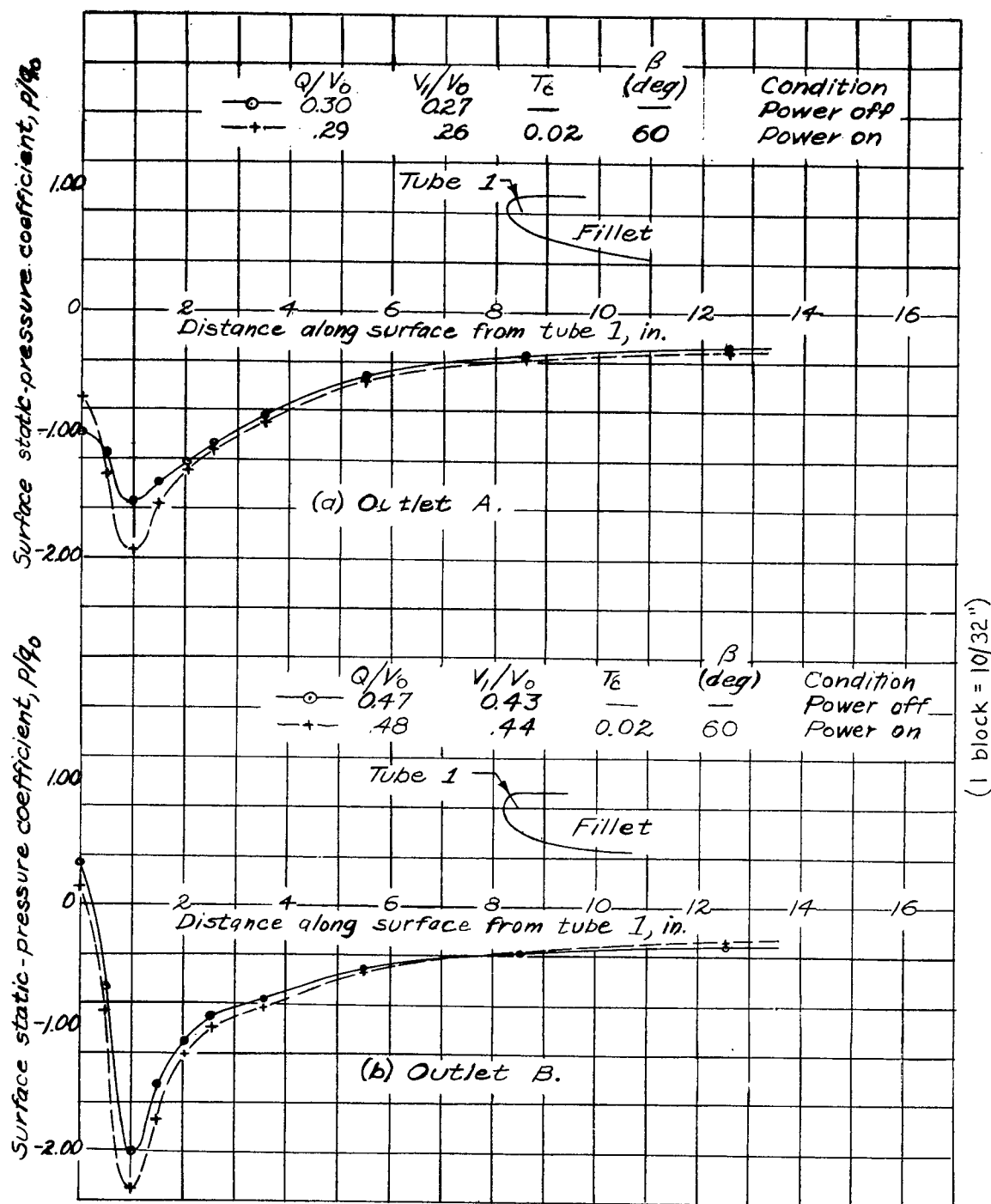


Figure 49. Effect of propeller slipstream on surface pressure distribution at left duct-fuselage fillet.  $\alpha$ ,  $0.2^\circ$ ;  $\Delta p/q_2$ , 109; inlet guide vanes in; Mach number, 0.08.

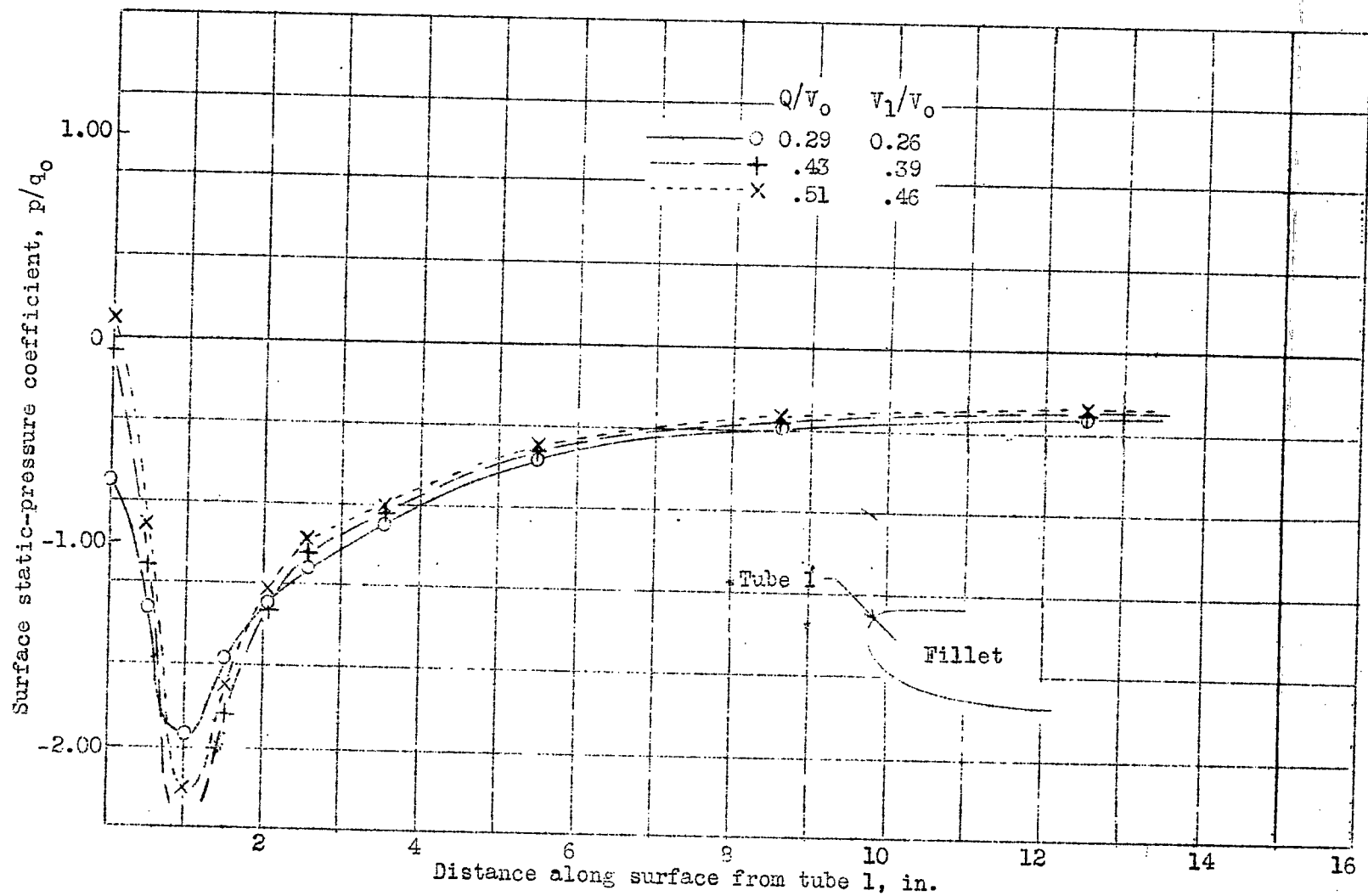


Figure 50.- Effect of  $V_1/V_0$  on surface pressure distribution at duct-fuselage fillet. Power on;  $\alpha$ ,  $0.2^\circ$ ;  $\beta$ ,  $50^\circ$ ;  $T_c$ , 0.02; inlet guide vanes in; Mach number, 0.08.